FABRICATION AND CHARACTERIZATION OF $Ni_{(1-x)}Co_xFe_2O_4$ ELECTROMAGNETIC CERAMIC

SYED AHAMMOD ALI

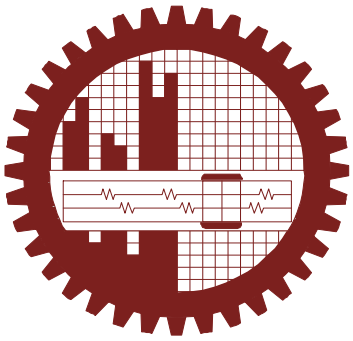

DEPARTMENT OF GLASS AND CERAMIC ENGINEERING

BANGLADESH UNIVERSITY OF ENGINEERING & TECHNOLOGY

2018

CANDIDATES' DECLARATION

IT IS DECLARED HEREBY THAT THIS THESIS PAPER OR ANY PART OF IT HAS NOT BEEN SUBMITTED TO ANYWHERE ELSE FOR THE AWARD OF ANY DEGREE

.....

Syed Ahammod Ali
M.Sc. Engineering, GCE, BUET

Dedication

I would like to dedicate my thesis to my beloved family.

The thesis titled **"FABRICATION AND CHARACTERIZATION OF $Ni_{(1-x)}Co_xFe_2O_4$ ELECTROMAGNETIC CERAMIC"** submitted by Syed Ahammod Ali, Roll No-0412172011 Session: April 2012 has been accepted as satisfactory in partial fulfillment of the requirement for for the degree of Master of Science in Glass and Ceramic Engineering on 25 June, 2018.

BOARD OF EXAMINERS

1. .....
Dr. Md. Abdul Matin
Associate Professor
Department of Glass and Ceramic Engineering
BUET, Dhaka
— Chairman

2. .....
Dr. Md. Abdul Matin
Head
Department of Glass and Ceramic Engineering
BUET, Dhaka
— Member (Ex-officio)

3. .....
Dr. Kazi Md. Shorowordi
Professor
Dept. of MME, BUET, Dhaka
— Member

4. .....
Dr. A. K. M. Abdul Hakim
Individual Consultant
Department of Glass and Ceramic Engineering
BUET, Dhaka
— Member

5. .....
Dr. Sheikh Manjura Hoque
Chief Scientific Officer, Material Science Division,
Atomic Energy Centre,
BAEC, Kazi Nazrul Islam Avenue, Ramna
P.O. BOX-162, DHAKA-1000
— Member (External)

Title: FABRICATION AND CHARACTERIZATION OF $Ni_{(1-x)}Co_xFe_2O_4$ ELECTROMAGNETIC CERAMIC

Contents

Page No.

Acknowledgement

Abstract

List of figures

List of tables

Chapter 1: General Introduction

1.1 Introduction 1
1.2 Objective of the present research 2
1.3 Possible outcomes 3
1.4 Outline of Methodology/Experimental design 3

Chapter 2: Theoretical Background

2.1 Review works 4

Chapter 3: Literature Review

3.1 General aspects 18
3.1.1 Historical background of magnetism 18
3.1.2 Magnetic dipole 19
3.1.3 Magnetic field 20
3.1.4 Magnetic moment 20
3.1.5 Magnetic behavior 22
3.1.6 Magnetic domains 23
3.1.7 Domain wall motion 25
3.1.8 Hysteresis 26
3.1.9 Magnetic anisotropy 28
3.1.10 Saturation magnetization 29
3.2 Ferrites 29
3.2.1 Soft ferrites 30
3.2.2 Hard ferrites 31
3.2.3 Spinel ferrites 31
3.2.4 Structure of unit cell of spinel ferrites 32
3.2.5 Cation distribution of ferrites 33

3.2.6 Exchange interaction 35
3.3 Various kind of magnetism 35
3.3.1 Diamagnetism 35
3.3.2 Paramagnetism 36
3.3.3 Ferromagnetism 38
3.3.4 Antiferromagnetism 39
3.3.5 Ferrimagnetism 40

Chapter 4: Experimental methods

4.1 Sample preparation 42
4.1.1 Compositions 42
4.1.2 Solid state reaction method. 42
4.1.3 Pre-sintering 44
4.1.4 Sintering 45
4.1.5 Flowchart of sample preparation 47
4.2 X-ray diffraction analysis 47
4.3 Microstructures analysis by FE-SEM 48
4.4 Magnetic properties analysis 48
4.5 Thermal properties analysis 48
4.6 Dielectric property measurement 49

Chapter 5: Results and Discussions

5.1 X-ray diffraction analysis 50
5.1.1 XRD pattern 50
5.1.2 Lattice parameter 52
5.1.3 Density and porosity 54
5.2 Microstructure 55
5.3 Magnetic properties 62
5.3.1 Temperature dependence of initial permeability 62
5.3.2 Compositional dependence of curie temperature 64
5.3.3 Frequency dependence of permeability 65
5.3.4 Magnetization measurement 67
5.4 Thermal properties 74
5.4.1 TG-DSC 74
5.4.2 Particle size analysis 76
5.5 Dielecetric properties 78
5.5.1 Frequency dependence dielectric constant 78

Chapter 6: Conclusion 80

References 83

Appendix-A
List of Symbols 89

Appendix-B
List of publication and Presented paper: 91

Acknowledgements

All the devotion and admiration to Almighty Allah, the most merciful, compassionate and beneficent to His creature, who blessed me with knowledge and potential to implement my research work.

Foremost, I would like to express my sincere gratitude to my supervisor Associate Professor Dr. Md. Abdul Matin, Head, Department of Glass and Ceramic Engineering, BUET, Dhaka. Without his enthusiasm, his inspiration and his great efforts this work would have remained a dream. I thank him from the bottom of my heart for his sincere cooperation, precious advice and consistent encouragement. His dedication and the drive for excellence in any task undertaken has been one of the primary motivating factors in this thesis. I am indebted to him for providing me all necessary facilities and opinions whenever required.

I am very much indebted to Dr. A. K. M. Abdul Hakim, Individual Consultant, Department of Glass and Ceramic Engineering, BUET, Dhaka for introducing the present research topic and for inspiring guidance and valuable suggestion throughout this research work. It would have not been possible for me to bring out this thesis without his help and constant encouragement.

I am deeply grateful to Professor Dr. Fakhrul Islam, Department of Glass and Ceramic Engineering, BUET, Dhaka, for his interest and encouragement in my thesis.

I am eternally grateful to Rubayyat Mahbub Turjo, Assistant Professor, GCE; Arman Hussain, Assistant Professor, GCE, Mehedi Hasan, Assistant Professor, GCE and All the ideas we shraed and discussed have proven very useful. This thesis would not go so well without their contribution at the forefront of this research.

I am also very much grateful to Md. Shahajalal Rana, Department of GCE, for his generous help in doing measurements and analysis of Microstructure. I also thankful to Mr. Sahahjalal, Md. Saiful Islam, Md. Yunus Ali of Department of GCE for their help during my research work

I convey my heartiest regards to Dr. Sheikh Manjura Hoque, Head, Materials science division, AEC, Dhaka. I am extremely grateful to her for sharing her wisdom and for generously letting me use Materials Science Division lab of AEC, Dhaka on such short notice.

I am also grateful to Dr. Md. Nazrul Islam, Chief Scientific Officer, Materials Science Division, Atomic Energy Centre, Dhaka for his generous help in doing measurements and analysis of XRD results and whose vast knowledge in the field of science has enlightened me of this research work.

I am thankful to Ms. Alhamra Parveen, Ms. Anjuman Ara Begum, Ms. Nazmunnahar Begum, and Ms. Halima Sadia of Materials Science Division, AECD for their constant help during my research work.

Above all, I would like to all my family members and friends whose direct and indirect support helped me completing my project in time. This thesis has been impossible without their perpetual moral support.

Last but not the least; I would like to thank my parents and my wife for their undying support, encouragement and endless love throughout my life.

Syed Ahamm

Abstract

Ni-Co ferrites with the composition $Ni_{1-x}Co_xFe_2O_4$ (x=0, 0.2, 0.4, 0.6, 0.8, 1) were synthesized by solid state reaction method. The starting materials for the preparation of the studied compositions were in the form of nano powder of ferrites ($NiFe_2O_4$ and $CoFe_2O_4$) of Inframat Advanced Materials, USA. The purity of materials was up to 99.99%. The $NiFe_2O_4$ and $CoFe_2O_4$ nano ceramic powders were mixed according to their molecular weight. Intimate mixing of materials was carried out using mortar and pestle and then ball milled for 10hrs and the slurry was dried and pressed into disc shaped sample. The disc shaped samples were pre-sintered at 850^0C for 4hrs. Final sintering of the samples were carried out at 1100^0C, 1125^0C, 1150^0C, 1175^0C, 1200^0C and1250^0C for 4 hrs respectively.

The phase identification and lattice parameter determination were performed on an X-ray diffraction patterns. The XRD patterns for all samples clearly showed their spinel phase and the formation of a spinel structure. The peaks (111), (220), (311), (222), (400), (511) and (440) correspond to the spinel phase. The lattice parameter was determined through the Nelson-Riley extrapolation method. The variation of lattice parameter as a function of Co^{2+} content was established. It was noticed that the lattice parameter increased with the Co content. This variation can be explained on the basis of an ionic size difference of the component ions. The Co^{2+} (0.745 Å) ions have a larger ionic radius than Ni^{2+} (0.69 Å) and Fe^{3+} ions (0.645 Å).The bulk density (d_B) and the X-ray density (d_X) of the prepared samples were also calculated.

The microstructural aspects were studied with a field emission scanning electron microscope (JEOL-JSM-7600F). Magnetic and electrical properties of ferrites highly depend on the microstructure. Between the grain size and porosity of microstructures, the grain size is more important parameter affecting the magnetic properties of a ferrite. Scanning electron micrographs of $Ni_{1-x}Co_xFe_2O_4$(x=0, 0.2, 0.4, 0.6, 0.8, 1) samples

sintered at 1100^0C, 1125^0C, 1150^0 C, 1175^0C, 1200^0C and 1250^0C were measured. As seen from the micrographs, the average dimension of the particles is below 10 μm.

Initial permeability as a function of frequency has been measured by an impedance analyzer. Phase transition temperature determined from DSC measurements and temperature dependence of initial permeability was found to display a good correlation.

Curie temperature, T_c of all the samples were determined from the temperature dependence of permeability and compared with the peak temperature of DSC thermograph. T_c is found to decrease with increasing $CoFe_2O_4$ substitution which ascribed due to weakening of J_{AB} super-exchange interaction between tetrahedral and octahedral sites.

The magnetization measurement of the sample was conducted by a vibrating sample magnetometer (model VSM-02, Hirstlab, UK) at 80K, 200K and 300K as a function of field. The detail hysteresis parameters such as M_s, M_r, H_c determined from M-H loop measured at 80, 200 and 300K. Saturation magnetization, M_s measured at 80K was found much higher compared with data at 300K. M_s was found to increase with decreasing temperature and attained a maximum value corresponding to $CoFe_2O_4$ at any measurement temperature which may be attributed to higher magnetic moment of $CoFe_2O_4$ compared with $NiFe_2O_4$. A gradual magnetic hardening was observed to increase with increasing $CoFe_2O_4$ content with a maximum value of H_c at x=0.8.

The dielectric behavior is one of the most important characteristics of ferrites which distinctly depend on the preparation conditions, e.g. sintering time and temperature, type and quantity of additives. The dielectric constant (ε') results are due to the heterogeneous structure of the material. The frequency dependence of the dielectric constant for all the samples were measured using an impedance analyzer. The change of dielectric properties was investigated varying modulating frequency (100 Hz to 10 MHz). All the samples showed similar behavior, i.e. dielectric constant decreased initially with increase in frequency and reached a constant value at higher frequency. After a certain increase in frequency all the samples exhibit a frequency-independent behavior.

List of Figures

Chapter-2		Page
Figure 2.1	FTIR spectrum for Ni_{1-X} $Co_XFe_2O_4$ (x=0.3)	5
Figure 2.2	X-ray diffraction pattern for Ni_{1-X} $Co_XFe_2O_4$ (X=0.3)	5
Figure 2.3	X-ray diffraction patterns of $Co_{1-x}Ni_xFe_2O_4$.	6
Figure 2.4	SEM images of $Co_{1-x}Ni_xFe_2O_4$.	7
Figure 2.5	Micro-Raman spectrum of $Co_{1-x}Ni_xFe_2O_4$.	7
Figure 2.6	FT-IR Spectrum of $Co_{1-x}Ni_xFe_2O_4$	8
Figure 2.7	Variation of loss tangent with frequency of $Co_{1-x}Ni_xFe_2O_4$	8
Figure 2.8	Variation of room temperature complex impedance spectra of $Co_{1-x}Ni_xFe_2O_4$	8
Figure 2.9	Variation of AC conductivity with respect to frequency of $Co_{1-x}Ni_xFe_2O_4$	8
Figure 2.10	(a) M-H curve of $Co_{1-x}Ni_xFe_2O_4$ at 30K and (b) M-H curve of $Co_{1-x}Ni_xFe_2O_4$ at 300K	9
Figure 2.11	XRD pattern of $Ni_{0.25}Co_{0.75}Fe_2O_4$ nano particles	10
Figure 2.12	EDX spectrum of $Ni_{0.25}Co_{0.75}Fe_2O_4$ nano particles	10
Figure 2.13	SEM image of $Ni_{0.25}Co_{0.75}Fe_2O_4$ nano particles	10
Figure 2.14	TG-DSC curve of $Ni_{0.25}Co_{0.75}Fe_2(cin)_3(N_2H_4)_5$	10
Figure 2.15	XRD graph of Co_xNi_{1-x} Fe_2O_4(Where x= 0.5,0.7 & 0.9) of synthesize	11
Figure 2.16	VSM (Vibration Sample Magnetometer) -Hystresses loop	12
Figure 2.17	(a) XRD Patterns (b) variation of Lattice parameters with Cobalt Content for the samples X=0.0, 0.1, 0.2, 0.3, 0.4 & 0.5 of the series of $Ni_{(1-X)}Co_xFe_2O_4$	12
Figure 2.18	Temperature dependence of ε' at 75 kHz and 50 kHz frequencies for the samples X=0.0, 0.1, 0.2, 0.3, 0.4 & 0.5 of the series of $Ni_{(1-X)}Co_xFe_2O_4$	13

Figure 2.19	Indexed X-ray pattern of $Ni_{1-x}Co_xFe_2O_4$	14
Figure 2.20	Composition variation of dc electrical resistivity *(*ln *ρ)* with $1/k_BT$ $(eV)^{-1}$	15
Figure 2.21	Temperature dependence of drift mobility (μ_d) in $Ni_{1-x}Co_xFe_2O_4$ nanoferrites	15
Figure 2.22	Frequency dependence of dielectric constant *(ε)* for $Ni_{1-x}Co_xFe_2O_4$ nanoferrites	15
Figure 2.23	Graph of ac conductivity as a function of frequency for various concentrations of cobalt	15
Figure 2.24	SEM micrographs for $Ni_{(1-x)}Co_xFe_2O_4$ ferrite.	16
Figure 2.25	Variation of dielectric permittivity with frequency for $Ni_{(1-x)}Co_xFe_2O_4$ ferrite	17
Figure 2.26	Variation of AC conductivity of $Ni_{(1-x)}Co_xFe_2O_4$ ferrite with frequency	17
Figure 2.27	IR absorption spectra for $Ni_{(1-x)}Co_xFe_2O_4$ ferrite.	17

Chapter -3

Figure 3.1	Magnetic dipole of a bar magnet	19
Figure 3.2	Magnetic domain	24
Figure 3.3	Bloch wall	25
Figure 3.4	The magnetization changes from one direction to another one	26
Figure 3.5	Hysteresis loop	27
Figure 3.6	Schematic of two sublattice of a unit cell of the spinel structure, showing octahedral and tetrahedral sites	33
Figure 3.7	Diamagnetism	36
Figure 3.8	Paramagnetism	37
Figure 3.9	Ferromagnetism	38
Figure 3.10	The inverse susceptibility varies with temperature T for (a) paramagnetic, (b) ferromagnetic, (c) ferrimagnetic, (d) antiferromagnetic materials. T_N and T_c are Neel temperature and Curie temperature, respectively.	39
Figure 3.11	Antiferromagnetism	40

Figure 3.12	Ferrimagnetism	41

Chapter -4

Figure 4.1	a. Pellets and b. Toroids shaped samples.	43
Figure 4.2	Pre- sintering and sintering program.	45
Figure 4.3	Flowchart of ferrite sample preparation.	47

Chapter -5

Figure 5.1	XRD pattern of $Ni_{1-x}Co_xFe_2O_4$(x = 0.0, 0.2, 0.4, 0.6, 0.8 &1.0)	50
Figure 5.2	XRD patterns of $NiFe_2O_4$	51
Figure 5.3	XRD patterns of $CoFe_2O_4$	52
Figure 5.4	Variation of Lattice Parameter with Co Content	53
Figure 5.5(a-f)	SEM micrographs of $Ni_{1-x}Co_xFe_2O_4$ samples are sintered at 1100ºC	56
Figure 5.6(a-f)	SEM micrographs of $Ni_{1-x}Co_xFe_2O_4$ samples are sintered at 1125ºC	57
Figure 5.7(a-f)	SEM micrographs of $Ni_{1-x}Co_xFe_2O_4$ samples are sintered at 1150ºC	58
Figure 5.8(a-f)	SEM micrographs of $Ni_{1-x}Co_xFe_2O_4$ samples are sintered at 1175ºC	59
Figure 5.9(a-f)	SEM micrographs of $Ni_{1-x}Co_xFe_2O_4$ samples are sintered at 1200ºC	60
Figure 5.10(a-f)	SEM micrographs of $Ni_{1-x}Co_xFe_2O_4$ samples are sintered at 1250ºC	61
Figure 5.11	Temperature dependence of permeability, μ' of Ni(1-x)CoxFe2O4 ferrites and determination of Curie temperature.	63
Figure 5.12	Variation of Curie temperature, T_c with Co content (x) of $Ni_{(1-x)}Co_xFe_2O_4$ ferrites.	64
Figure 5.13	Frequency dependence of the real part of the permeability, μ' of $Ni_{(1-x)}Co_xFe_2O_4$ ferrites sintered at 1100°C, 1125°C,11500C,117500C,12000C and 1250°C for 4hrs.	66
Figure 5.14(a-f)	The M-H loop for $Ni_{(1-x)}Co_xFe_2O_4$ at 80K	68
Figure 5.15(a-f)	The M-H loop for $Ni_{(1-x)}Co_xFe_2O_4$ at 200K	69
Figure 5.16(a-c)	The M-H loop for $Ni_{(1-x)}Co_xFe_2O_4$ at 300K	70
Figure 5.16(a-c)	The M-H loop for $Ni_{(1-x)}Co_xFe_2O_4$ at 300K	71

Figure 5.17	Saturation magnetization (M_s), Retentivity (M_r), Coercivity (H_c) for $Ni_{(1-x)}Co_xFe_2O_4$ at 80K , sintering condition 1200^0C	72
Figure 5.18	Saturation magnetization (M_s), Retentivity (M_r), Coercivity (H_c) for $Ni_{(1-x)}Co_xFe_2O_4$ at 200K , sintering condition 1200^0C	72
Figure 5.19	Saturation magnetization (M_s), Retentivity (M_r), Coercivity (H_c) for $Ni_{(1-x)}Co_xFe_2O_4$ at 300K , sintering condition 1200^0C	72
Figure 5.20(a-f)	DSC/TG curve of Ni-Co ferrites with the composition of $Ni_{1-x}Co_xFe_2O_4$(x=0.0,0.2,0.4,0.6,0.8 ,1.0)	75
Figure 5.21(a-f)	Particle size distribution of Ni-Co ferrites with the composition $Ni_{1-x}Co_xFe_2O_4$ (x=0, 0.2, 0.4, 0.6, 0.8 &1.0)	77
Figure 5.22	Frequency dependence of dielectric constant of $Ni_{1-x}Co_xFe_2O_4$	78

List of Tables

Chapter -5 **Page**

Table 5.1 The Chemical formula, cation distribution to A-site and B-site and theoretical calculation of lattice parameter with cobalt content in $Ni_{1-x}Co_xFe_2O_4$. 54

Table 5.2 Variation of lattice parameter, X-ray density, bulk-density, porosity and Curie temperature with cobalt content in $Ni_{1-x}Co_xFe_2O_4$. 55

Table 5.3 Saturation magnetization (M_S), retentivity(M_r), coercivity(H_C), and hysteresis loss of Ni-Co ferrite samples at 80K. 73

Table 5.4 Saturation magnetization (M_S), retentivity(M_r), coercivity(H_C), and hysteresis loss of Ni-Co ferrite samples at 200K. 73

Table 5.5 Saturation magnetization (M_S), retentivity(M_r), coercivity(H_C), and hysteresis loss of Ni-Co ferrite samples at 300K. 73

Chapter One

General Introduction

1.1 Introduction

Ferrites are commercially important magnetic materials. Ranging from the very ordinary radio sets to the complicated and exhaustive hardware involved in computers, ferrites have found their way to prove their importance. There are soft and hard magnetic ferrites. Both of these ferrites have enormous practical applications. Soft ferrites have been extensively used for many kinds of magnetic devices such as transformers, inductors, magnetic heads, in resonance circuit for high frequency (ranging from 10^3 to 10^{11}Hz) because of their electrical resistivity higher than those of the soft magnetic alloys (ranges from 10^3 to 10^{11} Ω-cm which is up to 15 order of magnitude higher than that of metals like iron), low eddy current losses, high initial permeability, high saturation induction, low hysteresis loss and reduced physical size. Due to these reasons extensive research activities has been carried out during the past 50 years to enhance their efficiency from the application point of view to various technical devices. Cubic spinel ferrite, has two sub-lattices, tetrahedral (A site) and octahedral (B site) in AB_2O_4 crystal structure. The important structural, electrical and magnetic properties of spinels, responsible for their application in various fields, are found to depend on the distribution of cations among the sites [1.1].Therefore the estimation of the cation distribution turns out to be important. Various cations can be placed in A site and B site to tune its magnetic properties. Depending on A site and B site cations it can exhibit various magnetic structures [1.2].

Both Nickel and Cobalt ferrites have inverse spinel structure in bulk. Some researchers have investigated various properties of bulk Ni-Co ferrites employing co-precipitation, hydrothrermal, sol-gel method but no detail study has been conducted yet to synthesize and characterize nano-power based Ni-Co mixed ferrites [1.3, 1.4].

In present work, we studied the structural and magnetic properties of functional magnetic materials of composition $Ni_{1-x}Co_xFe_2O_4$ (x=0, 0.2, 0.4, 0.6, 0.8, 1) prepared using $NiFe_2O_4$ (soft) and $CoFe_2O_4$ (semi-hard) nanomaterials following solid state synthesis technique.

Spinel ferrites commanded the attention first when S. Hilpert [1.5] focused on the usefulness of ferrites at high frequency applications. The ferrites were developed into commercially important materials, chiefly during the years 1933 - 1945 by Snoek [1.6] and his associates at the Philips Research Laboratories in Holland. At the same time, Takai [1.7] in Japan was engaged in the research work on the ferrite materials. In a classical paper published in 1948 by Neel [1.8] provided the theoretical key to an understanding of the ferrites. The subject has been covered at length in books by Smit. [1.9] and Standley [1.10] and reviewed by Smart [1.11], Wolf [1.12], and Gorter [1.13]. Snoek had laid the foundation of the physics and technology of practical ferrites by 1945 and now embrace a very wide diversity of compositions, properties and applications [1.14]. Technological advances in a variety of areas have generated a growing demand for the soft magnetic materials in devices. Among the soft magnetic materials, polycrystalline ferrites have received special attention due to their good magnetic properties and high electrical resistivity over a wide range of frequencies; starting from a few hundred Hz to several GHz. Spinel type ferrites are commonly used in many electronic and magnetic devices due to their high magnetic permeability and low magnetic losses [1.15, 1.16]. They are also used in electrode materials for high temperature applications because of their high thermodynamic stability, electrical resistivity, electrolytic activity and resistance to corrosion [1.17, 1.18].

1.2 Objectives of the present research

The present research work is carried out with the following objects:

- To a) To fabricate $Ni_{(1-x)}Co_xFe_2O_4$ electromagnetic ceramic using $(1-x)NiFe_2O_4.xCoFe_2O_4$ (x = 0.0, 0.2, 0.4, 0.6, 0.8 and 1.0)

- To establish a comprehensive microstructure-property relationship with determination of phases, structure, density and porosity of the samples, ferrimagnetic to paramagnetic transition temperature.

1.3 Possible outcomes

This research would develop a new $Ni_{(1-x)}Co_xFe_2O_4$ nanoceramic with superior electromagnetic properties that can find prospective applications such as biosensors and targeted drug delivery system

1.4 Outline of Methodology/Experimental design:

To fabricate new $Ni_{(1-x)}Co_xFe_2O_4$ electromagnetic nanoceramics, different $(1-x)NiFe_2O_4.xCoFe_2O_4$ (x=0.0, 0.2, 0.4, 0.6, 0.8 and 1.0) batches will be prepared from nano-sized powders of $NiFe_2O_4$ and $CoFe_2O_4$ followed by double stage sintering. The mixture will be milled in a ball mill and then pressed into disc shape. The sample then will be pre-sintered at 800^0C to 1000^0C. After crushing, the resulting powders will be pressed uniaxially under pressure to make pellets and toroids. The pressed pellets and toroids will then finally be sintered at a temperature from 1200^0C to 1400^0C for several hours. After sintering, phase identification and crystal structure analysis of the sintered samples will be conducted using X-ray diffractometer (XRD). Microstructure analysis will be carried out by field emission Scanning Electron Microscope (FESEM) of the polished and etched surface of the samples. Compositional analysis of $Ni_{(1-x)}Co_xFe_2O_4$ will be done by XRF. The frequency dependence of complex permeability and loss factor of the toroid samples will be measured over a wide range of frequency (1 KHz-15MHz) with an impedance analyzer. The initial permeability as a function of temperature for both heating and cooling cycle will be measured. Field dependence of magnetization at room temperature would be measure using Vibrating Sample Magnetometer (VSM). Finally, the dielectric measurement of the sintered samples will be carried out using impedance analyzer.

Chapter Two

Theoretical Background

2.1 Review works

Spinel ferrites are extremely important for academic and technological applications. The physical properties such as structural, electrical and magnetic properties are governed by the type of magnetic ions residing on the tetrahedral (A) site and octahedral (B) site of the spinel lattice and the relative strength of the inter- and intra- sublattice interactions. In recent years, the design and synthesis of magnetic particles have been the focus of fundamental and applied research owing to their enhanced or unusual properties [2.1]. It is possible to manipulate the properties of a spinel material to meet the demands of a specific application. A large number of scientists are research on the ferrites material. Before discussing our research work, we shall see the previous work done related to our work through literature survey.

Singh *et al.* [2.2] synthesized of pure and mixed Nickel-Cobalt spinel ferrite samples, Ni(1-x)CoxFe2O4 (x=0, 0.1, 0.3, 0.5), has been carried out with varying composition of Co as substituent. Solution combustion method has been employed for the synthesis of ferrites. For the combustion synthesis oxalic dihydrazide (ODH) was used as a fuel. Various techniques i.e. Fourier transform infrared spectroscopy (FT-IR), X-ray powder diffraction (XRD) and Mössbauer spectroscopy have been used to characterize ferrite samples. Magnetic studies have been carried out by using Vibrating sample magnetometer (VSM). Cobalt substituted ferrites showed variation in magnetic properties than pure nickel ferrite.

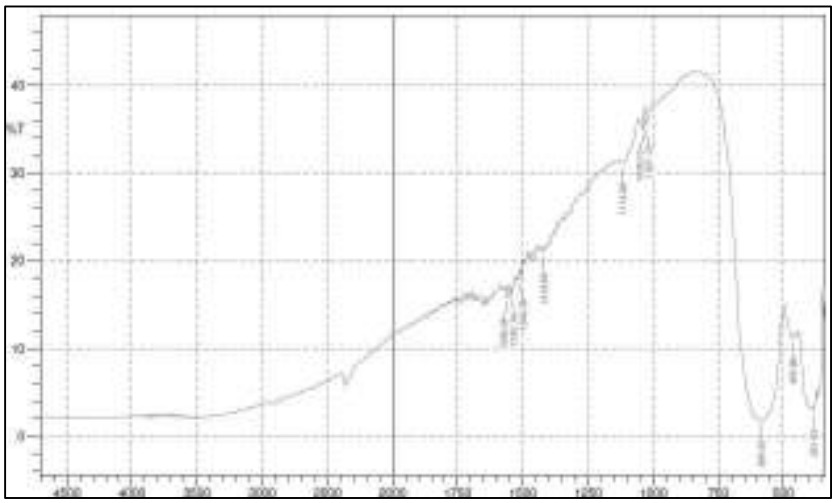

Figure 2.1: FTIR spectrum for Ni_{1-X} $Co_XFe_2O_4$ (X=0.3) [2.2]

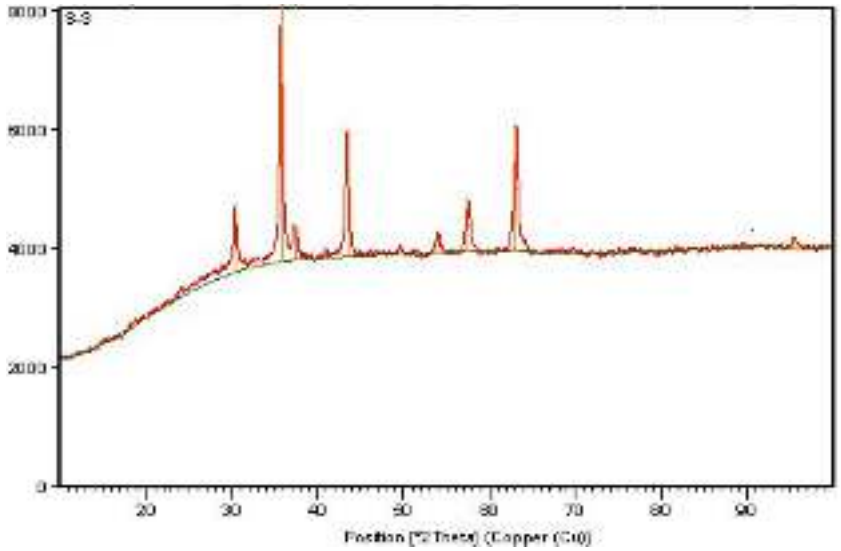

Figure 2.2: X-ray diffraction pattern for Ni_{1-X} $Co_XFe_2O_4$ (X=0.3) [2.2]

Velhal *et al*. [2.3] synthesized Nickel substituted cobalt ferrite nanoparticles with composition $Co_{1-x}Ni_xFe_2O_4$ ($0.0 \leq x \leq 1.0$) using low temperature auto combustion method. They reported that X-ray diffraction patterns reveal the formation of cubic phase spinel structure. The crystallite size varies from 30-44 nm with the nickel content. Porous and agglomerated morphology of the bulk sample was displayed in the scanning electron

microscopy. Micro Raman spectroscopy reveals continuous shift of E_g and $E_g(2)$ stokes line up to 0.8 Ni substitution. The dispersion behavior of the dielectric constant with frequency and the semicircle nature of the impedance spectra showed the cobalt nickel ferrite to have high resistance. The ferromagnetic nature was observed in all the samples, however, the maximum saturation magnetization was achieved by the 0.4 Ni substituted cobalt ferrite, which is up to the 92.87 emu/gm at 30K.

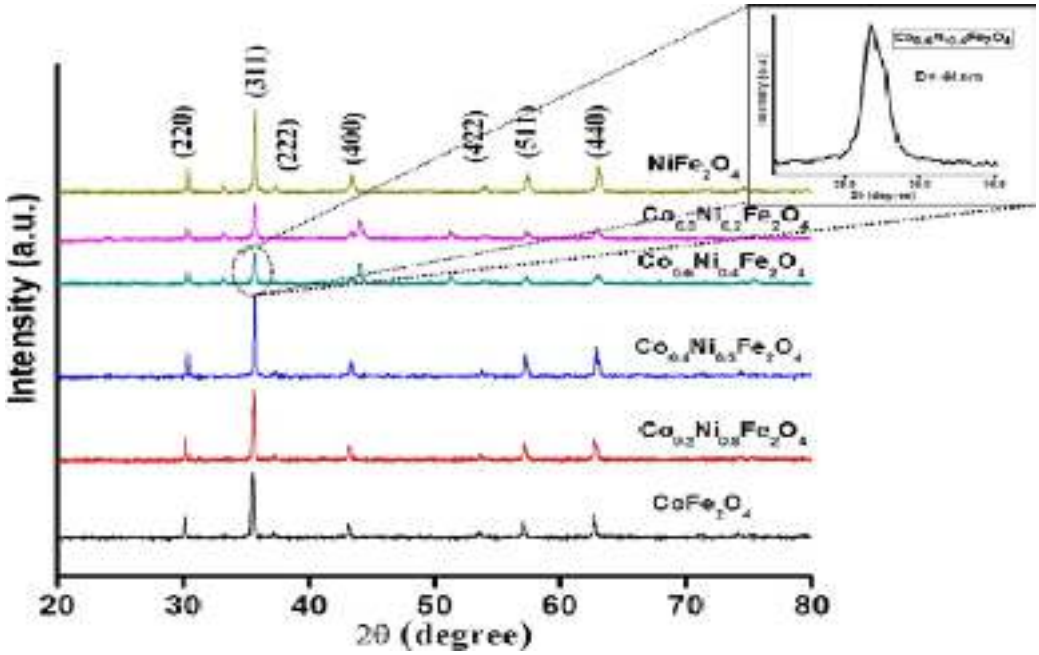

Figure. 2.3: X-ray diffraction patterns of $Co_{1-x}Ni_xFe_2O_4$. [2.3]

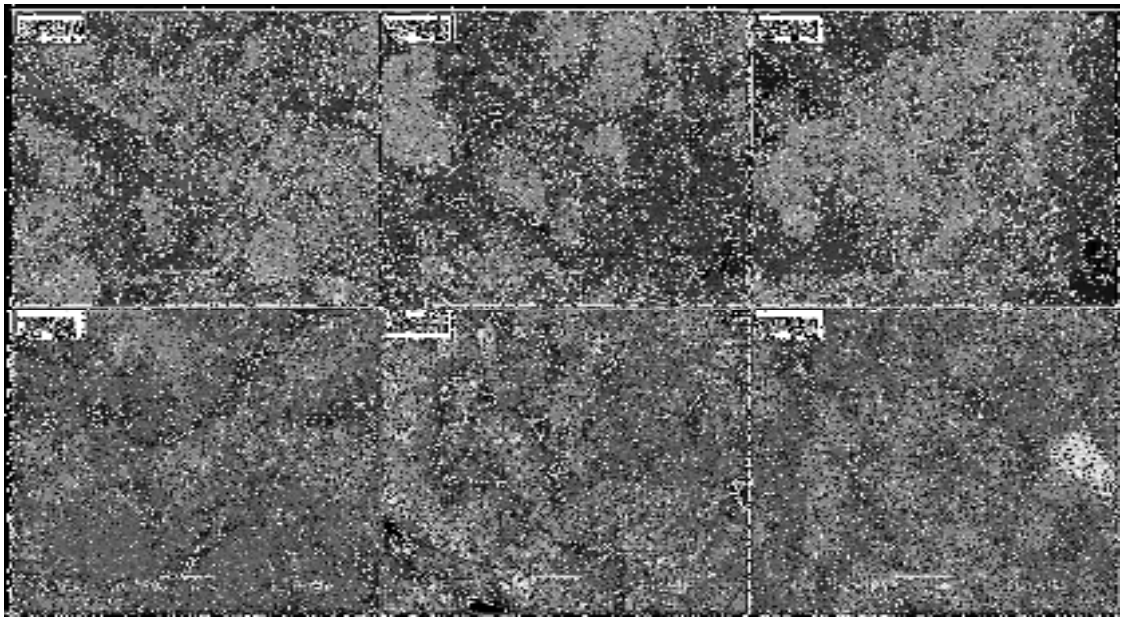

Figure. 2.4: SEM images of $Co_{1-x}Ni_xFe_2O_4$. [2.3]

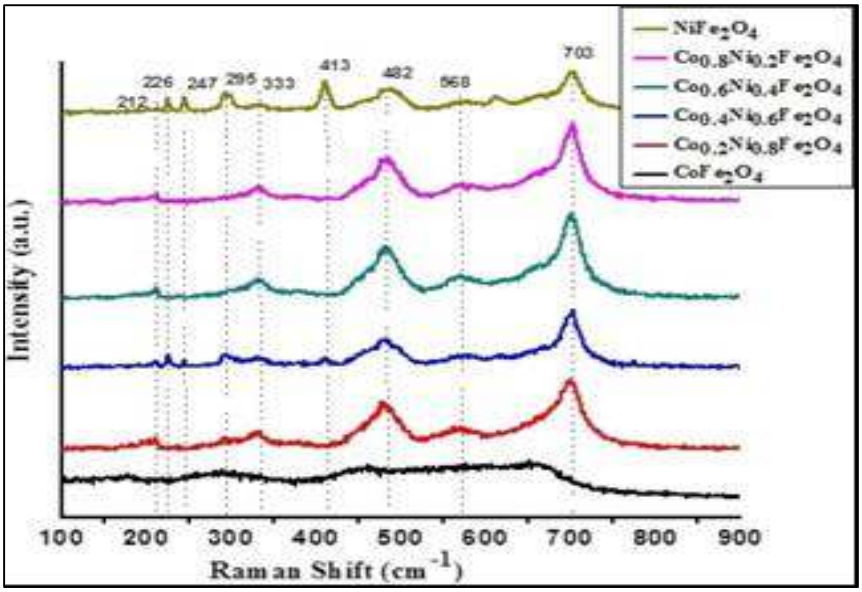

Figure 2.5.: Micro-Raman spectrum of $Co_{1-x}Ni_xFe_2O_4$. [2.3]

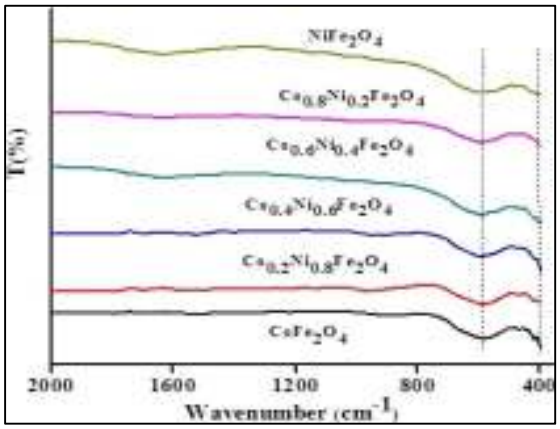

Figure 2.6.: FT-IR Spectrum of $Co_{1-x}Ni_xFe_2O_4$ [2.3]

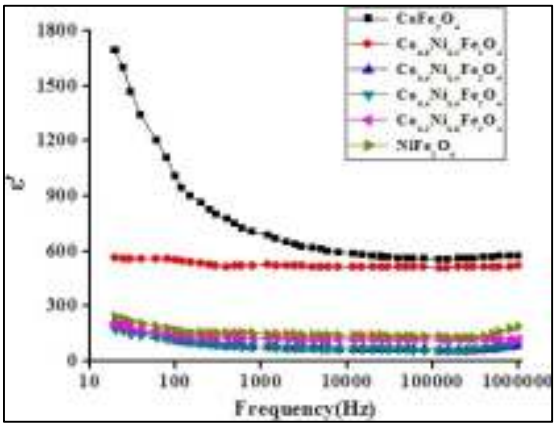

Figure 2.7: Variation of loss tangent with frequency of $Co_{1-x}Ni_xFe_2O_4$ [2.3]

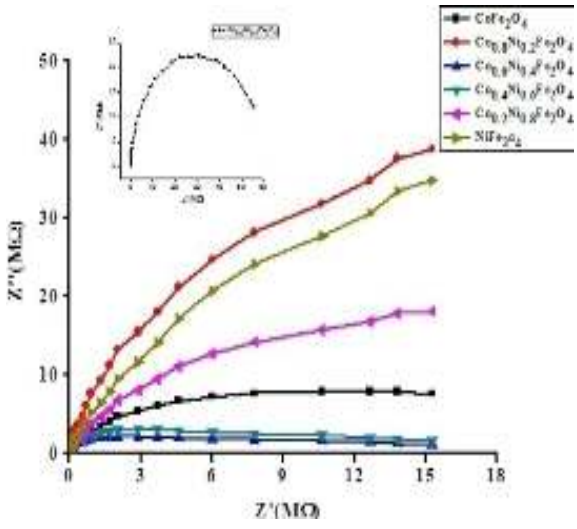

Figure 2.8: Variation of room temperature complex impedance spectra of $Co_{1-x}Ni_xFe_2O_4$ [2.3]

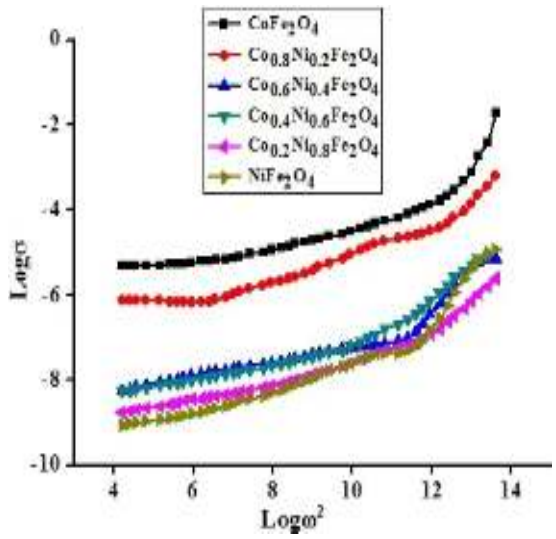

Figure 2.9: Variation of AC conductivity with respect to frequency of $Co_{1-x}Ni_xFe_2O_4$.[2.3]

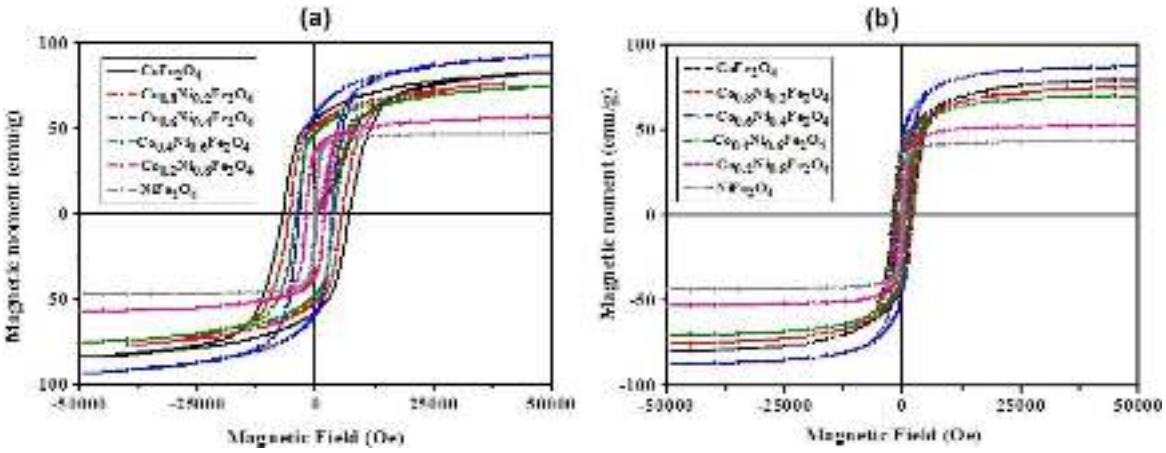

Figure 2.10: (a) M-H curve of $Co_{1-x}Ni_xFe_2O_4$ at 30K and (b) M-H curve of $Co_{1-x}Ni_xFe_2O_4$ at 300K [2.3]

Kalpanadevi *et al.* [2.4] synthesized of $Ni_{0.25}Co_{0.75}Fe_2O_4$ nanoparticles by a simple thermal decomposition method from the inorganic precursor, $Ni_{0.25}Co_{0.75}Fe_2$ $(cin)_3(N_2H_4)_5$, which was obtained by a novel precipitation method from the corresponding metal salts, cinnamic acid and hydrazine hydrate. The precursor was characterised by hydrazine and metal analyses, infrared spectral analysis and thermo gravimetric analysis. On appropriate annealing, $Ni_{0.25}Co_{0.75}Fe_2(cin)_3(N_2H_4)_5$ yielded $Ni_{0.25}Co_{0.75}Fe_2O_4$ nanoparticles, which were characterised for their size and structure using X-ray diffraction (XRD), high resolution transmission electron microscopic (HRTEM), selected area electron diffraction (SAED) and scanning electron microscopic (SEM) techniques.

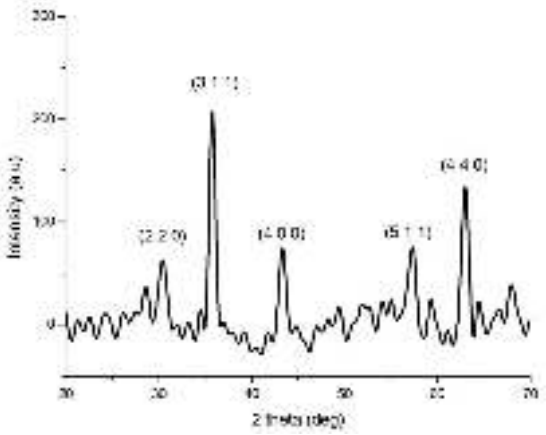

Figure 2.11: XRD pattern of $Ni_{0.25}Co_{0.75}Fe_2O_4$ nano particles [2.4]

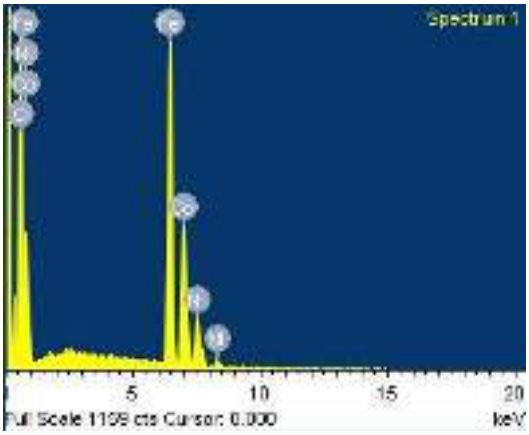

Figure 2.12: EDX spectrum of $Ni_{0.25}Co_{0.75}Fe_2O_4$ nano particles [2.4]

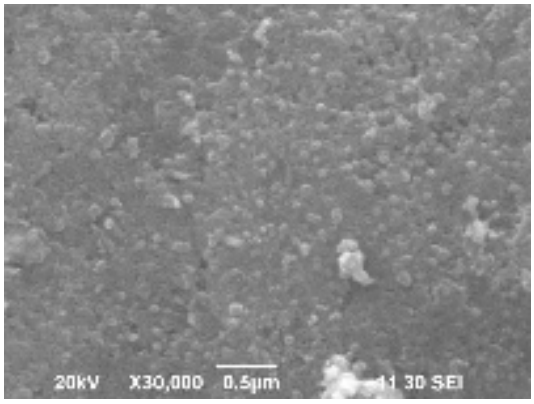

Figure 2.13: SEM image of $Ni_{0.25}Co_{0.75}Fe_2O_4$ nano particles [2.4]

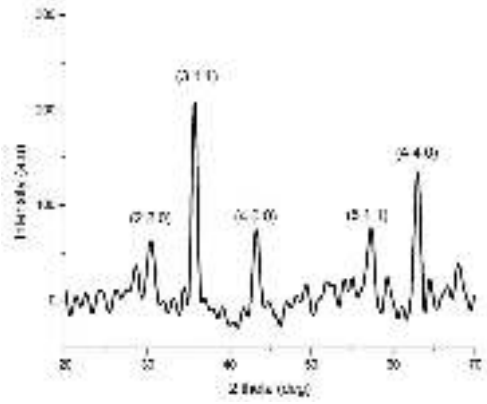

Figure 2.14: TG-DSC curve of $Ni_{0.25}Co_{0.75}Fe_2(cin)_3(N_2H_4)_5$[2.4]

Patil & Rathod [2.5] prepared $Co_x\ Ni_{1-x}\ Fe_2\ O_4$ (x= 0.5, 0.7, 0.9) nanoferrite powder using sol-gel auto combustion method at low temperature. Metal nitrates are used analytical grade, such as Nickel nitrate, Cobalt nitrate and ferric nitrate, were used as the source materials. Citric acid was used as the burning agent and the metal nitrate- to -citric acid taken as ratio 1:3. The pH of the precursor was maintained at 7. The synthesized powder was characterized by TGA/DTA .It showed that the phase formation, The FTIR spectroscopy used to deduce the structural investigation and confirmation of ferrite, The X-ray diffraction (XRD) used to determine the particle size and structural properties. The Vibrating Sample Magnetometer (VSM) used to obtain the Hysteresis parameters. The

magnetic property of the samples showed remarkable changes with change of Co $^{2+}$. The variation of Co^{2+} substitution had a significant influence on the grain size and magnetic properties. The mean crystalline size of the prepared ferrite was in the range of ~ 36 - ~45 nm.

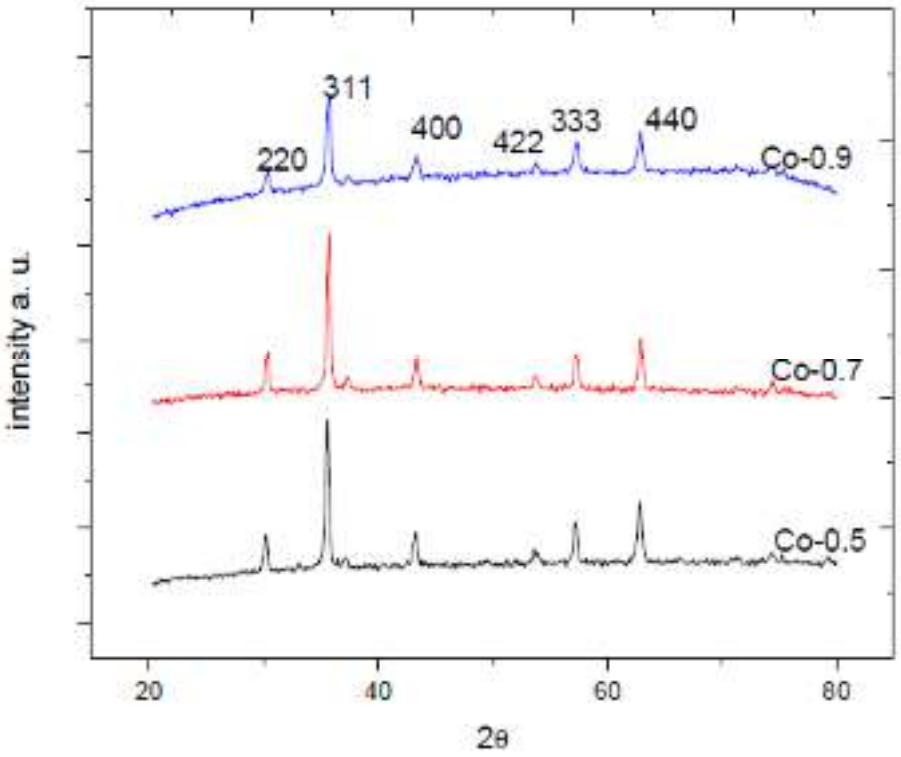

Figure 2.15: XRD graph of $Co_xNi_{1-x}Fe_2O_4$(Where x= 0.5,0.7 & 0.9) of synthesize [2.5]

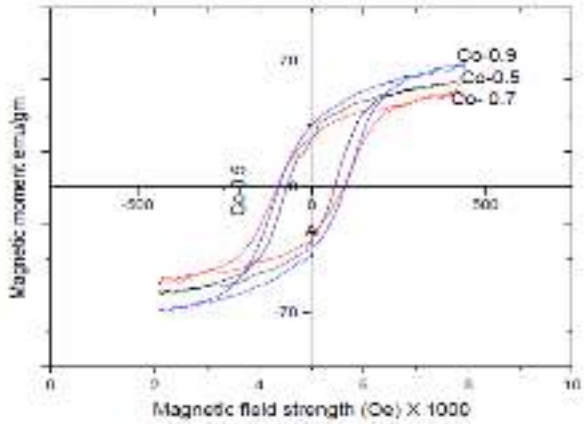

Figure 2.16:VSM (Vibration Sample Magnetometer) -Hystresses loop [2.5]

Joshi *et al.* [2.6] synthesized nano powder of $Ni_{1-x}Co_xFe_2O_4$ ferrite (where x= 0.0, 0.1, 0.2, 0.3, 0.4, 0.5) by wet chemical co-precipitation method. X-ray diffraction (XRD) confirmed single cubic spinel structure. The increase in lattice parameter was observed with increasing cobalt content. The effect of Co^{2+} ion substitution on dielectric constant ($\varepsilon^{/}$), dielectric loss (tanδ) and ac conductivity (σ_{ac}) were measured as a function of the frequency in range from 100 Hz to 1 MHz, at room temperature.The $\varepsilon^{/}$ increased with increasing Co^{2+} concentration due to the increase in the number of vacancies at the Fe site.

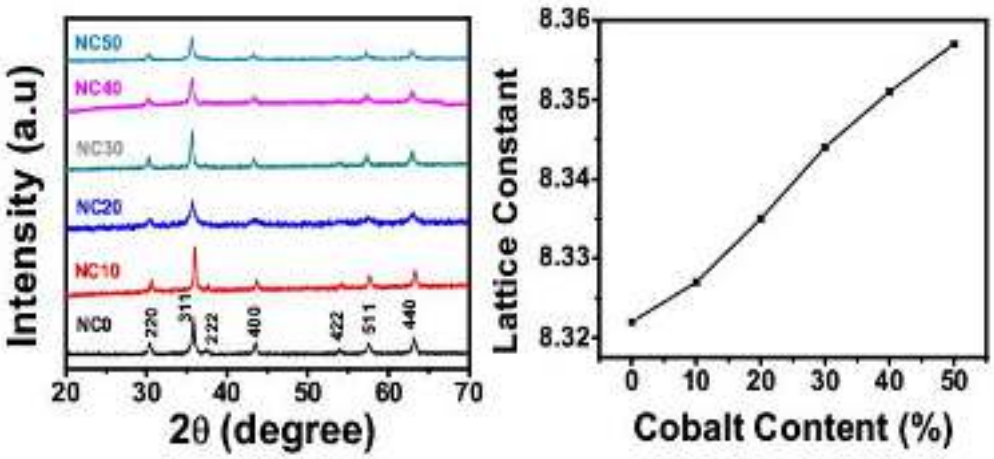

Figure 2.17: (a) XRD Patterns (b) variation of Lattice parameters with Cobalt Content for the samples X=0.0, 0.1, 0.2, 0.3, 0.4 & 0.5 of the series of $Ni_{(1-x)}Co_xFe_2O_4$[2.6]

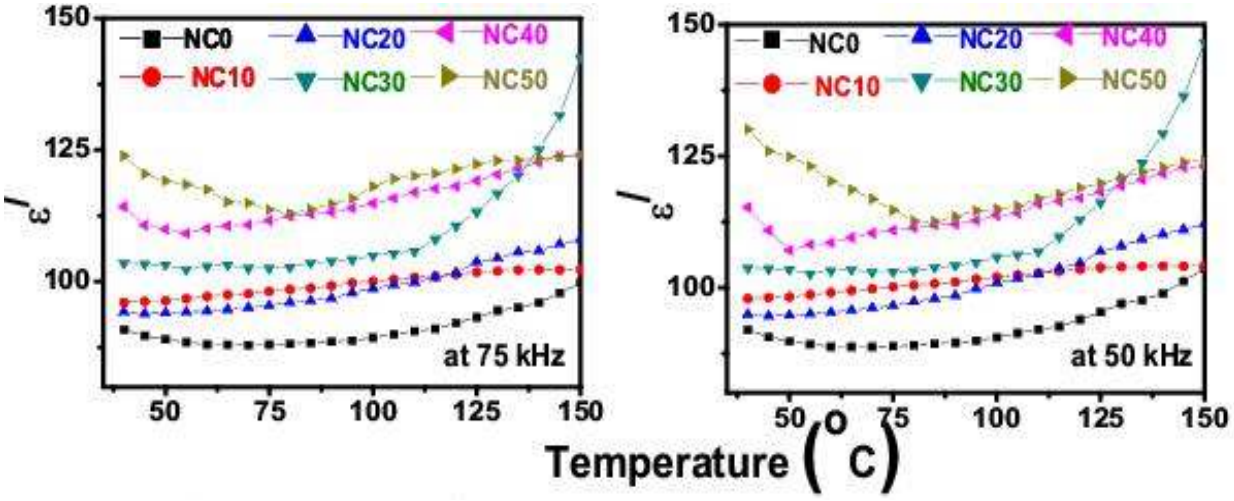

Figure 2.18: Temperature dependence of ε' at 75 kHz and 50 kHz frequencies for the samples X=0.0, 0.1, 0.2, 0.3, 0.4 & 0.5 of the series of $Ni_{(1-X)}Co_xFe_2O_4$[2.6]

Maqsood *et al.* [2.7] investigated the structural and electrical properties of Ni-Co nanoferrites prepared by Co-precipitation route. They used X-rays powder diffractometry (XRD) to characterize the synthesized materials. The obtained crystallite size variation was within 15 to 33 nm using the Scherrer formula. They also investigated electrical properties such as dc electrical resistivity was measured as a function of temperature. It is noticed that σ_{dc} increases with a rise in temperature. The dielectric measurements were carried out at room temperature as a function of frequency and composition (x). The dielectric constant (ε) and dielectric loss tangent (tan δ) showed a decreasing trend with increasing field frequency. The ac electrical conductivity is calculated from the dielectric measurements; it increases with the rise in frequency.

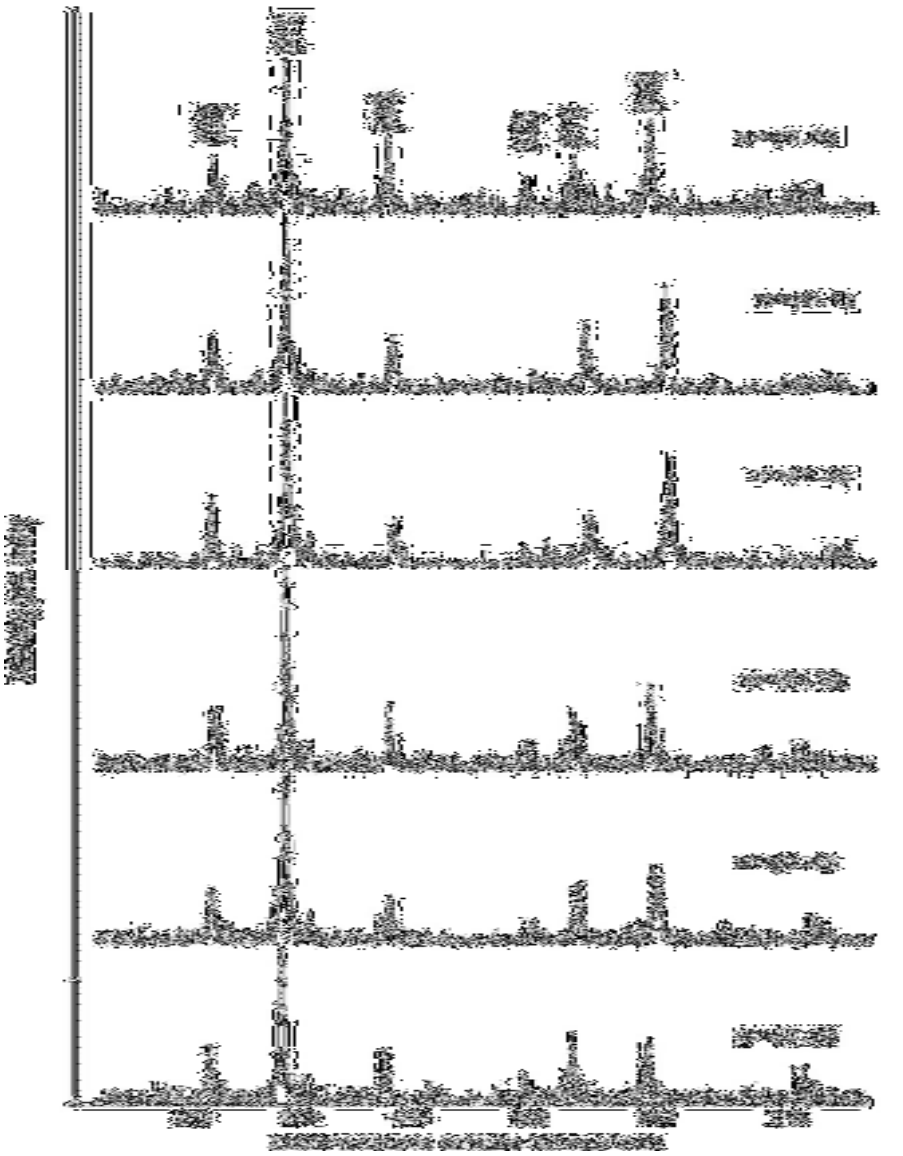

Figure 2.19: Indexed X-ray pattern of $Ni_{1-x}Co_xFe_2O_4$ [2.7]

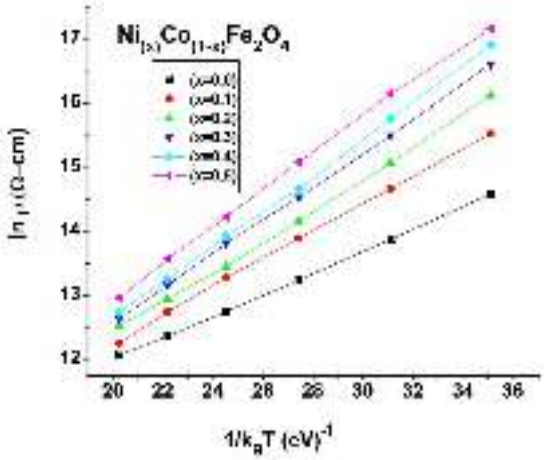

Figure 2.20: Composition variation of dc electrical resistivity *(*ln *ρ)* with 1*/ k*B*T* (eV)$^{-1}$[2.7]

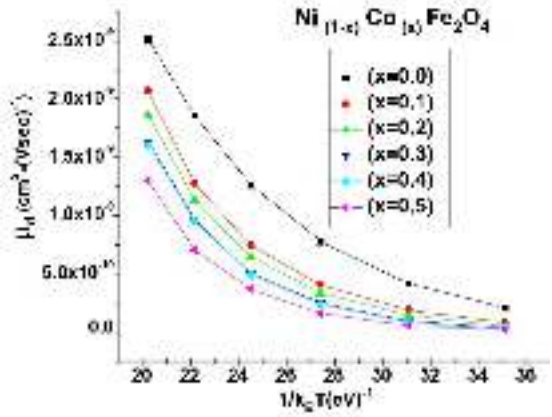

Figure 2.21: Temperature dependence of drift mobility (μ_d) in $Ni_{1-x}Co_xFe_2O_4$ nanoferrites [2.7]

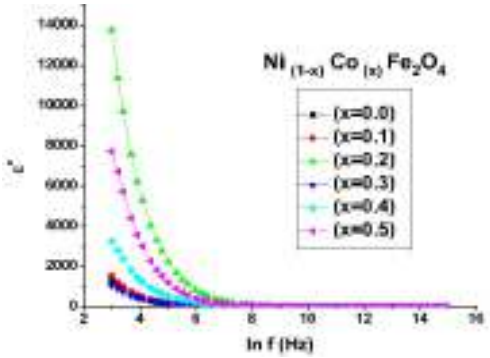

Figure 2.22: Frequency dependence of dielectric constant *(ε)* for $Ni_{1-x}Co_xFe_2O_4$ nanoferrites [2.7]

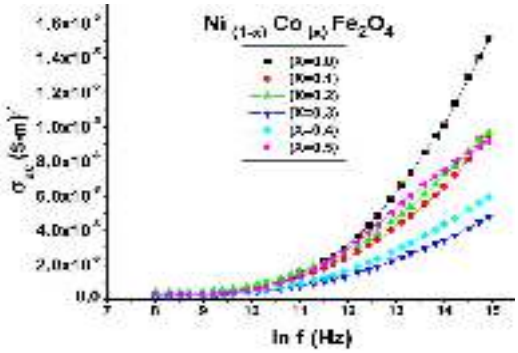

Figure 2.23: Graph of ac conductivity as a function of frequency for various concentrations of cobalt [2.7]

Kambale *et al.* [2.8] studied dielectric properties and complex impedance spectroscopy of mixed Ni–Co ferrites. They prepared samples with general formula $Ni_{(1-x)}$ Co_x Fe_2 O_4 (where x = 0.0, 0.2, 0.4, 0.6 and 0.8) by the conventional double sintering ceramic method. The microstructural features were observed by scanning electron microscopy. An infrared spectroscopy study showed the presence of absorption bands in the higher frequency range around 578 cm^{-1} *(ν_1)* and in the lower frequency range around 396 cm^{-1} *(ν_2)*; these indicate

the presence of tetrahedral and octahedral group complexes, respectively, within the spinel phase. Complex impedance measurements were carried out to understand the conduction mechanism.. The dielectric permittivity (ε) was measured at room temperature (300 K) as a function of frequency from 20 Hz to 1 MHz.

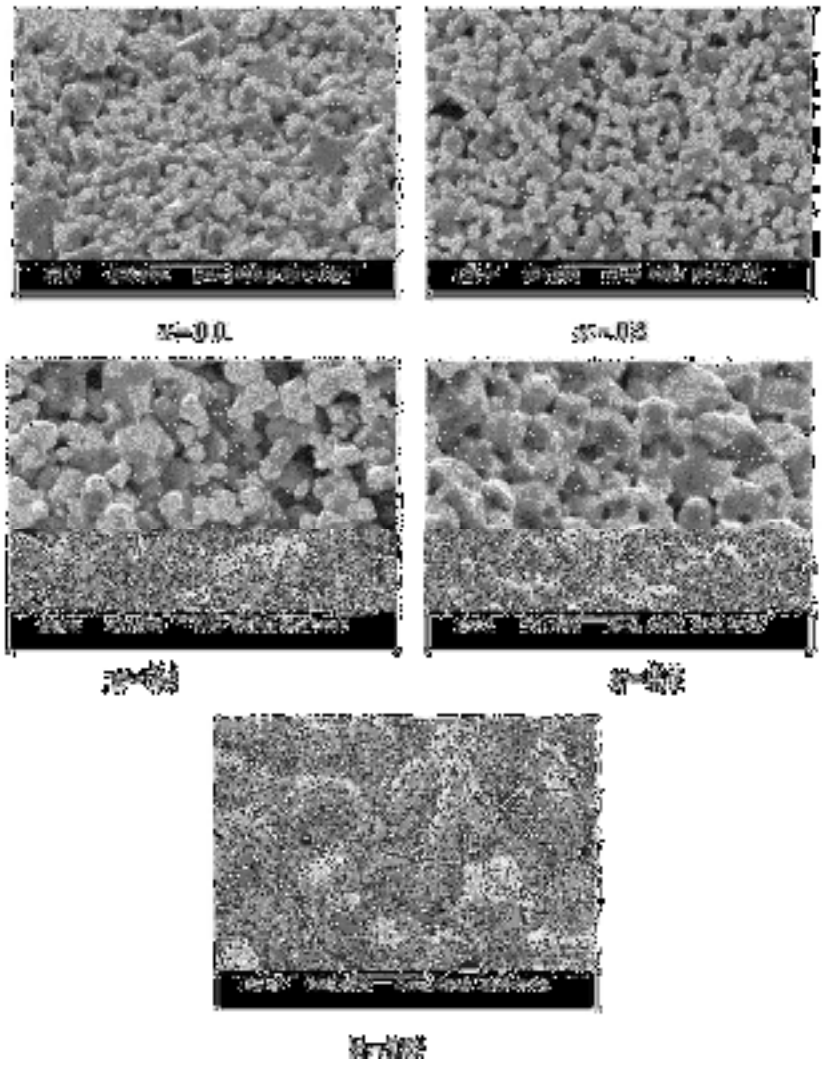

Figure 2.24: SEM micrographs for $Ni_{(1-x)}Co_x Fe_2O_4$ ferrite [2.8]

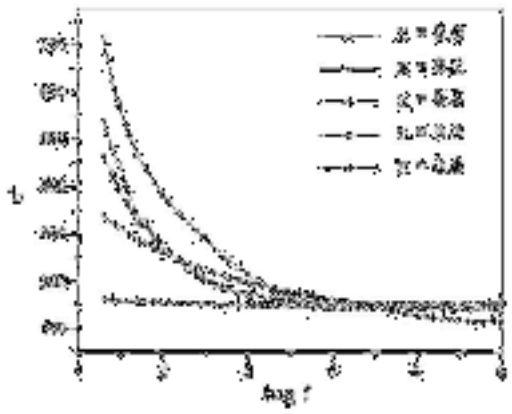

Figure 2.25: Variation of dielectric permittivity with frequency for $Ni_{(1-x)}Co_xFe_2O_4$ ferrite.[2.8]

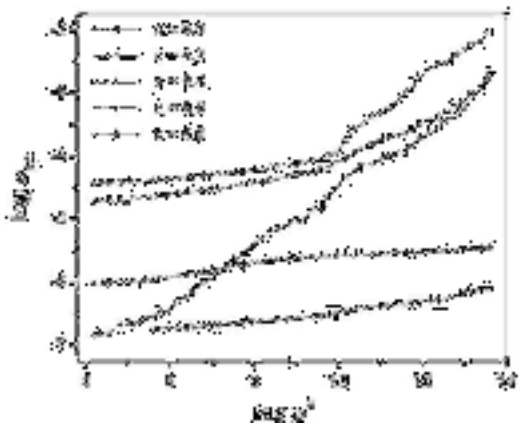

Figure 2.26: Variation of AC conductivity of $Ni_{(1-x)}Co_xFe_2O_4$ ferrite with frequency[2.8]

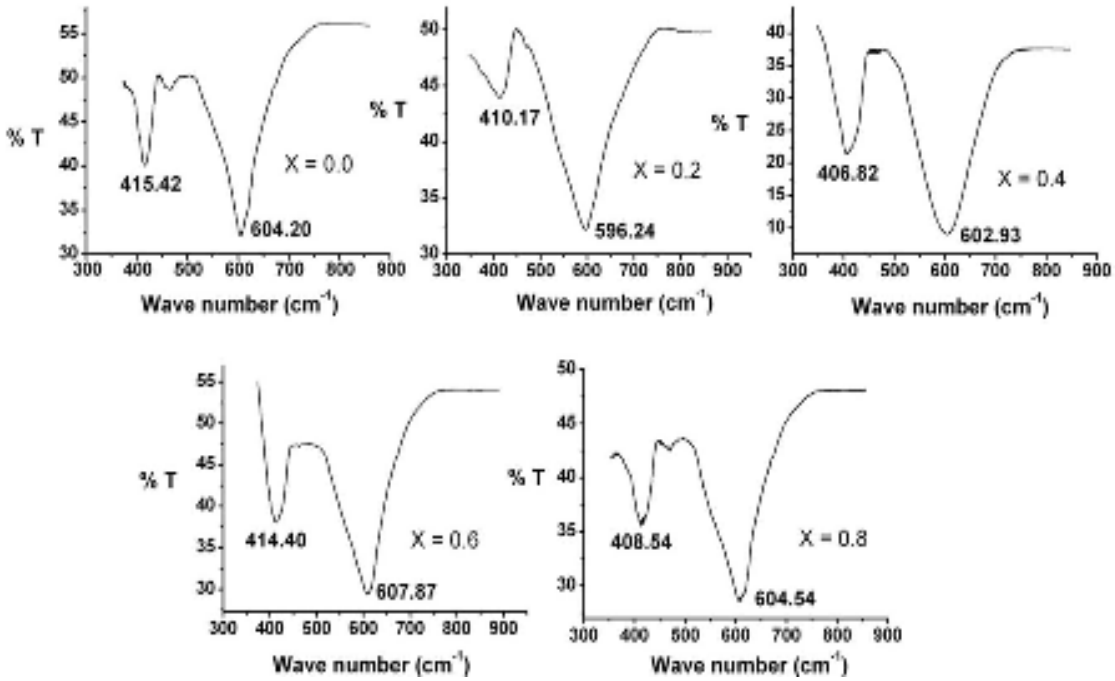

Figure 2.27: IR absorption spectra for $Ni_{(1-x)}Co_xFe_2O_4$ ferrite.[2.8]

Chapter Three

Literature Review

3.1 General aspects

3.1.1 Historical background of magnetism

Since ancient times, human beings were familiar with magnets, some properties of magnets and its uses. The history of magnetism begins with a mineral stone was found in Magnesia by the Greeks in 470 BC. These stones are called lodestones and chemically they are known as magnetite (Fe_3O_4). The first truly scientific study of magnetism was made by the Englishman William Gilbert (1540 – 1603), who published his classic book on the magnet in 1600. He experimented with lodestones and iron magnets, formed a clear picture of the Earth's magnetic field, and cleared away many superstitions that had clouded the subject. For more than a century and a half after Gilbert, no discoveries of any fundamental importance were made, although there were many practical improvements in the manufacture of magnets. Thus, in the eighteenth century, compound steel magnets were made, composed of many magnetized steel strips fastened together, which could lift 28 times their own weight of iron [3.1]. This is all the more remarkable when we realize that there was only one way of making magnets at that time: the iron or steel had to be rubbed with a lodestone, or with another magnet which in turn had been rubbed with a lodestone. In 1750, John Michell in England found that magnetic poles obey the inverse–square law. His results were confirmed by Charles Coulomb [3.2]. The first electromagnet was made in 1825, following the great discovery made in 1820 by Hans Christian Oersted that an electric current produces a magnetic field. Later on Bergmann, Becquerel, and Faraday discovered that all matter including liquids and gasses were affected by magnetism, but only a few responded to a noticeable extent. Magnets are very common items in the workplace and household. Uses of magnets range from holding pictures on the refrigerator to causing torque in electric motors. Most people are familiar with the general properties of magnets but are less familiar with the source of magnetism. The traditional concept of

magnetism centers around the magnetic field and a dipole. The term "magnetic field" simply describes a volume of space where there is a change in energy within that volume. This change in energy can be detected and measured. The location where a magnetic field can be detected exiting or entering a material is called a magnetic pole. Magnetic poles have never been detected in isolation but always occur in pairs, hence the name dipole which is defined as any two opposite poles separated by a distance l forms a magnetic dipole. A bar magnet can be considered as a dipole with north pole at one end and south pole at the other. A magnetic field can be measured leaving the dipole at north pole and returning the magnet at south pole. If a magnet is cut into two, two magnets or dipoles are created out of one. This sectioning and creation of dipoles can continue to the atomic level. Therefore, the source of magnetism lies in the basic building block (atom) of all matter. Now a day, ferrites are the most important types of magnetic materials. We are interested about it.

3.1.2 Magnetic dipole

A dipole is a pair of electric charges or magnetic poles of equal magnitude but opposite polarity, separated by a small distance. Dipoles can be characterized by their dipole moment, a vector quantity with a magnitude equal to the product of the charge or magnetic strength of one of the poles and the distance separating the two poles [Figure 3.1]. The direction of the dipole moment corresponds to the direction from the negative to the positive charge or from the south to the north pole.

Figure 3.1: Magnetic dipole of a bar

So we have two types of dipoles; one is electric dipole and another is magnetic dipole. A magnetic dipole is a closed circulation of electric current. A simple example of this is a single loop of wire with some constant current flowing through it [3.3]. Magnetic dipole experience torque in the presence of magnetic fields.

3.1.3 Magnetic field

A magnetic field (**H**) is a vector field which is created with moving charges or magnetic materials. It is also be defined as a region in which the magnetic lines of force is present. The magnetic field vector at a given point in space is specified by two properties:

(i) Its direction, which is along the orientation of a compass needle.

(ii) Its magnitude (also called strength), which is proportional to how strongly the compass needle orients along that direction.

The magnetic field inside a toroid or long solenoid is

$$H = \frac{0.4\pi nI}{l} \qquad (3.1)$$

and zero outside it. The field H is here expressed in oersted (Oe), the current I in amperes and the length in cm, n is the number of turns [3.4]. In matter, atomic circular currents may occur. Their strength is characterized by the magnetization M, which is the magnetic moment per cm^3. Then the matter provide the magnetic field is

$$H = 4\pi M \qquad (3.2)$$

The S.I. units for magnetic field strength H are Am^{-1}. The relation C.G.S and S.I. unit is $1Am^{-1} = \frac{4\pi}{10^3}$ Oe.

3.1.4 Magnetic moment

If a magnet is broken into small pieces, each part will be a magnet and we cannot get a separate north or south pole. That means, dipole moment exists in each. Each of them is called a magnetic dipole. Bar magnet, magnetic needle, current-carrying coil etc are considered as magnetic dipole. The moment associated with a magnetic dipole is called magnetic dipole moment or simply magnetic moment.

The magnetic moment or magnetic dipole moment is a measure of the strength of a magnetic source. In the simplest case of a current loop, the magnetic moment is defined as:

$$\mu_m = I \int dA \tag{3.3}$$

where A is the vector area of the current loop, and the current, I, is constant. By convention, the direction of the vector area is given by the right hand rule (moving one's right hand in the current direction around the loop, when the palm of the hand is "touching" the loop's surface, and the straight thumb indicate the direction).

In the more complicated case of a spinning charged solid, the magnetic moment can be found by the following equation:

$$\vec{\mu}_m = \frac{1}{2} \int \vec{r} \times \vec{J} d\tau \tag{3.4}$$

where, $d\tau = r^2 \sin\theta \, dr \, d\theta \, d\phi$, $\vec{J}$ is the current density.

Magnetic moment can be explained by a bar magnet which has magnetic poles of equal magnitude but opposite polarity. Each pole is the source of magnetic force which weakens with distance. Since magnetic poles come in pairs, their forces interfere with each other because while one pole pulls, the other repels. This interference is greatest when the poles are close to each other i.e. when the bar magnet is short. The magnetic force produced by a bar magnet, at a given point in space, therefore depends on two factors: on both the strength p of its poles, and on the distance d separating them. The force is proportional to the product , $\mu = Pd$, where, μ describes the "magnetic moment" or "dipole moment" of the magnet along a distance R and its direction as the angle between R and the axis of the bar magnet. Magnetism can be created by electric current in loops and coils so any current circulating in a planar loop produces a magnetic moment whose magnitude is equal to the product of the current and the area of the loop. When any charged particle is rotating, it behaves like a current loop with a magnetic moment.

The equation for magnetic moment in the current-carrying loop, carrying current I and of area vector $\vec{A}$ for which the magnitude is given by:

$$\vec{\mu}_m = I \vec{A} \tag{3.5}$$

where, $\vec{\mu}_m$ is the magnetic moment, a vector measured in Am^2, or equivalently joules per tesla, I is the current, a scalar measured in amperes, and $\vec{A}$ is the loop area vector.

3.1.5 Magnetic behavior

Every material is composed of atoms and molecules. There are protons and neutrons at the nucleus of an atom and electrons are revolving around the nucleus in different orbits. Also, electrons have rotation and spin motion are called respectively orbital motion moment and spin motion moment. Due to the resultant action of these moments different magnetic characters and properties of different materials.

Magnetic materials classified by their response to externally applied magnetic fields as diamagnetic, paramagnetic and ferromagnetic. These magnetic responses differ greatly in strength. Diamagnetism is property of all materials and opposes applied magnetic fields, but is very weak paramagnetism, when present, is stronger than diamagnetism and produces magnetization in the direction of the applied field and proportional to the applied field. Ferromagnetic effects are very large, producing magnetizations sometimes orders of magnitude greater than the applied field and as such arte much larger than either diamagnetic or paramagnetic effects. The magnetization of a material is expressed in terms of density of net magnetic dipole moments μ in the material. We define a vector quantity called the magnetization M by

$$M = \frac{\mu_{total}}{V} \quad , \tag{3.6}$$

when the total magnetic field B in the material is given by

$$B = B_0 + \mu_0 M \quad , \tag{3.7}$$

where μ_0 is the magnetic permeability of space and B_0 is the externally applied magnetic field. When magnetic fields inside of materials are calculated using Ampere's law or the Biot- Savart law, then the μ_0 in those equations is typically replaced by just μ with the definition

$$\mu = \mu_r \mu_0 \quad , \tag{3.8}$$

where μ_r is called the relative permeability. If the material does not respond to the external magnetic field by producing any magnetization then $\mu_r = 1$. Another commonly used magnetic quantity is the magnetic susceptibility

$$\chi = \mu_r - 1 \tag{3.9}$$

For paramagnetic and diamagnetic materials the relative permeability is very close to 1 and the magnetic susceptibility very close to zero. For ferromagnetic materials, these quantities may be very large. Another way to deal with the magnetic fields which arise from magnetization of materials is to introduce a quantity called magnetic field strength H. It can be defined by the relationship

$$H = \frac{B_0}{\mu_0} = \frac{B}{H_0} - M \tag{3.10}$$

and has the value of unambiguously designating the driving magnetic influence from external currents in a material independent of the materials magnetic response. The relationship for B above can be written in the equivalent form

$$B = \mu_0 (H + M) \tag{3.11}$$

H and M will have the same units, amperes/meter

The magnetic susceptibility (χ) is defined as the ratio of magnetization to magnetic field

$$\chi = \frac{M}{H} \tag{3.12}$$

The permeability and susceptibility of a material is correlated with respect to each other by

$$\mu = \mu_0 (1 + \chi) \tag{3.13}$$

3.1.6 Magnetic Domain

A magnetic domain is an atom or group of atoms within a material that have some kind of uniform electron motion. A fundamental property of any charged particle is that when it is in motion, it creates a magnetic field around its path of travel. Electrons are negatively charged particles, and they create electromagnetic fields about themselves as they move. We know that electrons orbit atomic nuclei, and they create magnetic fields while doing so. If we take one or more atoms or groups of atoms and align them so that they have some

kind of uniform electron motion, an overall magnetic field will be present in this region of the material. The individual magnetic fields of some electrons will be added together. The uniform motion of the electrons about atoms in this area creates a magnetic domain [Figure 3.2]. In regular iron, these magnetic domains are randomly arranged. But if we align a large enough group of these magnetic domains, we shall have created a magnet.

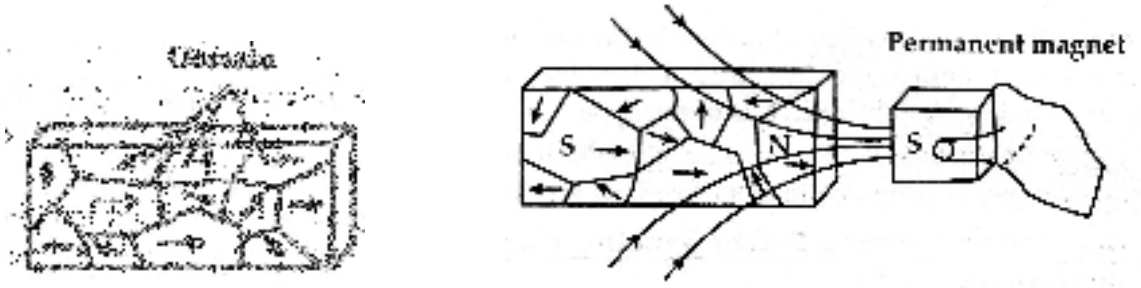

Figure 3.2: Magnetic Domain

In 1907 Weiss proposed that a magnetic material consists of physically distinct regions called domains and each of which was magnetically saturated in different directions (the magnetic moments are oriented in a fixed direction) as shown schematically in figure 3.5. Even each domain is fully magnetized but the material as a whole may have zero magnetization. The external applied field aligns the domains, so there is net moment. At low fields this alignment occurs through the growth of some domains at the cost of less favorably oriented ones and the intensity of the magnetization increases rapidly. Growth of domains stops as the saturation region is approached and rotation of unfavorably aligned domain occurs. Domain rotation requires more energy than domain growth. In a ferromagnetic domain, there is parallel alignment of the atomic moments. In a ferrite domain, the net moments of the antiferromagnetic interactions are spontaneously oriented parallel to each other. Domains typically contain from 10^{12} to 10^{15} atoms and are separated by domain boundaries or walls called Bloch walls [Figure 3.3].

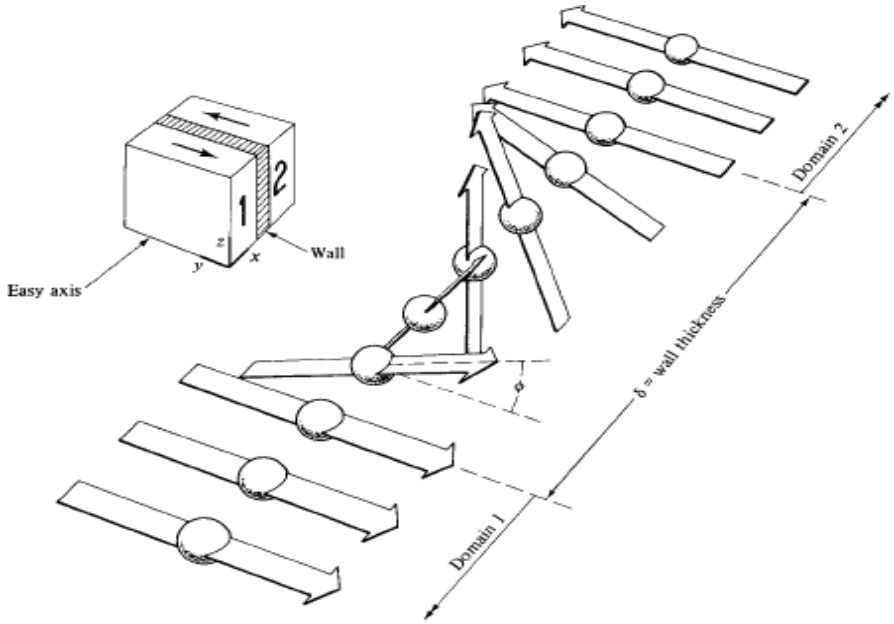

Figure 3.3: Bloch wall.

3.1.7 Domain wall motion

In magnetism, a domain wall is an interface separating magnetic domains. It is a transition between different magnetic moments and usually undergoes an angular displacement of 90° or 180°. Although they actually look like a very sharp change in magnetic moment orientation, when looked at in more detail there is actually a very gradual reorientation of individual moments across a finite distance [3.5]. The energy of a domain wall is simply the difference between the magnetic moments before and after the domain wall was created. This value is more often than not expressed as energy per unit wall area. The width of the domain wall varies due to the two opposing energies that create it: the magnetocrystalline anisotropy energy and the exchange energy, both of which want to be as low as possible so as to be in a more favorable energetic state. The anisotropy energy is lowest when the individual magnetic moments are aligned with the crystal lattice axes thus reducing the width of the domain wall, whereas the exchange energy is reduced when the magnetic moments are aligned parallel to each other and thus makes the wall thicker, due to the repulsion between them (where anti-parallel alignment would bring them closer working to reduce the wall thickness).

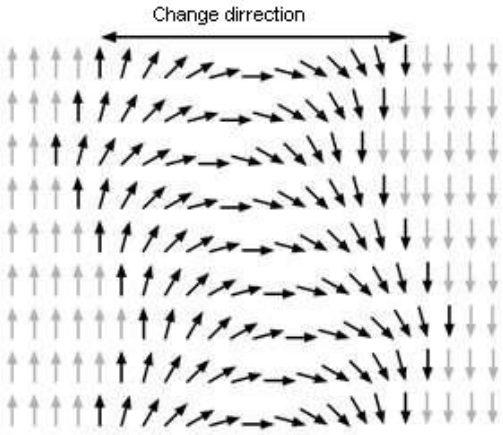

Figure 3.4: The magnetization changes from one direction to another one.

In the end equilibrium is reached between the two and the domain wall's width is set as such is shown in figure 3.4. An ideal domain wall would be fully independent of position; however, they are not ideal and so get stuck on inclusion sites within the medium, also known as crystallographic defects. These include missing or different (foreign) atoms, oxides, and insulators and even stresses within the crystal. In most bulk materials, we find the Bloch wall: the magnetization vector turns bit by bit like a screw out of the plane containing the magnetization to one side of the Bloch wall. In thin layers (oft the same material), however, Neél walls will dominate. The reason is that Bloch walls would produce stray fields, while Neél walls can contain the magnetic flux in the material [3.6].

3.1.8 Hysteresis

We know that, the value of magnetic induction or flux density B depends on the magnetic field intensity H. This is because that B is created due to H. If the value of magnetic field intensity H is changed in cyclic order an unusual behavior is observed which is shown in figure 3.5. Scientist J. A. Euwong invented this phenomenon after many experiments. This graph of H versus B is called B-H graph or hysteresis loop. A piece of ferromagnetic substance can be magnetized by placing it in a solenoid and passing current through it. If we increase the value of current gradually, the magnetic field intensity H also increases. As a result, the magnetic induction B produced in the specimen also increases.

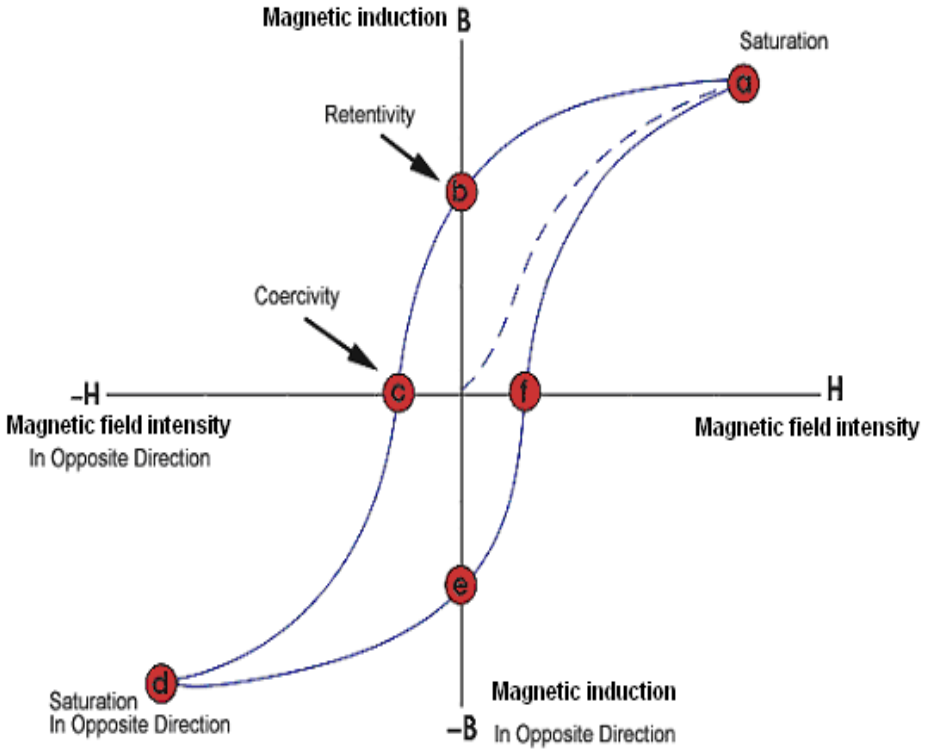

Figure 3.5: Hysteresis loop.

The ferromagnetic material that has never been previously magnetized or has been thoroughly demagnetized will follow the dashed line as H is increased. As the line demonstrates, the greater the amount of current applied, the stronger the magnetic field in the component . At point "a" almost all of the magnetic domains are aligned and an additional increase in the magnetic field intensity will produce very little increase in magnetic induction. The material has reached the point of magnetic saturation. When H is reduced to zero, the curve will move from point "a" to point "b." At this point, it can be seen that some magnetic induction remains in the material even though the magnetic field intensity H is zero. This is referred to as the point of retentivity on the graph and indicates the remanence or level of residual magnetism in the material. As the magnetic field intensity is reversed, the curve moves to point "c", where the flux has been reduced to zero. This is called the point of coercivity on the curve. The force required to remove the

residual magnetism from the material is called the coercive force or coercivity of the material.

As the magnetic field intensity H is increased in the negative direction, the material will again become magnetically saturated but in the opposite direction (point "d"). Reducing H to zero brings the curve to point "e." It will have a level of residual magnetism equal to that achieved in the other direction. Increasing H back in the positive direction will return B to zero. Notice that the curve did not return to the origin of the graph because some force is required to remove the residual magnetism. The curve will take a different path from point "f" back to the saturation point where it with complete the loop.

3.1.9 Magnetic anisotropy

Magnetic anisotropy is the direction dependence of material's magnetic properties. In the absence of an applied field, a magnetically isotropic material has no preferential direction for its magnetic moment while a magnetically anisotropic material will align with one of the easy axis. An easy axis is an energetically favorable direction of spontaneous magnetization that is determined by the sources of magnetic anisotropy. In some magnetic materials the domain magnetization tends to align in a particular crystal direction. The material is easiest to magnetize to saturation or demagnetize from saturation if the field is applied along an easy axis. The energy difference between aligning the domain in the easy and another direction (hard direction) is called magnetocrystalline anisotropy energy. Anisotropy energy is the energy needed to rotate the moment from the easy direction to a hard direction. For materials with cubic crystalline structure (such as ferrites), the energy is expressed in terms of anisotropy constants and the direction to which the magnetization rotates.

It has been found experimentally that the crystal anisotropy can be described by the first two or three terms of an infinite power series in the direction cosines of the magnetization vector with respect to the crystal axis (easy axis) [3.7]. For hexagonal crystals the anisotropy energy is a function of only one parameter, that is the angle between the magnetization and easy axis. So for hexagonal structure,

$$E_k = -k_1 \cos^2 \theta + k_2 \cos^4 \theta. \quad (3.14)$$

For cubic crystals we have,

$$E_k = k_1(\alpha_1^2\alpha_2^2 + \alpha_2^2\alpha_3^2 + \alpha_3^2\alpha_1^2) + k_2(\alpha_1^2\alpha_2^2\alpha_3^2 + \ldots \quad \ldots) \quad (3.15)$$

where, k is the anisotropy constant, θ is the angle between the easy axis and the direction of magnetization, and α's are the direction cosines, which are the ratios of the individual components of the magnetization projected on each axis divided by the magnitude of the magnetization. A crystal is higher in anisotropy energy when the magnetization points in the hard direction rather than along the easy direction. The formation of domains permits the magnetization to point along the easy axis, resulting in a decrease in the net anisotropy energy.

3.1.10 Saturation magnetization

The saturation magnetization M_S is a measure of the maximum amount of field that can be generated by a material. It will depend on the strength of the dipole moments on the atoms that make up the material and how densely they are packed together. The atomic dipole moment will be affected by the nature of the atom and the overall electronic structure. The packing density of the atomic moments will be determined by the crystal structure (i.e. the spacing of the moments) and the presence of any non-magnetic elements within the structure. At finite temperatures, for ferromagnetic materials, M_S will depend on how well these moments are aligned, as thermal vibration of the atoms causes misalignment of the moments and a reduction in M_S. For ferromagnetic materials, all moments are aligned parallel even at zero Kelvin and hence M_S will depend on the relative alignment of the moments as well as the temperature.

3.2 Ferrites

There are two basic types of magnetic materials; one is metallic and another is metallic oxides or ceramics. These metallic oxides are called ferrites. Ferrites are chemical compounds with the formula AB_2O_4, where A and B represent various metal cations; usually including iron [3.8]. Ferrites are a class of spinels i.e. materials that adopt a crystal motif consisting of cubic closed pack oxides with A cations occupying 1/8th of the

octahedral voids and B cations occupying half of the octahedral voids. For inverse spinel structure, half the B cations occupy tetrahedral sites and both the A and B cations occupy the octahedral sites. Divalent, trivalent and quadrivalent cations can occupy the A and B sites and they include Mg, Zn, Fe, Mn, Al, Cr, Ti and Si. At high frequencies ferrites are considered superior to other magnetic materials because they have low eddy current losses and high DC electrical resistivity. The DC electrical resistivity of ferrites at room temperature can very depending upon the chemical composition between about 10^{-2} Ω-cm and higher than 10^{11} Ω-cm. They are considered superior to other magnetic materials because they have low eddy current losses and high electrical resistivity.

Ferrites are classified into two categories based on their coercive field strength. They are:

(i) Soft ferrites

(ii) Hard ferrites.

3.2.1 Soft ferrites

Soft Ferrites are those that can be easily magnetized or demagnetized. This shows that soft magnetic materials have low coercive field and high magnetization that is required in many applications. The hysteresis loop for a soft ferrite should be thin and long, therefore the energy loss is very low in soft magnetic material. Examples are nickel, iron, cobalt, manganese etc. The magnetically soft ferrites first came into commercial production in 1948. Additionally, part of the family of soft ferrite are the microwave ferrites e.g.Ytrium iron garnet .These ferrite are used in the frequency range from 100 MHz to 500 GHz. For waveguides for electromagnetic radiation and in microwave device such as phase shifters. They are used in transformer cores, inductors, recording heads and microwave devices [3.9].

Soft ferrites have certain advantages over other electromagnetic materials including high resistivity and low eddy current losses over wide frequency ranges. They have high permeability and are stable over a wide temperature range. These advantages make soft ferrites paramount over all other magnetic materials.

3.2.2 Hard ferrites

Hard ferrites are difficult to magnetize or demagnetize. They are used as permanent magnets. A hard magnetic material has high coercive field and a wide hysteresis loop. Examples are alnico, rare earth metal alloys etc. The development of permanent magnets began in 1950s with the introduction of hard ferrites. These materials are ferrimagnetic and have quite a low remanence (~400mT). The coercivity of these magnets (> 125Oe), however, is far in excess of other materials. The magnets can also be used to moderate demagnetizing fields and hence can be used for applications such as permanent magnet motors. The hexagonal ferrite structure is found in both $BaO.6Fe_2O_3$ and $SrO.6Fe_2O_3$, but Sr ferrites have superior magnetic properties. Hard ferrite likes Ba-ferrite, Sr-ferrite, Pb ferrite are used in communication device operating with high frequency currents because of their high resistivity, negligible eddy currents and lower loss of energy due to Joule heating and hysteresis. These are found useful in many applications including fractional horse-power motors, automobiles, audio and video recorders, earphones, computer peripherals, clocks etc.

According to the crystallographic structures ferrites can be classified into three different types [3.10].

(i) Spinel ferrites (Cubic ferrites)

(ii) Hexagonal Ferrites

(iii) Garnets.

Our research work is on spinel ferrites; therefore we shall discuss in detail the spinel ferrites only.

3.2.3 Spinel ferrites

Cubic ferrite with spinel structure is the most widely used family of ferrites. High values of electrical resistivity and low eddy current losses make them ideal for their use at microwave frequencies. The spinel structure of ferrites as possessed by mineral spinel $MgAl_2O_4$ was first determined by Bragg [3.11]. The chemical composition of a spinel ferrite can be written in general as $MO.Fe_2O_3$ where M is a divalent cation such as Mn^{2+},

Ni^{2+}, Mg^{2+}, Zn^{2+}, Cd^{2+}, Cu^{2+}, Co^{2+} etc. A combination of these ions is also possible and it can be named as solid solution of two ferrites or mixed spinel ferrites. Generally, M represents a combination of ions which has an average valence of two. The trivalent iron ion in $MO.Fe_2O_3$ can partially be replaced by another trivalent ion such as Al^{3+} or Cr^{3+}, giving rise to mixed crystals.

3.2.4 Structure of unit cell of spinel ferrites

This ferrite is also called ferrospinels because they crystallize in the same crystal structure as the mineral spinel and they derive their general formula $MeFe_2O_4$. In this formula Me represents a divalent ion of metal. Spinel ferrites crystallize in the FCC structure. The lattice is composed of a close-packed oxygen arrangement in which 32 oxygen ions form the unit cell (the smallest repeating unit in the crystal network). These anions are packed in a face centered cubic (FCC) arrangement leaving two kinds of spaces between anions: tetrahedral sites (A), surrounded by four nearest oxygen atoms, and octahedral sites (B), surrounded by six nearest neighbor oxygen atoms. Figure 3.6 shows the unit cell of spinel structure. There are two groups of four cubes (octants). The ionic positions are different in two octants sharing a face or a corner and the same in two octants sharing an edge. Thus, to give a complete picture, it is necessary only to show the positions of the ions in two adjacent octants. Note that each octants contains, in the center a metal ion (small green sphere) surrounded by the tetrahedral of oxygen ions, this ion is said to occupy an A site. The right hand octant shows four metal ions (small red spheres) each surrounded by an octahedral (one of which is shown) formed by six oxygen ions. Such ions are said to occupy B sites. In a unit cell, there are 64 of A sites, 8 of which are occupied, and 32 of B sites, 16 of which are occupied. The divalent metal ions commonly used in ferrites can be classified roughly into those preferring B sites Co, Fe, Ni and those preferring A sites Mn and Zn. In the normal spinel structure the 8 divalent metal ions go into the A sites and the 16 trivalent iron ions have preference for B sites, they will displace eight of the trivalent iron ions which with go over into the A sites. This results in an inverted spinal. As two ionic species are then distributed over the octahedral sites a certain number of randomness may be present, contributing to the line width (loss) of the materials. These are however,

limiting cases [3.12].

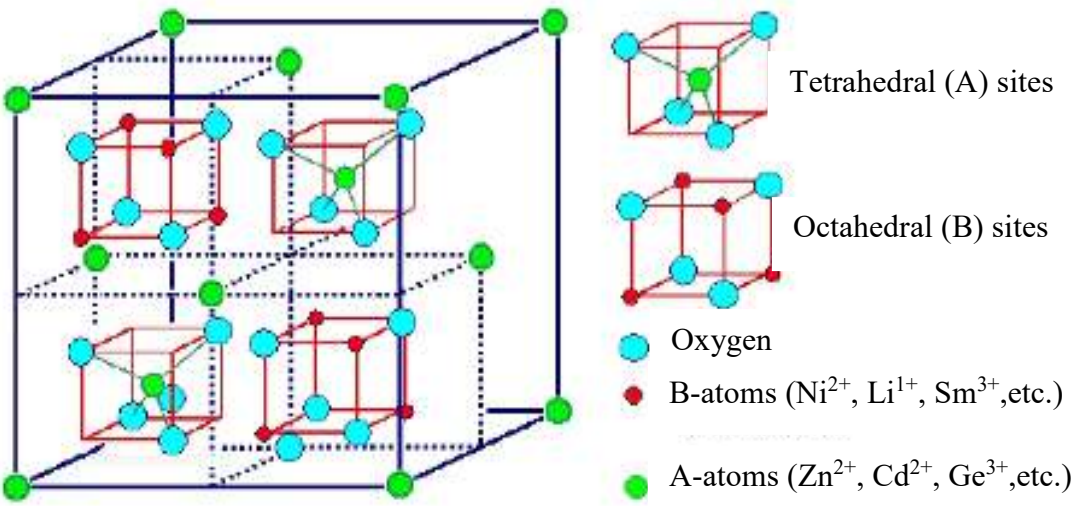

AB_2O_4: spinel structure.

Figure 3.6: Schematic of two sublattice of a unit cell of the spinel structure, showing octahedral and tetrahedral sites.

3.2.5 Cation distribution in ferrites

The cation distribution in the spinel $Me^{2+}Me_2^{3+}O_4$ can be as follows [3.13]. The spinel ferrites have been classified into three categories due to the distribution of cations on tetrahedral (A) and octahedral (B) sites. These are

(1) Normal spinel ferrites

(2) Inverse spinel ferrites

(3) Mixed or random spinel ferrites.

(¡). Normal spinel ferrites : The divalent cation (Me^{2+}) are in tetrahedral A-sites and two trivalent (Fe^{3+}) cations are in octahedral B- site which is represented as $(Me^{2+})_A[Fe^{3+}Fe^{3+}]_BO_4$. A typical example of normal spinel ferrite is bulk $ZnFe_2O_4$.

(¡¡). Inverse spinel ferrites : In this case divalent (Me^{2+}) cations are in octahedral B-sites and the trivalent (Fe^{3+}) cations are equally divided between A and B sites (the divalent and trivalent ions normally occupy the B sites in a random fashion i.e. they are disordered)

arrangement is as $(Fe^{3+})_A[Me^{2+}Fe^{3+}]_BO_4$. Iron, cobalt and Nickel ferrites have the inverse structure, and they are all ferromagnetic.

(¡¡¡). Mixed or random spinel ferrites: The arrangement of the from $(Fe^{3+}{}_{1-x}Me^{2+}{}_x)_A[Fe^{3+}{}_{1+x}Me^{2+}{}_{1-x}]_BO^{2-}{}_4$ is often referred as mixed spinel, where cations in the parentheses are at (A) sites and those in the brackets are at [B] sites and x is called the inversion parameter. The extreme case x = 1 corresponds to the normal spinel structure, and x = 0 corresponds to the inverse structure $0 < x < 1$ for intermediate used commercially are mixed ferrites. Typical example of mixed spinel ferrites are $MgFe_2O_4$ and $MnFe_2O_4$ [3.14].

The factor affecting the cation distribution over A and B sites are as follows :

- The size of the cations
- The electronic configuration of cations
- The electronic energy
- The saturation magnetization of the lattice

Smaller cations (trivalent ions) prefer to occupy the A-sites. The cations have special preference for A and B sites and the preference depends on the following factors:

- Ionic radius
- Size of interstices
- Temperature
- Orbital preference for the specific coordination.

The preference of cations is according to Verway- Heilmar scheme [2.15, 2.16]

- Ions with strong preference for A-sites Zn^{2+}, Cd^{2+}, Ga^{2+}, In^{3+}, Ge^{4+}.
- Ions with strong preference for B-sites Ni^{2+}, Cr^{3+}, Ti^{4+}, Sn^{4+},Sm^{3+}, Gd^{3+}.
- Indifferent ions are Mg^{2+}, Al^{3+}, Fe^{2+}, Co^{2+}, Mn^{2+}, Fe^{3+}, Cu^{2+}.

Moreover the electrostatic energy also affects the cation distribution in the spinel lattice.

3.2.6 Exchange interaction

The difference of energy of two electrons in a system with anti-parallel and parallel and parallel spins is called the exchange energy. The electron spin of the two atoms S_i and S_j, which is proportional to their product .The exchange energy can be written as universally in terms of Heisenberg Hemiltonian [3.17].

$$E_{ex} = -\sum J_{ij} S_i.S_j = -\sum J_{ij} S_i S_j \cos\varphi, \qquad (3.16)$$

where J_{ij} is the exchange integral represents the strength of the coupling between the spin angular momentum i and j and φ is the angle between the spins. It is well known that the favored situation is the one with the lowest energy and it turns out that there are two ways in which the wave functions can combine there are two possibilities for lowering the energy by E_{ex}. These are:

(i) If J_{ij} is positive and the parallel spin configuration ($\cos\varphi = 1$) the energy is minimum,

(ii) If J_{ij} is negative and the spins are antiparallel ($\cos\varphi = -1$) energy is maximum. This situation leads to antiferromagnetism.

3.3 Various kinds of magnetism

In most atoms, electrons occur in pairs. Electrons in a pair, spin in opposite directions. When electrons are paired together, their opposite spins cause their magnetic fields to cancel each other. Therefore, no net magnetic field exists. Alternately, materials with some unpaired electrons will have a net magnetic field and will react more to an external field. The magnetic behavior of materials can be classified into the following major groups:

- Diamagnetism
- Paramagnetism
- Ferromagnetism, Antiferromagnetism and ferrimagnetisms are considered as subclasses of ferromagnetism.

3.3.1 Diamagnetism

Diamagnetic substances consist of atoms or molecules with no net angular momentum. When an external magnetic field is applied, there creates a circulating atomic current that

produces a very small bulk magnetization opposing the applied field [3.18]. Diamagnetism is exhibited by all common materials but so feeble that it is covered if material also exhibits paramagnetism or ferromagnetism. When a material is placed in a magnetic field, electrons in the atomic orbital tend to oppose the external magnetic field by moving the induced magnetic moment in a direction opposite to the external magnetic field. Due to this fact, the material is very weakly repelled in the magnetic field. This is known as diamagnetism. The induced dipole moments disappear when the external field is removed. The diamagnetic effect in a material can be observed only if the paramagnetic effect or the ferromagnetic effect does not hide the weak diamagnetic effect. In Figure 3.7 magnetic moment of two electrons A and B are shown. When a external field **H**=0 those two moments cancel each other in figure 3.7(a); but as magnetic field is applied magnetic moment does not disappear; a net magnetic moment results a shown in figure 3.7(b). The direction of this net moment is opposite to the applied magnetic field **H.**

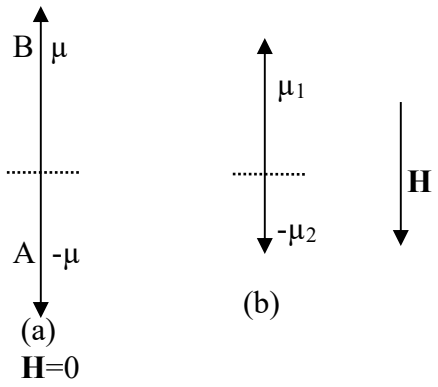

Figure 3.7: Diamagnetism

Due to this fact, a diamagnetic material is weakly repelled in the magnetic field. When the field is removed, its magnetization becomes zero. Examples of some diamagnetic materials are gold, silver, mercury, copper and zinc [3.19].

3.3.2 Paramagnetism

Paramagnetism is a form of magnetism, which occurs only in the presence of an externally applied magnetic field [3.20]. Paramagnetic materials are attracted to magnetic fields; hence have a relative magnetic permeability greater than one, while the positive magnetic

susceptibility. However, unlike ferromagnets, which are also attracted to magnetic fields, paramagnets do not retain any magnetization in the absence of an externally applied magnetic field. Constituent atoms of paramagnetic materials have permanent magnetic dipoles moments, even in the absence of an applied field. This generally occurs due to the presence of unpaired electrons in the atomic orbital. In pure paramagnetism, the dipoles are randomly oriented in the absence of an external field and do not interact with one another, resulting in zero net magnetic moment [Figure 3.8 (a), (b)].

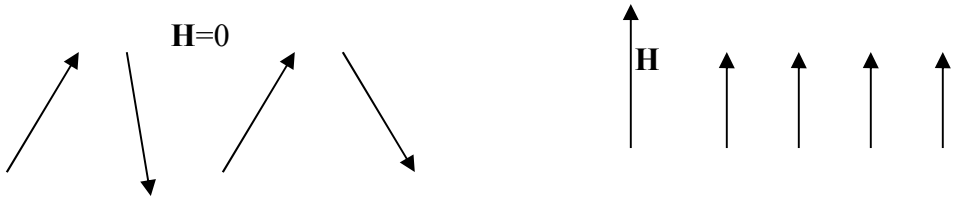

(a) : Randomly oriented magnetic dipoles (b) : Regularly aligned magnetic dipoles

Figure 3.8: Paramagnetism

When a magnetic field is applied, the dipole gets aligned along the applied field. In the classical description, this alignment can be understood to occur due to a torque being provided on the magnetic moments by an applied field, which tries to align the dipoles parallel to the applied field. However, the truer origins of the alignment can only be understood via the quantum-mechanical properties of spin and angular momentum. If there is sufficient exchange energy between neighboring dipoles, they will interact and spontaneously aligned parallel or anti-parallel, forming the magnetic domains, resulting in ferromagnetism or anti-ferromagnetism respectively. Paramagnetic behaviour can also be observed in ferromagnetic materials only above their Curie temperature, and in anti-ferromagnetic above their Neel temperature.

The magnetic moment can be oriented along an applied field to give rise to a positive susceptibility, and the values of susceptibility are very small with the order of 10^{-5} to 10^{-3}. O_2, NO, Mn and Cr are just a few examples of the paramagnetic materials. The susceptibility of a paramagnetic material is inversely dependent on temperature, which is known as Curie law [figure 3.10(a)]

$$\chi = C/T \tag{3.17}$$

where C is the Curie constant

3.3.3 Ferromagnetism

Ferromagnetism is a phenomenon of spontaneous magnetization. It has the alignment of an appreciable fraction of molecular magnetic moments in some favorable direction in the crystal. Ferromagnetism appears only below a certain temperature, known as Curie temperature. Above Curie temperature, the moments are randomly oriented and resulting the zero net magnetization [3.21]. Ferromagnetism is only possible when atoms are arranged in a lattice and the atomic magnetic moment can interact to align parallel to each other [Figure 3.9]. A ferromagnetic material has spontaneous magnetization due to the alignment of its atomic magnetic moments even in the absence of external magnetic field.

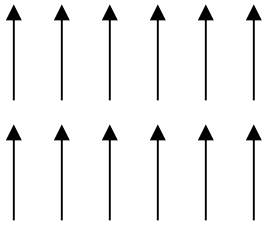

Figure 3.9: Ferromagnetism

Ferromagnetic materials generally can acquire a large magnetization even in the absence of a magnetic field, since all magnetic moments are easily aligned together. The susceptibility of a ferromagnetic material does not follow the Curie law, but displayed a modified behavior defined by Curie-Weiss law [Figure 3.10(b)].

$$\chi = \frac{C}{T - \theta} \tag{3.18}$$

Where, C is a constant and θ is called Weiss constant. For ferromagnetic materials, the Weiss constant is almost identical to the Curie temperature (T_c). At temperature below T_c, the magnetic moments are ordered whereas above T_c material losses magnetic ordering and show paramagnetic character. The elements Fe, Ni, and Co and many of their alloys are typical ferromagnetic materials.

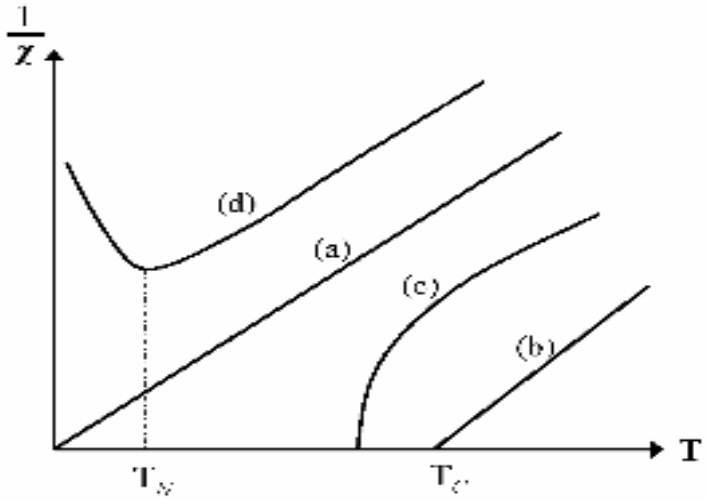

Figure 3.10: The inverse susceptibility varies with temperature T for (a) paramagnetic, (b) ferromagnetic, (c) ferrimagnetic, (d) antiferromagnetic materials. T_N and T_c are Neel temperature and Curie temperature, respectively.

Saturation magnetization is an intrinsic property independent of particle size by dependent on temperature. Even through electronic exchange forces in ferromagnets are very large thermal energy eventually overcomes the exchange energy and produces a randomizing effect. This occurs at a particular temperature called the Curie temperature (T_c). Below the Curie temperature the ferromagnetic is ordered and above it, disordered. The saturation magnetization goes to zero at the Curie temperature.

3.3.4 Antiferromagnetism

In this type of materials exchange integral strongly keeps the nearby ions into antiparallel arrangement [Figure 3.11]. In the simplest case adjacent magnetic moments are equal in magnitude and opposite therefore these is no over all magnetization. The natural state

makes it different for the material to become magnetized in the direction of the applied field but still demonstrates a relative permeability slightly greater than above a critical temperature known as the Neel temperature the material becomes paramagnetic [3.22]. The antiferromagnetic susceptibility is followed by the Curie-Weiss law with a negative θ as in the inverse susceptibility as a function of temperature is shown in figure. 3.10(d). Common examples of materials with antiferromagnetic ordering include MnF_2, FeO, CoO and NiO.

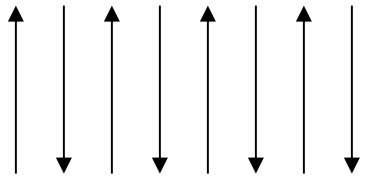

Figure 3.11: Antiferromagnetism

3.3.5 Ferrimagnetism

This type of material contains two different types of ions. Moments of the ions remain antiparallel [3.23] but since their values are not same figure 3.12. As a result a net magnetic moment remains in the absence of external magnetic field, the behavior of susceptibility of a ferrimagnrtic material also obeys Curie-Weiss law and has a negative Q as well as in figure 3.10 (c). While these materials may also demonstrate a relative permeability >1, their temperature dependence are not as consistent as with ferromagnetic materials and can result is some very unusual results. Ferrimagnetism is therefore similar to ferromagnetism. It exhibits all the hallmarks to ferromagnetic behavior like spontaneous magnetization, Curie temperature hysteresis, and remanence. However ferro and ferrimagnets have very different magnetic ordering. In ionic compounds, such as oxides, more complex forms of magnetic ordering can occur as a result of the crystal structure. The magnetic structure is composed of two magnetic sublattices (called A and B) separated by oxygens. The exchange interactions are mediated by the oxygen anions. When this happens, the interactions are called indirect or super exchange interactions.

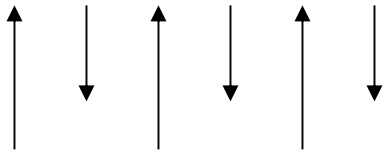

Figure 3.12: Ferrimagnetism

Ferrimagnetism is exhibited by ferrites and magnetic garnets. The oldest known magnetic substance, magnetite (Fe_3O_4), is ferrimagnetic. It was originally classified as a ferromagnetic before Neel‟s discovery of ferrimagnetisms and antiferromagnetism. Some ferrimagnetic materials are YIG (yttrium iron garnet) and ferries composed of iron oxides and other elements such as aluminum, cobalt, nickel, manganese and zinc.

Chapter Four

Experimental Method

4.1 Sample preparation

4.1.1 Compositions

In present work, we studied the structural and magnetic properties of functional magnetic materials of composition $Ni_{1-x}Co_xFe_2O_4$ (x=0, 0.2, 0.4, 0.6, 0.8, 1) prepared using $NiFe_2O_4$ (soft) and $CoFe_2O_4$ (semi-hard) nanomaterials following solid state synthesis technique [4.1]. The following compositions were fabricated, characterized and investigated thoroughly.

- NiF_3O_4 (x=0.0)
- $Ni_{0.8}Co_{0.2}Fe_3O_4$ (x=0.2)
- $Ni_{0.6}Co_{0.4}Fe_3O_4$ (x=0.4)
- $Ni_{0.4}Co_{0.6}Fe_3O_4$ (x=0.6)
- $Ni_{0.2}Co_{0.8}Fe_3O_4$ (x=0.8)
- $CoFe_3O_4$ (x=1.0)

4.1.2 Solid state reaction method

Sample preparation technique is an important part for ferrites sample. Knowledge and control of the chemical composition, homogeneity and microstructure are very crucial. The preparation of polycrystalline ferrites with optimized properties has always demanded delicate handling and cautious approach. The ferrite is not completely defined by its chemistry and crystal structure but also requires knowledge and control of parameters of its microstructure such as grain size, porosity, intra- and inter-granular distribution. There are many processing methods such as solid state reaction method [4.2]; high energy ball milling [4.3]; sol-gel [4.4]; chemical co-precipitation method [4.5]; microwave sintering method [4.6]; auto combustion method [4.7] etc for the preparation of polycrystalline

ferrite materials. The normal methods of preparation of ferrites comprise of the conventional ceramic method i.e., solid state reaction method involving milling of reactions following by sintering at elevated temperature range and non-conventional method, also called wet method. Chemical co-precipitation method and sol-gel method etc. are examples of wet method.

Our samples were synthesized by solid state reaction method. The starting materials for the preparation of the studied compositions were in the form of nano powder of ferrites ($NiFe_2O_4$ and $CoFe_2O_4$) of Inframat Advanced Materials, USA. The purity of our materials is up to 99.99%. The reagent nano powders were weighed precisely according to their molecular weight.The weight percentage of the oxide to be mixed for various samples was calculated by using formula:

$$\text{Weight \% of oxide} = \frac{M.wt.of\ oxide \times required\ \ weight\ of\ the\ sample}{Sum\ of\ Mol.wt.of\ each\ oxide\ in\ a\ sample}$$

Intimate mixing of the materials was carried out using agate mortar (hand milled) for 8 hours for fine homogeneous mixing and strong concentration. Then ball milled in a planetary ball mill in ethyl alcohol media for 24 hours with Y_2O_3-stabilized zirconia balls of different sizes in diameter. Then the mixed sample was pre-sintered at temperature at 850^0C for 4 hours at a heating rate of 3°C/min in air to form ferrite through chemical reaction. The sample was then cooled down to room temperature at a cooling rate of 5°C/min. The mixture was dried and a small amount of saturated solution of polyvinyl alcohol was added as a binder. The resulting powders were pressed uniaxially under a pressure of (15-20) $KN.cm^{-2}$ in a stainless steel die to make pellets and toroids [Figure 4.1], respectively. The pressed pellet and toroid shaped samples were then finally sintered at 1200^0C temperatures in air and then cooled in the furnace.

Figure 4.1: a. Pellets and b. Toroids shaped samples.

4.1.3 Pre-sintering

After ball milled, the mixture was dried and required again hand milled for 4 hours. Then the mixed powder was transferred in a small ceramic pot for pre-sintering at temperature at 850°C in the furnace named Muffle Furnace (Nabertherm Gmbh Bahnhofstr, 20, Lilienthal/Bremen Germany) at Glass and Ceramic Engineering Dept. of BUET. The cooling and heating rates were 3°C/min and the holding time was 4 hours [Figure 3.2(a)]. The pre-sintering is very crucial because in this step of sample preparation a ferrite is formed from its component oxides. The solid-state reactions, leading to the formation of ferrites, actually achieved by counter diffusion. This means that the diffusion involves two or more species of ions, which move in opposite direction initially across the interface of two contacting particles of different component oxides. During the pre-sintering stage, the reaction of Fe_2O_3 with metal oxide (MO or M'_2O_3 where M is divalent and M' is the trivalent metal atom) takes place in the solid state to form spinel according to the reactions [4.8]:

$MO + Fe_2O_3 \rightarrow MO.Fe_2O_3$ (spinel)

$2M'_2O_3 + 4Fe_2O_3 \rightarrow 4M'Fe_2O_4$ (spinel) + O_2

For Ni-Co ferrite,

$$Ni_{(1-x)}Fe_2O_4+Co_xFe_2O_4 \rightarrow (Fe^{3+})\,[Ni_{(1-x)}^{2+}.C0_x^{2+}.Fe^{3+}]O_4^{2-}$$

For example,

When, x=0.0,then :$NiFe_2O_4 \rightarrow (Fe^{3+})\,[Ni^{2+}.Fe^{3+}]O_4^{2-}$

When,x=0.2,then :$Ni_{(1-0.2)}Fe_2O_4+Co_{0.2}Fe_2O_4 \rightarrow (Fe^{3+})\,[Ni_{(1-.02)}^{2+}.C0_{0.2}^{2+}.Fe^{3+}]O_4^{2-}$ or

$Ni_{0.8}Fe_2O_4+Co_{0.2}Fe_2O_4 \rightarrow (Fe^{3+})\,[Ni_{0.8}^{2+}.C0_{0.2}^{2+}.Fe^{3+}]O_4^{2-}$

When,x=1.0,then :$CoFe_2O_4 \rightarrow (Fe^{3+})\,[Co^{2+}.Fe^{3+}]O_4^{2-}$

Now in order to produce chemically homogeneous, dense and magnetically better material of desired shape and size, sintering at an elevated temperature is needed.

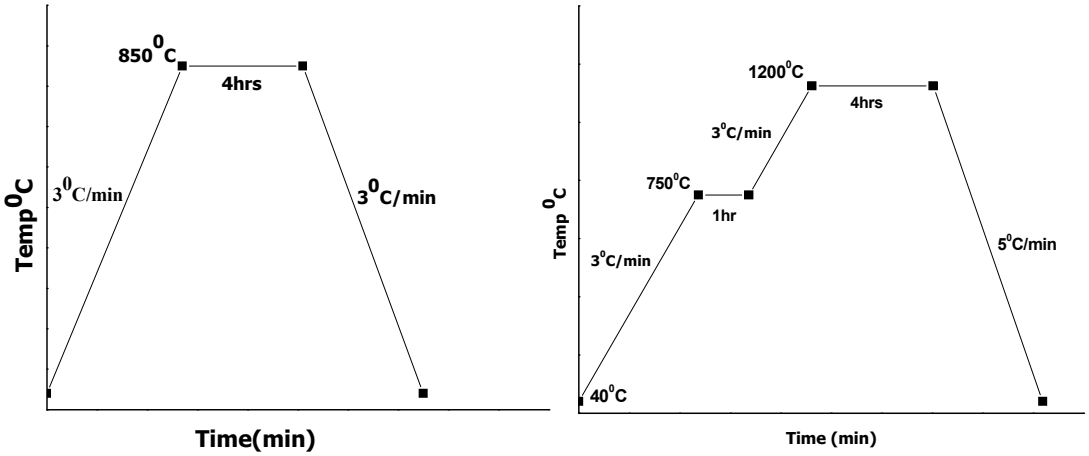

a. Pre- sintering program b.Sintering program

Figure 4.2: Pre- sintering and sintering cycle of $Ni_{1-x}Co_xFe_2O_4$

4.1.4 Sintering

Sintering is a widely used but very complex phenomenon. The fundamental quantification of change in pore fraction and geometry during sintering can be attempted by several techniques, such as: dilatometry, buoyancy, gas absorption, porosimitry indirect methods (e.g. hardness) and quantitative microscopy etc. The description of the sintering process has been derived from model experiments (e.g. sintering of a few spheres) and by observing powdered compact behavior at elevated temperatures.

Sintering is the final and a very critical step of preparing a ferrite with optimized properties. The sintering time, temperature and the furnace atmosphere play very important role on the magnetic property of final materials. Sintering commonly refers to processes involved in the heat treatment by which a mass of compacted powder is transformed into a highly densified object by heating it in a furnace below its melting point. Ceramic processing is based on the sintering of powder compacts rather than melting/ solidifications/cold working (characteristic for metal), because:

- Ceramics melt at high temperatures
- As solidified microstructures cannot be modified through additional plastic deformation and re-crystallization due to brittleness of ceramics

- The resulting course grains would act as fracture initiation sites
- Low thermal conductivities of ceramics (< 30 - 50 W/mK) in contract to high thermal conductivity of metals (in the range 50 - 300 W/mK) cause large temperature gradients, and thus thermal stress and shock in melting-solidification of ceramics.

For our samples, these are sintered at temperature between 1100^0C to 1250°C in the furnace named Muffle Furnace (Nabertherm Gmbh Bahnhofstr, 20, Lilienthal/Bremen Germany) at Glass and Ceramic Engineering Dept. of BUET. The heating rates was 3°C/min and cooling rates was 5^0C and holding period 1 hour at 750^0C [Figure 3.2(b)]. Sintering is the bonding together of a porous aggregate of particles at high temperature. The thermodynamic driving force is the reduction in the specific surface area of the particles. The sintering mechanism usually involves atomic transport over particle surfaces, along grain boundaries and through the particle interiors. Any un-reacted oxides form ferrite, inter diffusion occurs between adjacent particles so that they adhere (sinter) together, and porosity is reduced by the diffusion of vacancies to the surface of the part. Strict control of the furnace temperature and atmosphere is very important because these variables have marked effects on the magnetic properties of the product. Sintering may result in densification, depending on the predominant diffusion pathway. It is used in the fabrication of metal and ceramic components, the agglomeration of ore fines for further metallurgical processing and occurs during the formation of sandstones and glaciers. Sintering must fulfill three requirements:

- to bond the particles together so as to impart sufficient strength to the product
- to densify the grain compacts by eliminating the pores and
- to complete the reactions left unfinished in the pre-sintering step [4.8]

The theory of heat treatment is based on the principle that when a material has been heated above a certain temperature, it undergoes a structural adjustment or stabilization when cooled at room temperature. The cooling rate plays an important role on which the structural modification is mainly based.

4.1.5 Flowchart of sample preparation

The sample preparation process can be easily presented by the following flowchart:

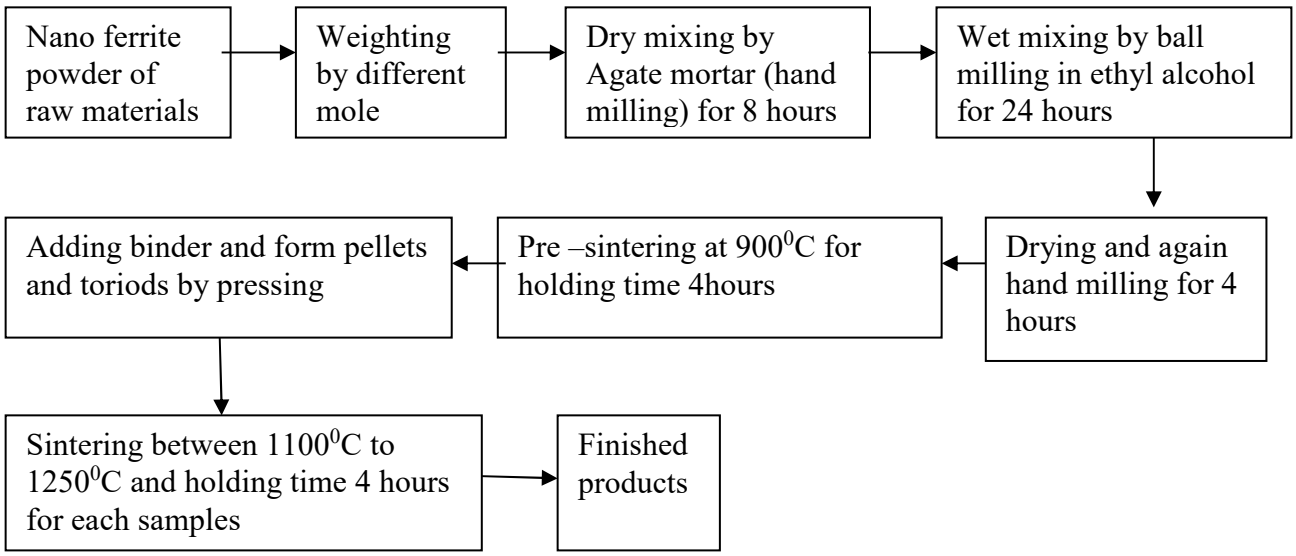

Figure 4.3: Flow-chart of ferrite sample

4.2 X-ray diffraction (XRD) Analysis

Crystal structure of $Ni_{1-x}Co_xFe_2O_4$ (x=0, 0.2, 0.4, 0.6, 0.8, 1) sintered at 1200^{0}C were examined by XRD in powder form. X-ray diffraction analysis was conducted using the XRD facility available at AECD *Phillips X'Pert Pro* & BCSIR *Brucker D8 Advance*, Dhaka in order to determine the phases present in the samples. We also calculated lattice parameter, X-ray density, Bulk density and Porosity of $Ni_{1-x}Co_xFe_2O_4$ (x=0, 0.2, 0.4, 0.6, 0.8, 1) sintered at 1200^{0}C.

4.3 Microstructure analysis by using FE-SEM

The SEM analysis was conducted using the FE-SEM (JEOL JSM-7600F) facility available at GCE, BUET. Since the sintered samples were meant to be observed under FE-SEM which is a very powerful tool, no further sample preparation was needed for the analysis. The FE-SEM is such a strong tool that it is capable of revealing the grains and the boundaries among them without the help of any etching given that a proper sintering cycle is operated.

4.4 Magnetic properties analysis

In the present study magnetic properties such as the temperature dependence of initial permeability at constant frequency (100 KHz) for toroid shaped samples of $Ni_{1-x}Co_xFe_2O_4$ (x=0, 0.2, 0.4, 0.6, 0.8, 1) sintered at 1200^0C was conducted by using a Impedance analyzer, facility available at BCSIR, Dhaka. From this analysis we determined the Curie temperature of $Ni_{1-x}Co_xFe_2O_4$ (x=0, 0.2, 0.4, 0.6, 0.8, 1) sintered at 1200^0C. We also analysis frequency dependence of the real part of the permeability of $Ni_{1-x}Co_xFe_2O_4$ (x=0, 0.2, 0.4, 0.6, 0.8, 1) sintered at 1100^0C, 11250C, 11500^0C, 1175^0C, 1200^0C & 1250^0C at frequency level 10KHz to 100000KHz by using same Impedance analyzer. By using a Vibrating Sample Magnetometer (Model-VSM-02, Hirstlab, UK) we studied saturation magnetization (M_s), retentivity (M_r), coercivity (H_c) 80K, 200K and 300K temperature of the investigated compositions $Ni_{(1-x)}Co_xFe_2O_4$ sintered at 1200^0C.

4.5 Thermal properties analysis

The TG-DSC analysis for the solid precursor of $Ni_{1-x}Co_xFe_2O_4$(where x=0,0.2,0.4,0.6,0.8 and 1.0) sintered at 1200^0C recorder under N_2 atmosphere with a heating rate 10^0 C min was conducted using the NETZSCH DSC Instrument (STA 449 F1 Jupiter) facility available at GCE, BUET. The Differential Scanning Calorimetry (DSC) analysis showed tetragonal to Cubic phase change for the solid samples of $Ni_{1-x}Co_xFe_2O_4$(where x=0,0.2,0.4,0.6,0.8 and 1.0) and compared the result with the curie temperature measured by Impedance analyzer. TG curves showed that no weight loss during TG-DSC analysis.

The TG experiment was conducted 25^0C to 600^{o}C. By the TG analysis we confirmed about the purity of the sintered samples

The Particle size distribution analysis was conducted using the NanoSight NS300 series available at Atomic Energy Centre. Particle size analysis was used to characterize the size distribution of particles in investigated compositions $Ni_{(1-x)}Co_xFe_2O_4$ sintered at 1200^0.

4.6 Dielectric property measurement

Dielectric property measurement for $Ni_{1-x}Co_xFe_2O_4$ (x=0, 0.2, 0.4, 0.6, 0.8, 1) sintered at 1200^0C as a function of frequency in the range 1KHz-15MHz at room temperature were carried out by using Wayne Kerr 6500B series Impedance Analyzer in the Department of Glass and Ceramic Engineering, Bangladesh University of Engineering and Technology (BUET). For this purpose silver paint was applied on both sides of the pellets to make good ohmic contacts with conducting wires. The real part of dielectric constant was calculated using the formula

$$\varepsilon' = \frac{cd}{\varepsilon_o A}, \qquad (3.1)$$

where c is the capacitance of the pellet in Farad, d the thickens of the pellet in meter , A the cross-sectional area of the flat surface of the pellet in m^2 and ε_o the constant of permittivity for free space. Where, $\varepsilon_o = 8.85\times10^{-12}Fm^{-1}$

Chapter Five

Results and Discussion

5.1 Structural Characterization

5.1.1 XRD pattern

The structural analysis of Ni(1-x)CoxFe2O4 (x = 0.0, 0.2, 0.4, 0.6, 0.8 &1.0) samples was done by powder X-ray diffraction technique, recorded at room temperature with CuKα radiation of wavelength λ = 1.54178 A^0 using a Philips X'Pert PRO X-ray diffractometer. The X-ray diffraction (XRD) patterns for series of samples $Ni_{1-x}Co_xFe_2O_4$(x = 0.0, 0.2, 0.4, 0.6, 0.8 &1.0) sintered at 1200^0 for 4h are shown in Figure 4.1

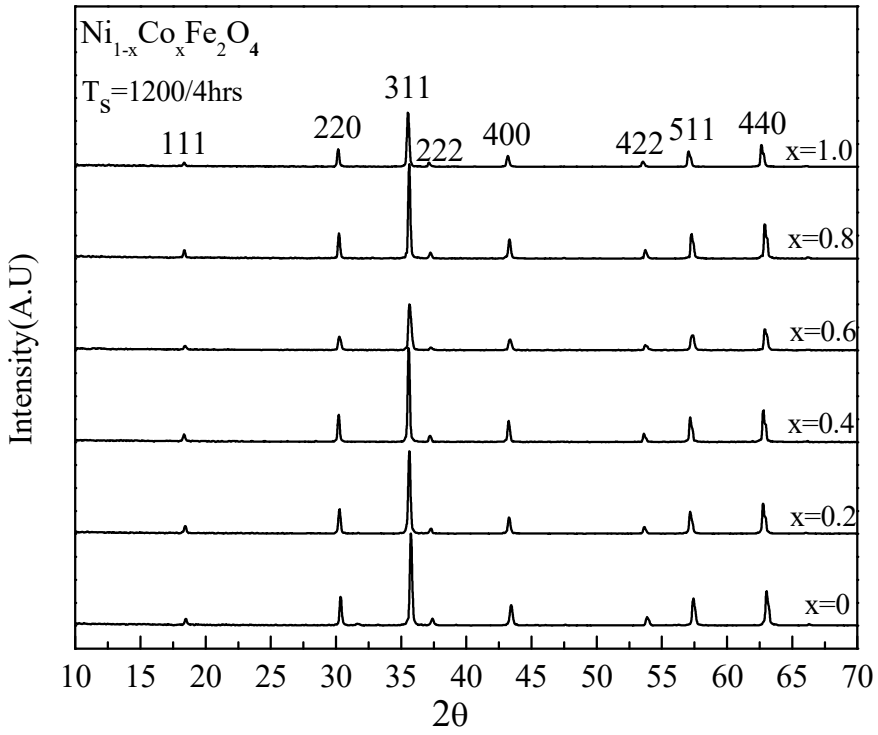

Figure 5.1: XRD pattern of $Ni_{(1-x)}Co_xFe_2O_4$ (x = 0.0, 0.2, 0.4, 0.6, 0.8 &1.0), sintering temperature 1200^0C

All the observed reflection lines were indexed as a single fcc structure corresponding to spinel phase. There are no extra peaks indicating purity of the samples synthesized. It is also noted that the peaks were broad, signifying ultra fine nature and small crystallite size of particles. Analyzing the XRD patterns, it is noted that the position of the peaks comply with the reported value [4.11]. The (hkl) values corresponding to the diffraction peaks of different planes (111), (220), (331), (222), (400), (422), (511) and (440) which represents either odd or even indicating the samples are spinel cubic phase. The peak intensity of spinel ferrites depends on the concentration of magnetic ions in the lattice. From the figure 4.1 also observed that the peaks are found to shift slightly towards the lower d-spacing values which indicate that the lattice parameters are increasing with the increase of Co content. The reflections also demonstrate the homogeneity of the studied samples. Therefore single phase spinel structure is confirmed for all the samples with increasing trend of the lattice parameter as the Co content is increased. The diffraction pattern from the sample $NiFe_2O_4$ and $CoFe_2O_4$ are shown separately in figure 4.2 and figure 4.3.Using X-ray data, it is also calculated the lattice parameter "a" and hence the X-ray density.

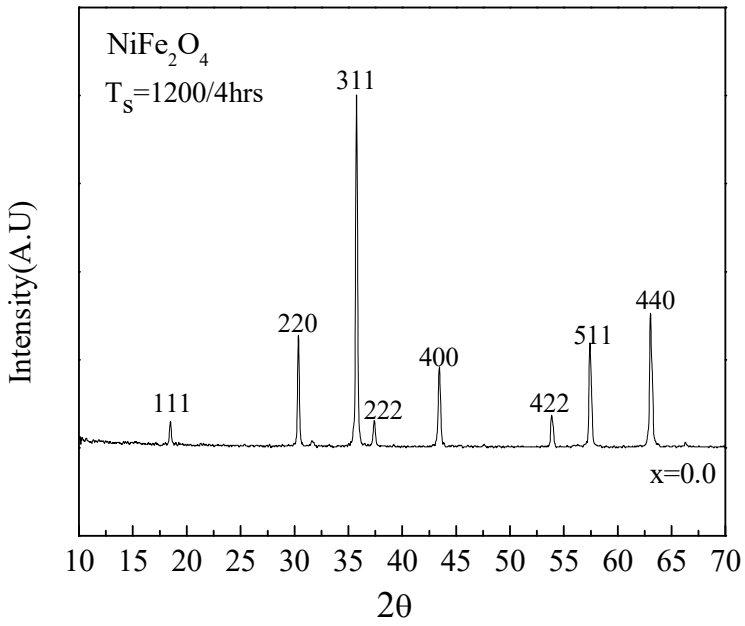

Figure 5.2 : XRD patterns of $NiFe_2O_4$, sintering temperature 1200^0C

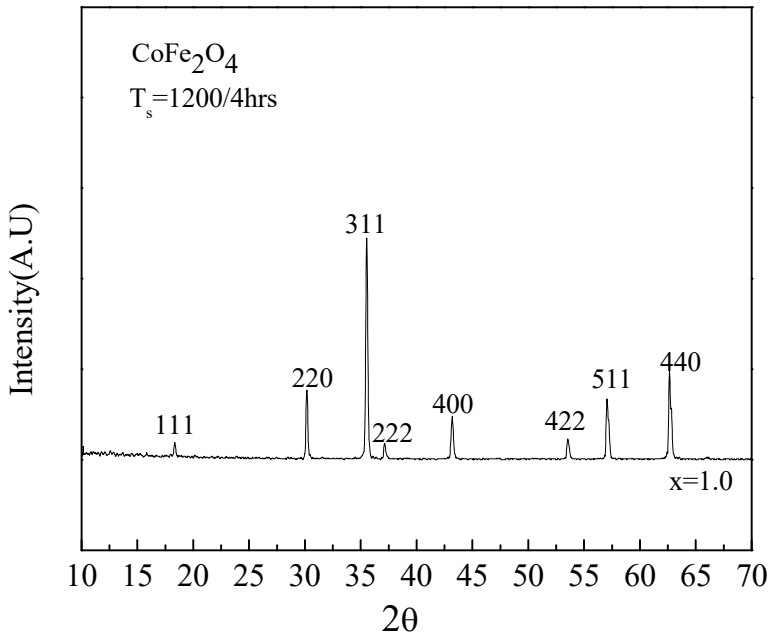

Figure 5.3: XRD patterns of $CoFe_2O_4$, sintering temperature 1200^0C

5.1.2 Lattice parameter

The lattice parameter for each peak of each sample was calculated by using the formula: a = d $\sqrt{h^2+k^2+l^2}$, where h, k and l are the Miller indices of the crystal planes. To determine the exact lattice parameter for each sample, Nelson-Riley [4.12] method was used. The Nelson-Riley function F(θ) is given as $F(\theta)=\frac{1}{2}\left[\frac{\cos^2\theta}{\sin\theta}+\frac{\cos^2\theta}{\theta}\right]$, where θ is the Bragg's angle, by extrapolating the lattice parameter values to F(θ) = 0 or θ = 90°. Variation of lattice parameter 'a' as a function of Co content x is shown in Fig.[4.4] and also shown in Table [4.2]. From Figure 4.4 it is observed that the lattice parameter increases linearly with increasing Co content obeying Vegard's law [4.2]. This enhancement of lattice parameter is attributed to Co^{2+} with larger ionic radius (0.745Å) which replaces Ni^{2+} having smaller ionic radius (0.69 Å) [4.3, 4.4]. It is well known that the distribution of cations on the octahedral B-sites and tetrahedral A-sites determines to a great extent the physical, electrical and magnetic

properties of ferrites. There exists a correlation between the ionic radius and the lattice constant, the increase of the lattice constant is proportional to the increase of the ionic radius [4.5]. Similar results for Ni-Co ferrite system have been reported by A. Maqsood *et.al* [4.3], O. M. Hemeda et.al [4.4],K. H. Maria *et.al* [4.6]. It is also found that the values for $NiFe_2O_4$ and $CoFe_2O_4$ are 8.31 Å and 8.38 Å which is values in good agreement with the reported values [4.7].

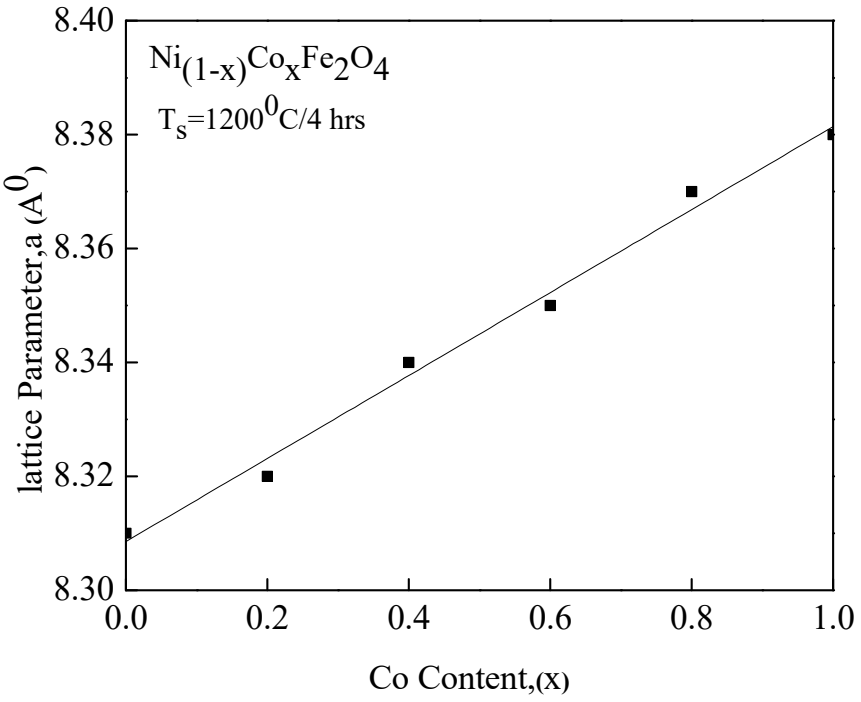

Figure 5.4 : Variation of Lattice Parameter with Co Content of $Ni_{(1-x)}Co_xFe_2O_4$ (x = 0.0, 0.2, 0.4, 0.6, 0.8 &1.0), sintering temperature 1200^0C

5.1.3 Density and Porosity

The X-ray density d_x was calculated from the molecular weight and the volume of the unit cell for each sample by using equation (3.5). The bulk density d_B was measured by usual mass and total volume by using equation (3.6). The X-ray density is higher than the apparent density value due to the existence of pores which depends on the sintering condition. The X-ray density and bulk density decrease significantly with the increasing Co content. This is because the atomic weight and density of Ni are 58.693 and 8.908 g-cm^{-3} while these values of Co are 58.933 and 8.9 g-cm^{-3} [4.8]. The percentage of porosity was calculated using the equation (3.7).It is well known that the porosity of the samples come from two sources, intra-granular porosity and inter-granular porosity. The inter-granular porosity mainly depends on the grain size [4.9]. At higher sintering temperatures the density is decreased because the intra-granular porosity is increased resulting from discontinuous grain growth.

Table [5.1]. The Chemical formula, cation distribution to A-site and B-site and theoretical calculation of lattice parameter with cobalt content in Ni(1-x)CoxFe2O4

x[a]	Chemical formulae	A-site	B-site	r_A (Å)	r_B (Å)	a_{th} (Å)
0.0	$Ni.Fe_2O_4$	(Fe^{3+})	$[Ni^{2+}\ Fe^{3+}]O_4^{2-}$	0.645	0.667	8.32
0.2	$Ni_{0.8}Co_{0.2}Fe_2O_4$	(Fe^{3+})	$[Ni_{0.8}^{2+}\ Co_{0.2}^{2+}\ Fe^{3+}]O_4^{2-}$	0.645	0.673	8.33
0.4	$Ni_{0.6}Co_{0.4}Fe_2O_4$	(Fe^{3+})	$[Ni_{0.6}^{2+}\ Co_{0.4}^{2+}\ Fe^{3+}]O_4^{2-}$	0.645	0.678	8.35
0.6	$Ni_{0.4}Co_{0.6}Fe_2O_4$	(Fe^{3+})	$[Ni_{0.4}^{2+}\ Co_{0.6}^{2+}\ Fe^{3+}]O_4^{2-}$	0.645	0.684	8.36
0.8	$Ni_{0.2}Co_{0.8}Fe_2O_4$	(Fe^{3+})	$[Ni_{0.2}^{2+}\ Co_{0.8}^{2+}\ Fe^{3+}]O_4^{2-}$	0.645	0.689	8.38
1.0	$CoFe_2O_4$	(Fe^{3+})	$[Co^{2+}\ Fe^{3+}]O_4^{2-}$	0.645	0.695	8.39

a :Cobalt (Co) content

r_A: ionic radius of A-site, r_B: ionic radius of B-site, a_{th}: theoretical lattice parameter.

Table [5.2]. Variation of lattice parameter, X-ray density, bulk-density, porosity and Curie temperature with cobalt content in $Ni_{1-x}Co_xFe_2O_4$.

x^a	a_{th} (A^0)	a_{exp} (A^0)	ρ_x (gm/cm^3)	ρ_b (gm/cm^3)	P (%)	T_c (C) Impendence Analyzer	T_c (C) DSC
0	8.32	8.31	5.42	5.02	7.38	538	556
0.2	8.33	8.32	5.40	4.41	18.33	527	538
0.4	8.35	8.34	5.36	4.34	19.02	515	520
0.6	8.36	8.35	5.35	4.32	19.25	505	510
0.8	8.38	8.37	5.31	4.39	17.32	490	498
1	8.39	8.38	5.29	5.03	4.91	480	485

a Cobalt (Co) content

a_{th}: theoretical lattice parameter, **a_{exp}**: experimental lattice parameter, **ρ_x**: X-ray density, **ρ_b**: bulk density, **P**: porosity, **T_c**: Curie temperature.

5.2 Microstructure

It is well known that the characteristics of soft ferrites are influenced by the composition, densification and microstructure [4.10]. During the sintering process, the thermal energy generates a force that drives the grain boundaries to grow over pores, thereby the pore volume and hence the materials become denser. At higher sintering temperature, density is decreased because the intra-granular porosity is increased. The crystal grain growth depends on grain boundaries migrating and larger crystal grains swallowing the small ones. During the growth the more different in size of crystal grains, the more beneficial for larger crystal grains to swallow smaller ones, so some pores inside the sintered ferrites are eliminated and the crystal growth improves. When the grain growth rate is very high, pores may be left behind by rapidly moving boundaries. As a result in pores that are trapped inside the grains. Between the grain size and porosity of microstructures, grain size is more important parameter affecting the magnetic properties of ferrites. The grain growth, being a result of inter-particle mass transport, appears to be dominated by the bimodal diffusion mechanism [4.11], lattice and grain boundary diffusion. It is seen from the micrographs

that the dense microstructures are obtained for all the samples. The average grain size (D_m) obtained from SEM picture by linear intercept method.

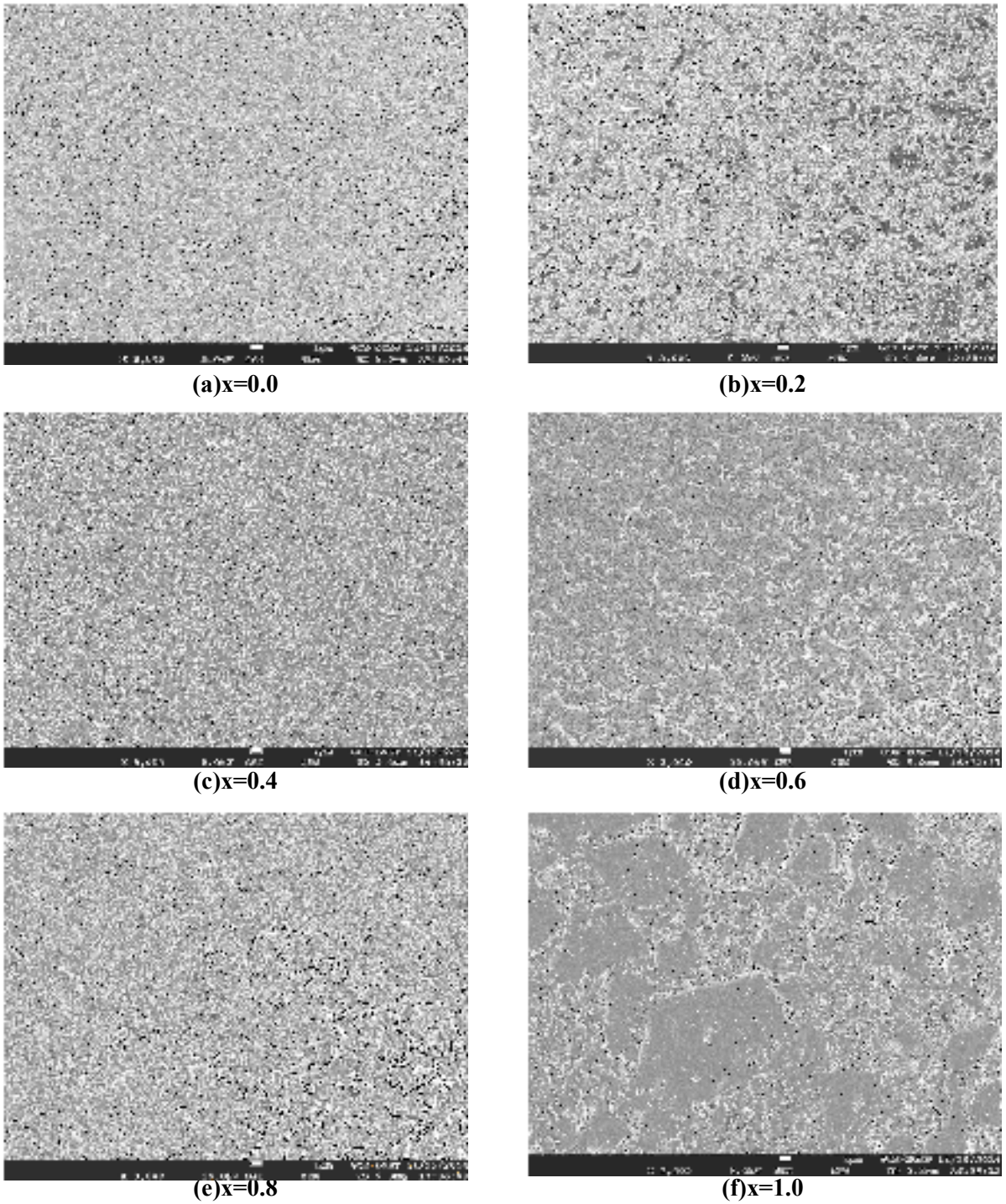

(a)x=0.0 **(b)x=0.2**

(c)x=0.4 **(d)x=0.6**

(e)x=0.8 **(f)x=1.0**

Figure 5.5 :(a-f) SEM micrographs of $Ni_{(1-x)}Co_xFe_2O_4$ samples, sintered at 1100°C.

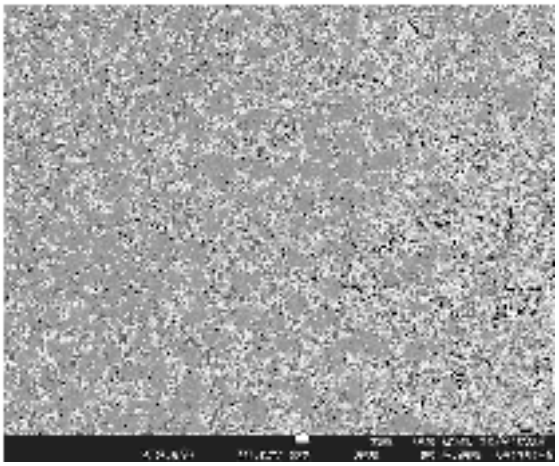

(a)x=0.0

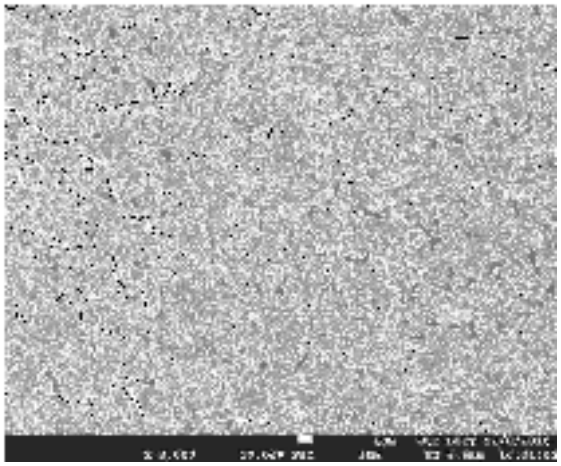

(b)x=0.2

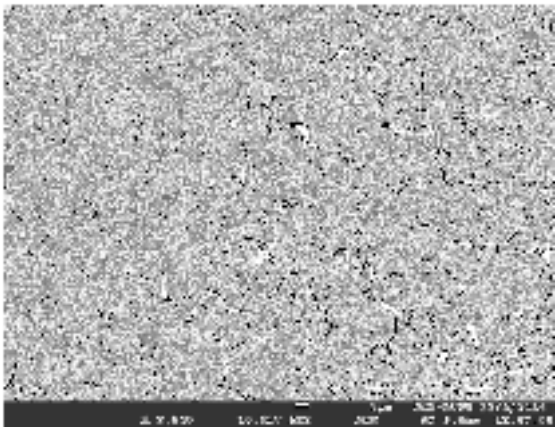

(c)x=0.4

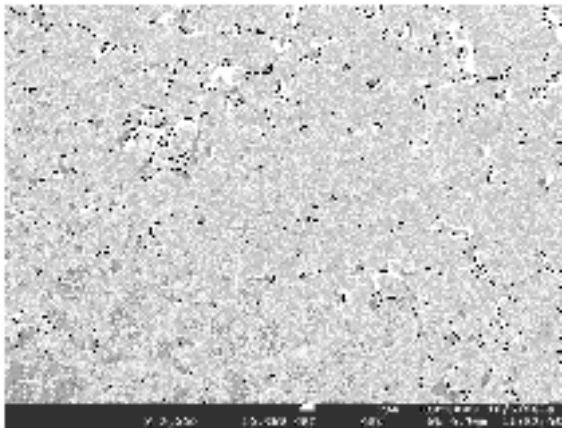

(d)x=0.6

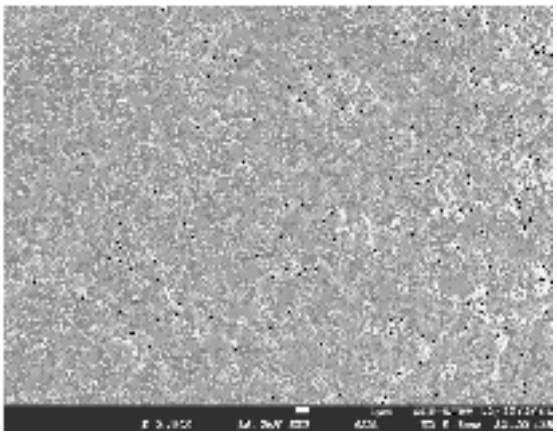

(e)x=0.8

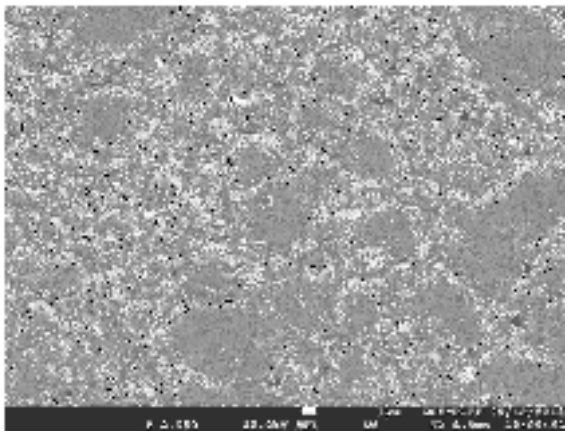

(f)x=1.0

Figure 5.6: (a-f) SEM micrographs of $Ni_{(1-x)}Co_xFe_2O_4$ samples sintered at 1125°C.

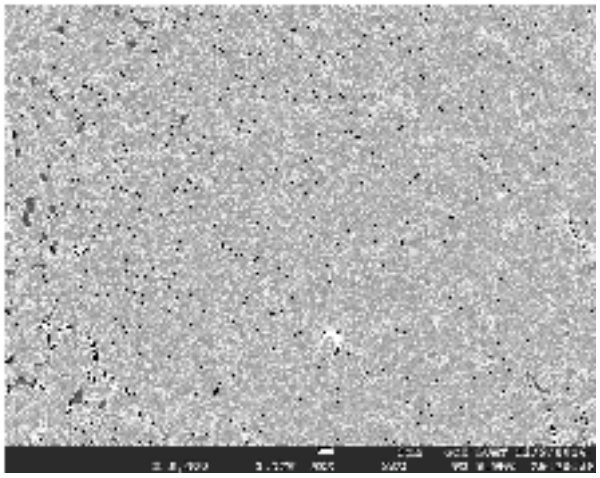

(a)x=0.0

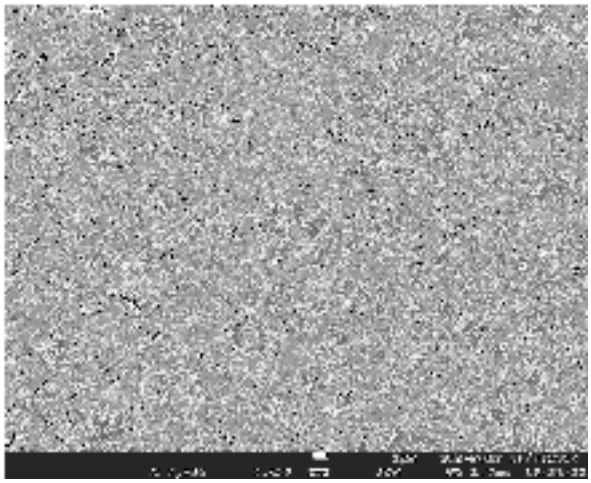

(b)x=0.2

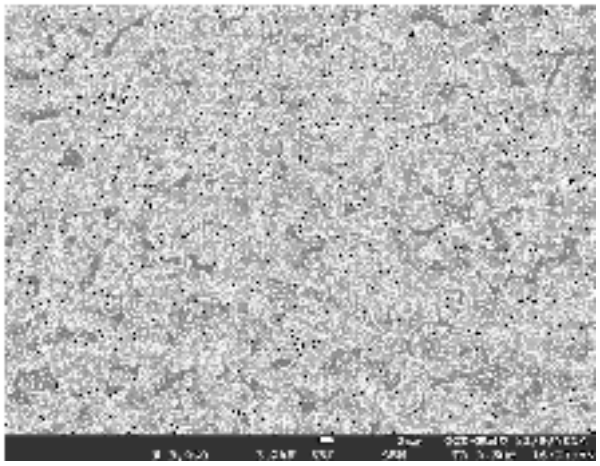

(c)x=0.4

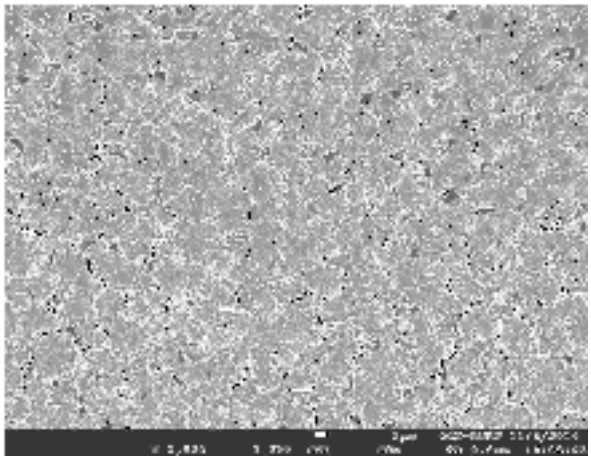

(d)x=0.6

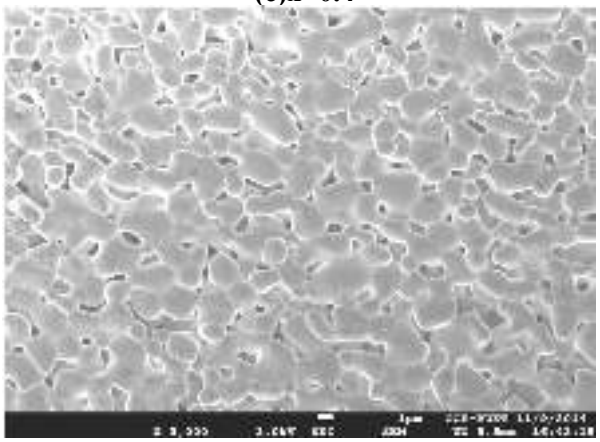

(e)x=0.8

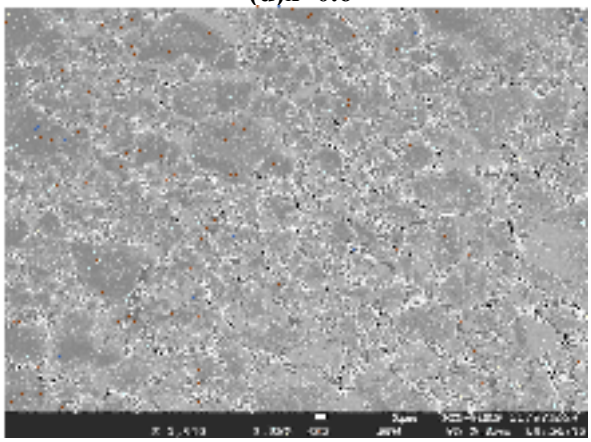

(f)x=1.0

Figure 5.7 :(a-f) SEM micrographs of $Ni_{(1-x)}Co_xFe_2O_4$ samples are sintered at 1150°C.

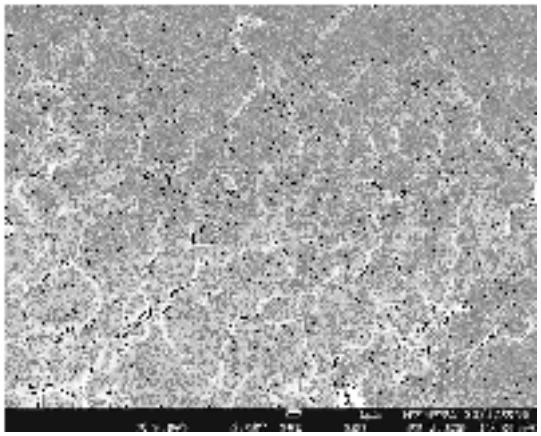

(a)x=0.0,average grain size 5.83µm

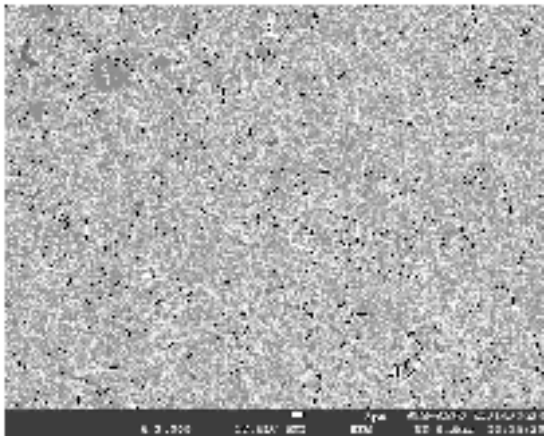

(b)x=0.2,average grain size 1.95µm

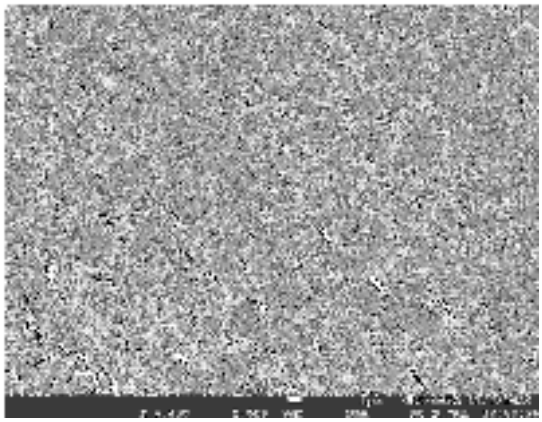

(c)x=0.4,average grain size 2.64µm

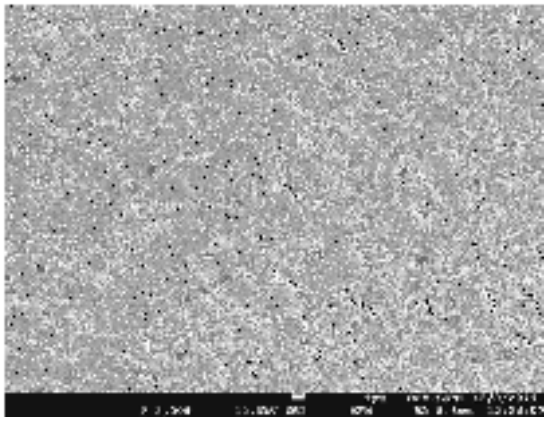

(d)x=0.6,average grain size 3.42µm

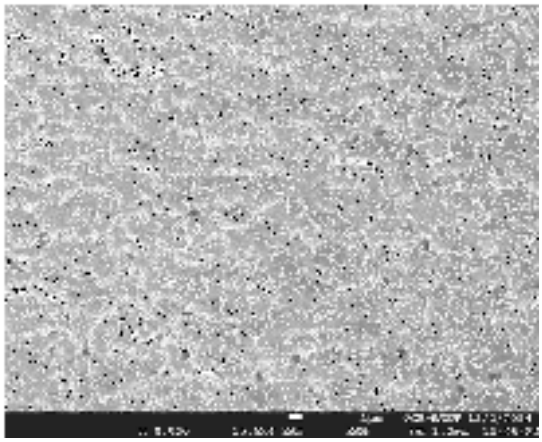

(e)x=0.8,avarge grain size 3.06µm

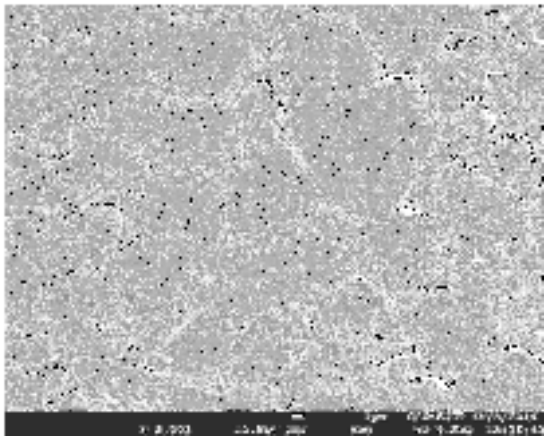

(f)x=1.0,average grain size 7.2µm

Figure 5.8:(a-f) SEM micrographs of $Ni_{(1-x)}Co_xFe_2O_4$ samples sintered at 1175°C.

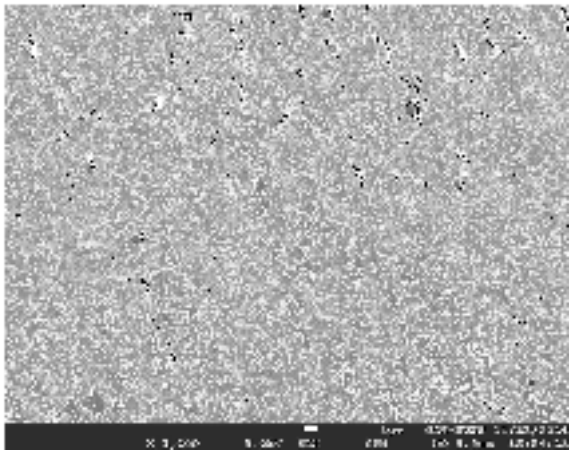

(a)x=0.0,average particle size 5.62µm

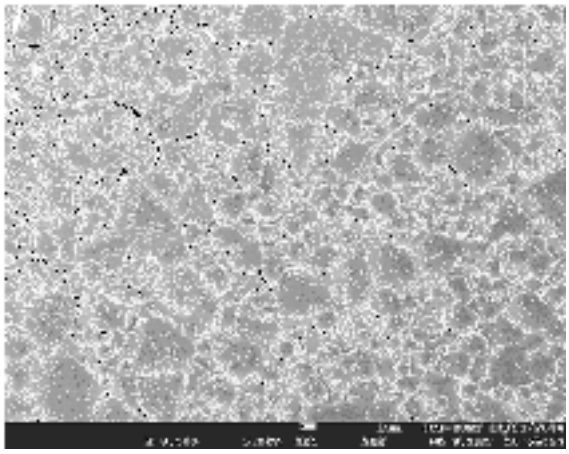

(b)x=0.2,average particle size 2.83µm

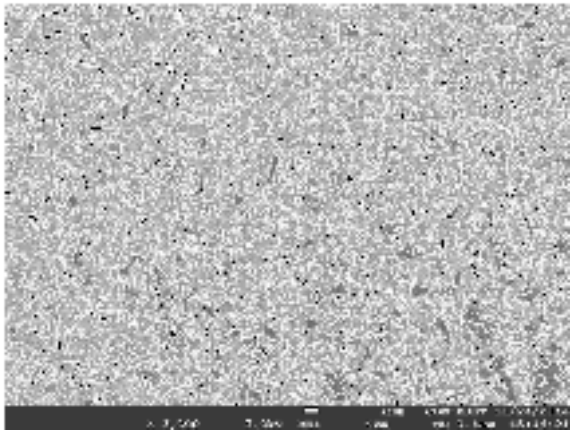

(c)x=0.4,average particle size 3.15µm

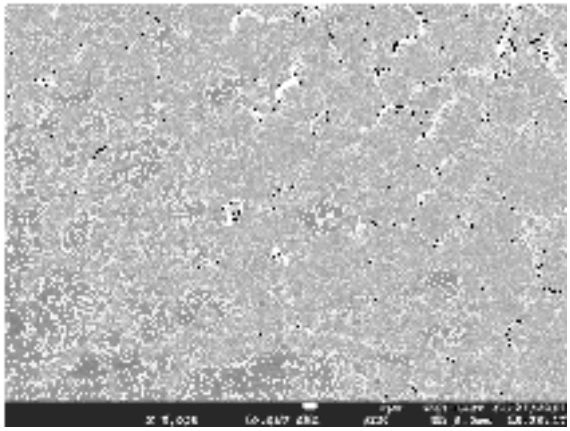

(d)x=0.6,average particle size 6.59µm

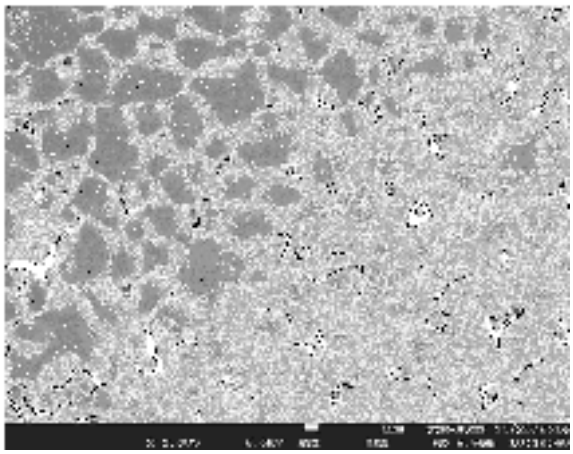

(e)x=0.8,average particle size 6.28µm

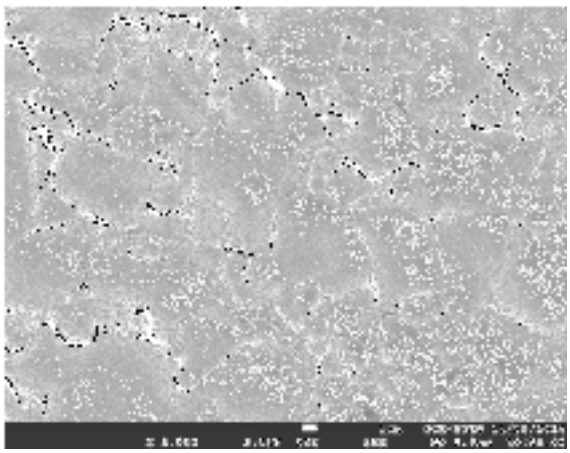

(f)x=1.0,average particle size 4.71µm

Figure 5.9:(a-f) SEM micrographs of $Ni_{(1-x)}Co_xFe_2O_4$ samples sintered at 1200°C.

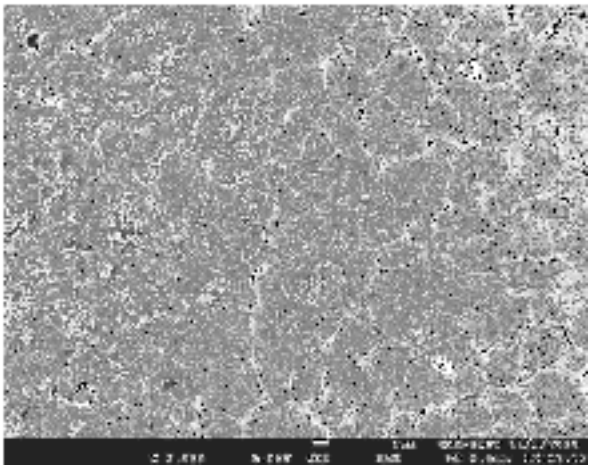

(a)x=0.0,average particle size 7.02µm

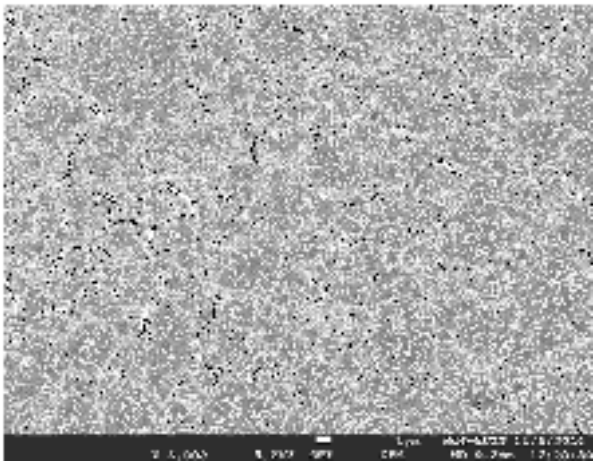

(b)x=0.2,average particle size 3.57µm

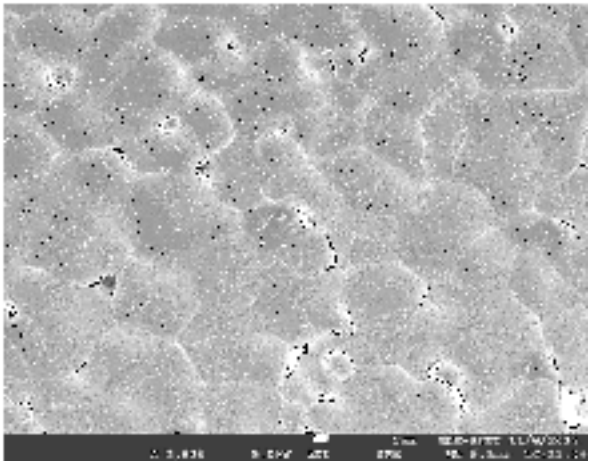

(c)x=0.4,average particle size 13.87µm

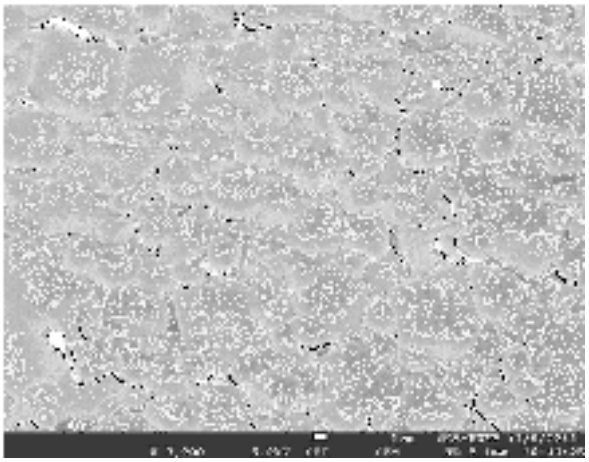

(d)=0.6,average particle size 4.93µm

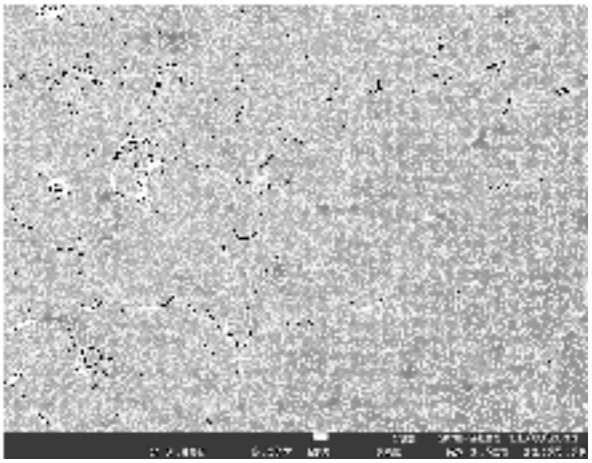

(e)x=0.8,average particle size 11.65µm

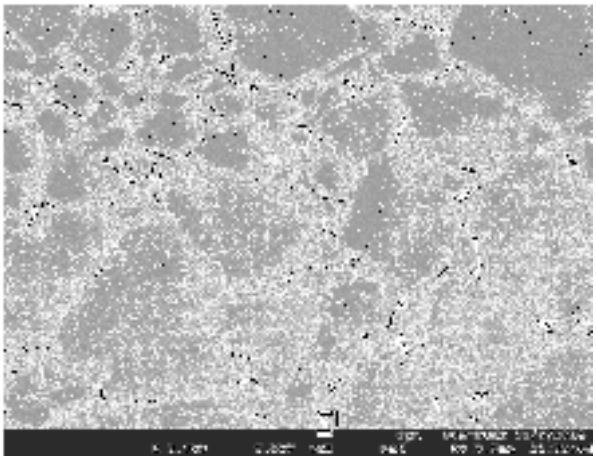

(f)x=1.0,average particle size 9.71µm

Figure 5.10 :(a-f) SEM micrographs of $Ni_{(1-x)}Co_xFe_2O_4$ samples, sintered at 1250°C.

The scanning electronic micrographs of Ni(1-x)CoxFe2O4 samples sintered at 1100^0C, 1125^0C, 1150^0C, 1175^0C, 1200^0C and 1250^0C are shown in Figure. 4.5.(a-f)], figure 4.6.(a-f),figure 4.7.(a-f), figure 4.8.(a-f), figure 4.9.(a-f) and figure 4.10.(a-f), respectively. From Figure 4.5(a-f) we observed that both grain boundary and grain growth were not clear at low magnification sintered at 1100^0C. At low magnification we found many pores due to addition of PVA which was volatile at higher temperature. We also observed that grains were attached with one another with pores. Similar case found at figure 4.6(a-f) and Figure 4.7(a-f). The sintering temperature has great influence on microstructure. It is observed that the average grain size of the sample increased with increasing sintering temperature. As seen from the micrographs sintered at 1175^0C,1200^0C and 1250^0C the dimension of the grain size is varying in the range of 1-7μm,3-6μm and 4-13μm.The possible reason for increase in grain size with increase in value x is relatively higher value of ionic radius of Co^{2+}($0.745A^0$) then Ni^{2+}($0.69A^0$) [4.3, 4.4]. Also increased grain size may results in an increase of mean free path of the electrons and hence causes the change in resistivity [4.12].

5.3 Magnetic Properties

5.3.1 Temperature dependence of initial permeability

Figure 4.11 shows the temperature dependence of initial permeability, μ' for the toroid shaped samples (where x = 0.0, 0.2, 0.4, 0.6, 0.8 and 1.0), which is measured at a constant frequency (100 kHz) of an AC signal by using Impedance Analyzer. It is observed that the initial permeability increases with the increase in Co content while it falls abruptly close to the Curie point. This is because Co in these compositions not only increases the magnetic moment and, but also lowers anisotropy, K_1 [4.13]. On the other hand, permeability increases with the decrease of K_1 as the temperature increases according to the relation $\mu' \propto \frac{M_s^2 D}{\sqrt{K_1}}$ [4.14, 4.15].

It is observed from Fig. 4.11 that the permeability falls density sharply when the magnetic state of the ferrite samples changes from ferromagnetic to paramagnetic. When the anisotropy constant reaches to zero just below the Curie temperature, μ' attains its maximum value and then drops off sharply to minimum value at the Curie point. The sharpness of the permeability drop at the Curie point can be used as a measure of the degree of compositional homogeneity [4.16] which has also been confirmed by X-ray diffraction that no impurity phases could be detected.

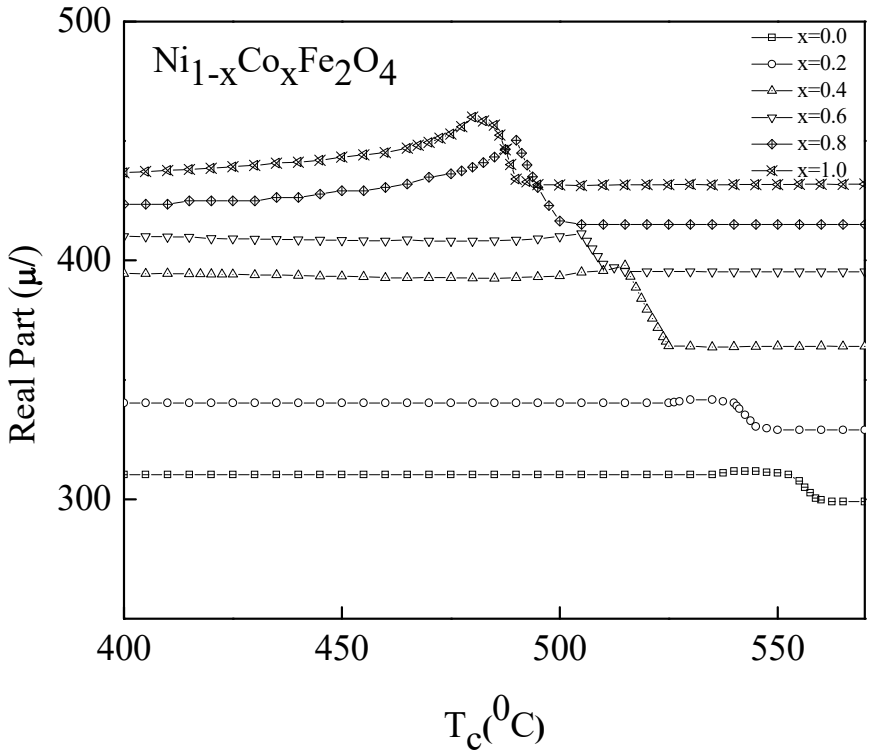

Figure 5.11: Temperature dependence of permeability, μ' of of $Ni_{(1-x)}Co_xFe_2O_4$ (x = 0.0, 0.2, 0.4, 0.6, 0.8 &1.0) ferrites sintered at 1200^0C and determination of Curie temperature.

5.3.2 Compositional Dependence of Curie Temperature

Figure 4.12 shows the variation of Curie temperature T_c with Co content of Ni(1-x)CoxFe2O4 ferrites. T_c of the studied sample was determined from μ'-T curve. The T_c values are shown in Table - 4.1. T_c is the transition temperature above which the ferrite material losses its magnetic properties. The Curie temperature gives an idea of the amount of energy required to break up the long-range ordering in the ferromagnetic material. The Curie temperature mainly depends upon the strength of A-B exchange interaction. According to Neel's sub lattice field model [4.17] sub-lattice field model, the A-B exchange interaction is stronger than the A-A or B-B interaction.

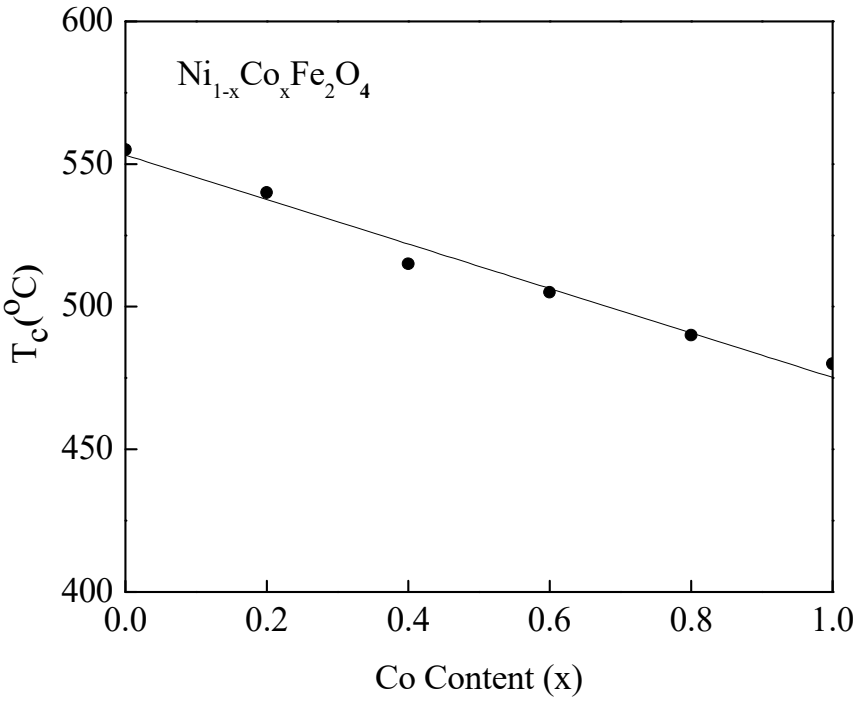

Figure 5.12: Variation of Curie temperature, T_c with Co content (x) of $Ni_{(1-x)}Co_xFe_2O_4$ ferrites sintered at 1200^0C

From figure 4.12 it is observed that Curie temperature linearly decreases with increasing Co content. The magnetic Co^{2+} ions replaced the magnetic F^{3+} ions on B-sites and thus the number of Fe^{3+} decreases on B-sites. This tends to decrease the strength of A-B exchange interactions. The decrease of T_c is due to the weakening of the A-B exchange interaction as well as due to increase of lattice parameter with Co^{2+} content which increases the distance between the magnetic cations. A linear dependence of T_c with Co content is observed for x = 0.0, 0.2, 0.4, 0.6, 0.8 and 1.0. The linear decrease of T_c with *x* content is attributed to the progressive weakening of J_{AB} exchange interactions resulting from substitution of magnetic Co in the Octahedral (B-site) occupancy.

5.3.3 Frequency dependence of permeability

Figure 4.13 shows the variation of the initial permeability spectra as a function of the Co content. It is noticed that the real part of the initial permeability (μ′) decreases with increasing Co^{2+} substitution in $Ni_{1-x}Co_xFe_2O_4$samples sintered at 1100^0C, 1125^0C, 1150^0C, 1175^0C, 1200^0C and 1250 ^{0}C. However the decrease in μ′ with the increase of Co content was not consistent with the variation of microstructures shown in figure 4.5(a-f) to figure 4.10(a-f). According to the Globus and Duplex model [4.18], the static permeability and their product are micro-structurally dependent. Ferrites with large grains are preferred to high permeability values because of the contribution of the domain wall motion. A decrease in the grain size results in a decrease in the number of domain walls in each grain. Moreover the decrease in initial permeability is closely related to the densification of the sample. A decrease in the density of ferrites not only results in an increase of the demagnetizing field due to the presence of pores but also reduces the spin rotational contribution, which in turn decreases the permeability [4.19, 4.20]. Therefore, the decrease of the initial permeability of Ni-Co ferrites with the increase of the Co content was attributed to the decrease in bulk densities

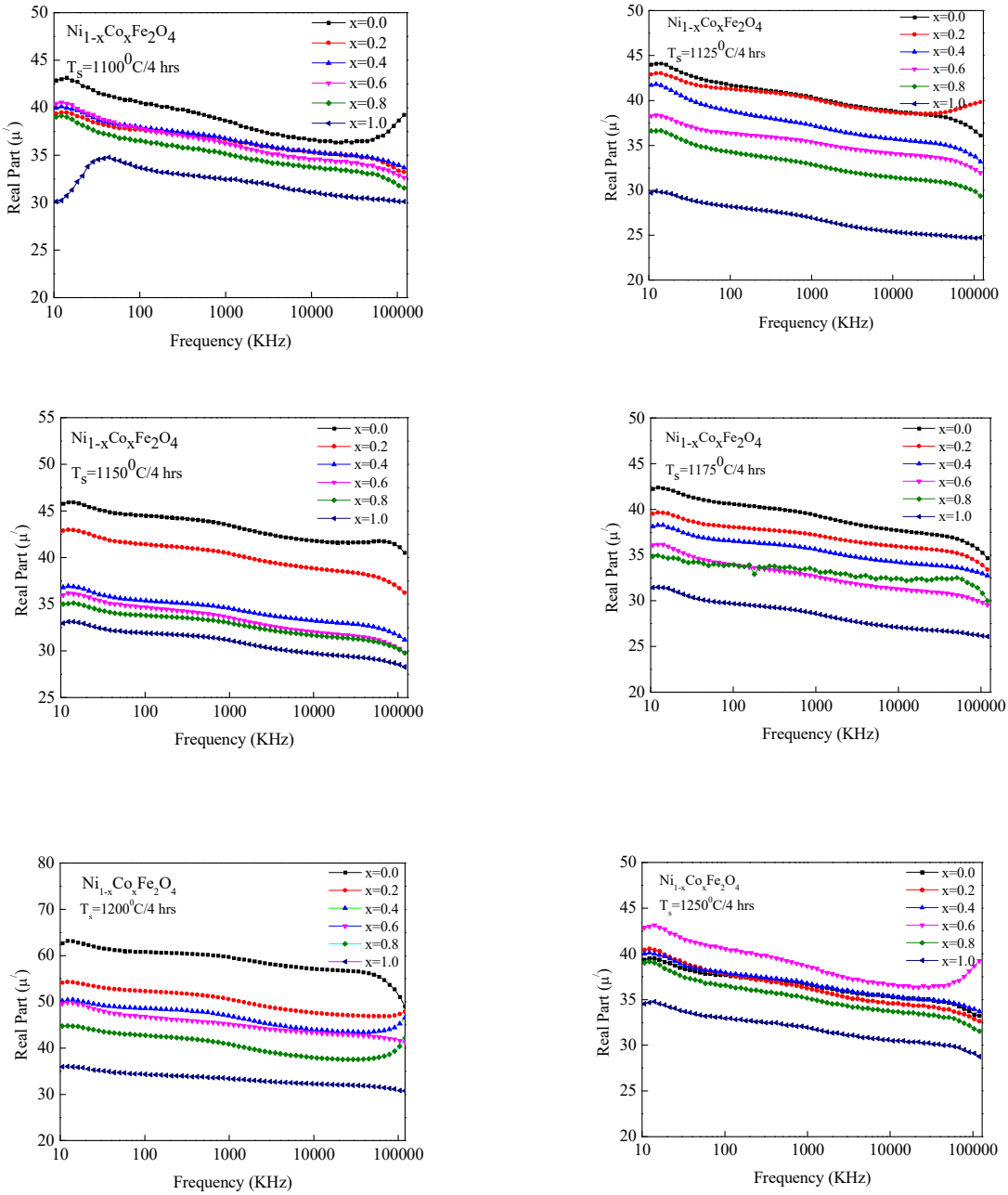

Figure 5.13: Frequency dependence of the real part of the permeability, μ' of $Ni_{(1-x)}Co_xFe_2O_4$ ferrites sintered at 1100°C, 1125°C,1150^{0}C,11750^{0}C,1200^{0}C and 1250°C

5.3.4 Magnetization measurement

Measurement of a hysteresis loop is a very simple and fast method to characterize ferromagnetic materials. The magnetic properties such as the saturation magnetization (M_s), retentivity (M_r), coercivity (H_c) measured by the VSM at 80K, 200K and 300K temperature of the investigated compositions Ni(1-x)CoxFe2O4 shown in figures 17(a-f) to figure 19(a-f). The hysteresis (M-H) loops for the sample sintered at 1200^0C temperatures are shown in figure 4.14(a-f) to figure 4.16(a-f). The magnetization under applied magnetic field for the as-prepared samples exhibits clear hysteretic behaviors. In this study, the hysteresis measurements were based on the following conditions; an applied magnetic field 15kOe, field angle 0 degree and at 80K,200K and 300K temperature. The hysteresis curves and their properties such as the saturation magnetization (M_s), retentivity (M_r), coercivity (H_c), and hysteresis loss are extracted from the application point of view. Tables 2-4 summarize hysteresis parameters such as M_s, M_r, H_c determined from M-H loop measured at 80, 200 and 300K. Saturation magnetization, M_s measured at 80K was found to be much higher compared with data at 300K. M_s has shown to increase with decreasing temperature and attained a maximum value for CoFe2O4 at any measurement temperature which may be attributed to higher magnetic moment of $CoFe_2O_4$ compared to $NiFe_2O_4$. A gradual increase in magnetic hardening was observed with increasing $CoFe_2O_4$ content attaining a maximum value of H_c at x=0.8. The saturation magnetization defined as the maximum possible magnetization of a material. We can find the saturation magnetization of a ferrite system by knowing

(i) The moment on each ion.

(ii) The distribution of ions between A and B sites.

(iii) The exchange interaction between A and B sites is negative.

In reality, AB, AA, and BB interactions all tend to be negative, but they can't all be negative simultaneously. AB interactions are usually the strongest so that all the A moments are parallel to one another but antiparallel to B moments [4.21].

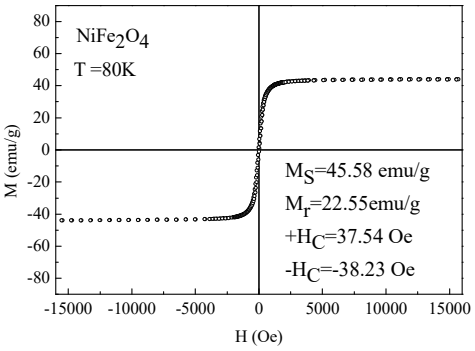

(a) The M-H loop for Ni(1-x)CoxFe2O4 , where x=0.0

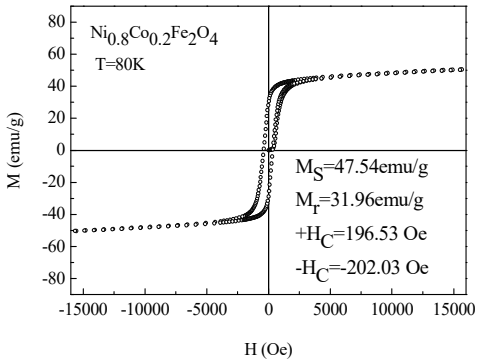

(b) The M-H loop for Ni(1-x)CoxFe2O4 , where x=0.2

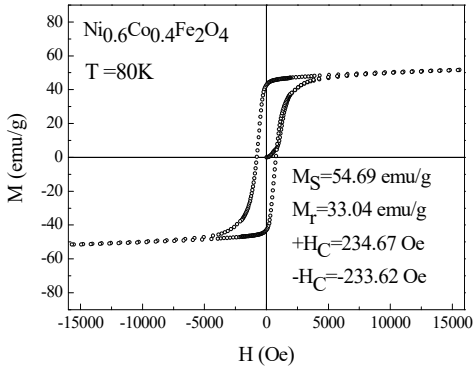

(c) The M-H loop for Ni(1-x)CoxFe2O4 , where x=0.4

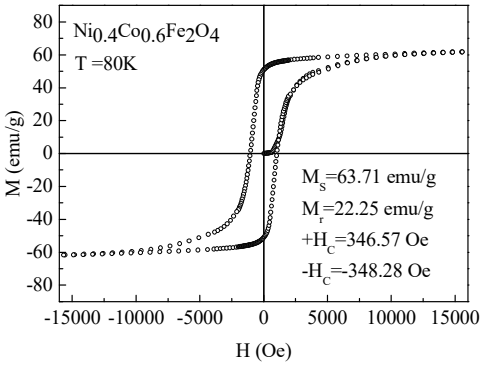

(d) The M-H loop for Ni(1-x)CoxFe2O4 , where x=0.6

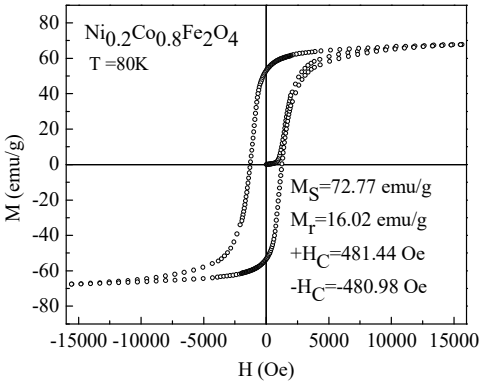

(e) The M-H loop for Ni(1-x)CoxFe2O4 , where x=0.8

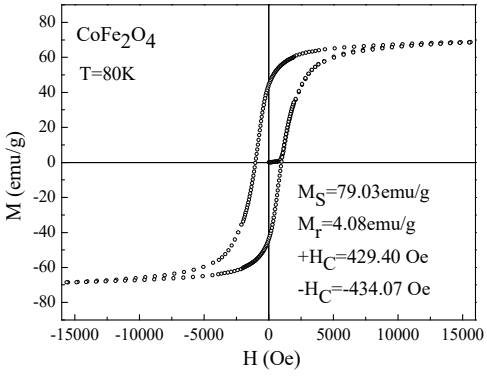

(f) The M-H loop for Ni(1-x)CoxFe2O4 , where x=1.0

Figure 5.14:(a-f)The M-H loop for $Ni_{(1-x)}Co_xFe_2O_4$ at 80K, sintered at 1200^0C

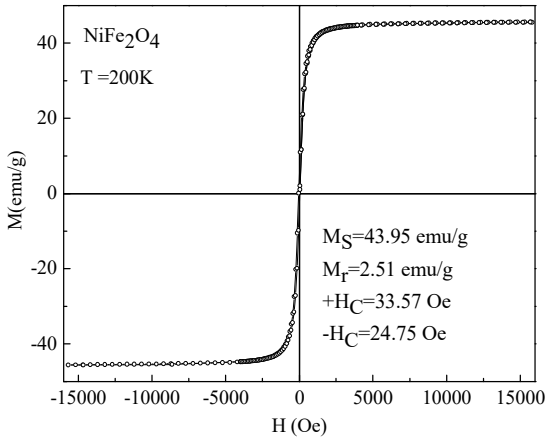

(a) The M-H loop for Ni(1-x)CoxFe2O4 , where x=0.0

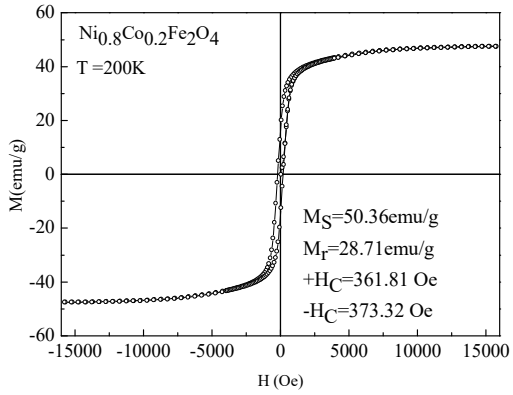

(b) The M-H loop for Ni(1-x)CoxFe2O4 , where x=0.2

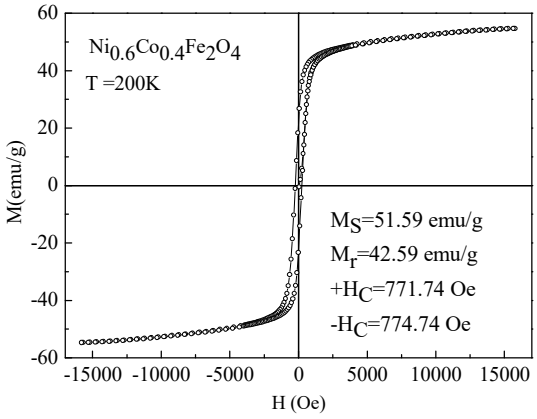

(c) The M-H loop for Ni(1-x)CoxFe2O4 , where x=0.4

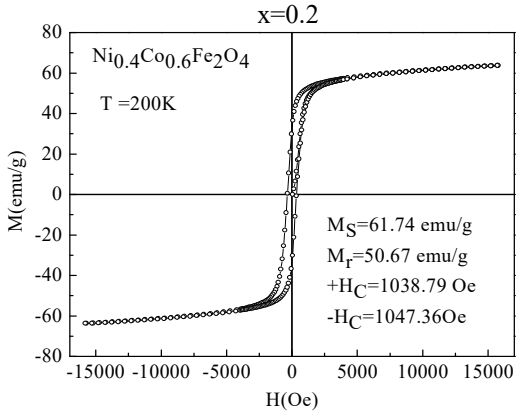

(d) The M-H loop for Ni(1-x)CoxFe2O4 , where x=0.6

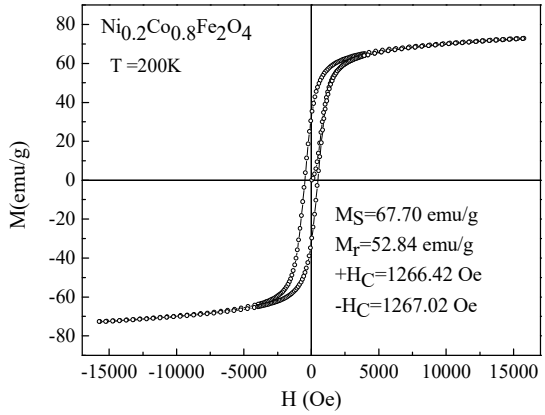

(e) The M-H loop for Ni(1-x)CoxFe2O4 , where x=0.8

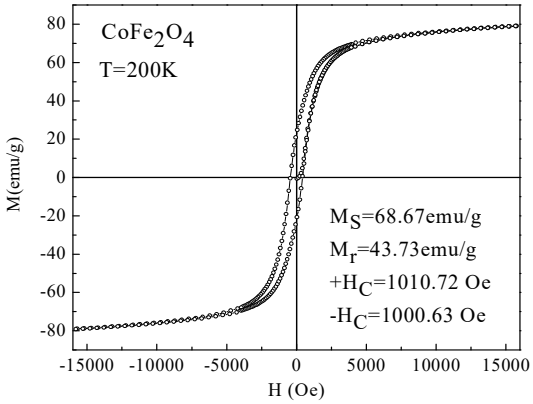

(f) The M-H loop for Ni(1-x)CoxFe2O4 , where x=1.0

Figure 5.15: (a-f).The M-H loop for $Ni_{(1-x)}Co_xFe_2O_4$ at 200K, sintered at 1200^0C

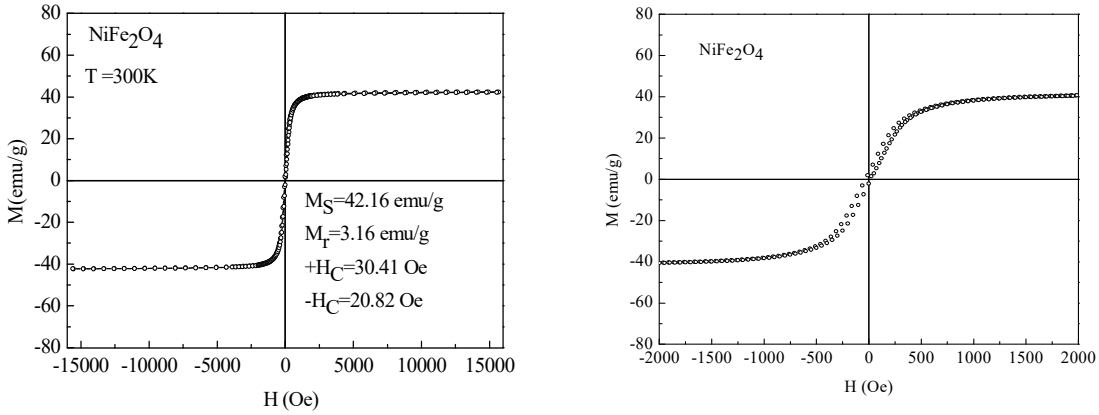

(a)The M-H loop for $Ni_{1-x}Co_xFe_2O_4$, where x=0.0

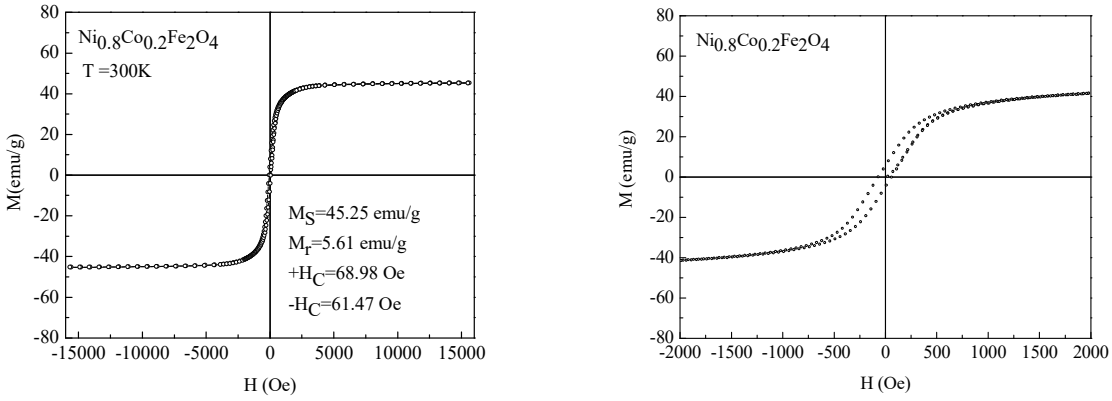

(b) The M-H loop for Ni(1-x)CoxFe2O4 , where x=0.2

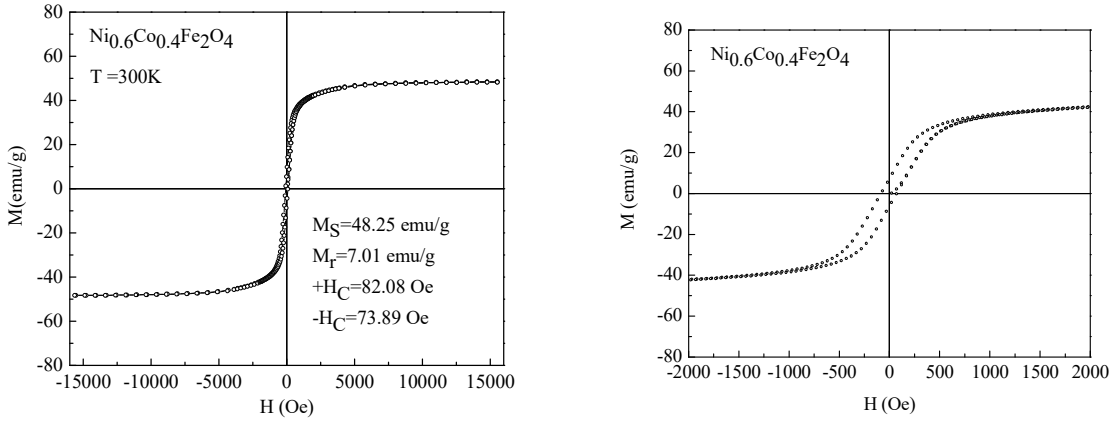

(c) The M-H loop for Ni(1-x)CoxFe2O4 , where x=0.4

Figure 5.16:(a-c) The M-H loop for $Ni_{(1-x)}Co_xFe_2O_4$ at 300K, sintered at 1200^0C

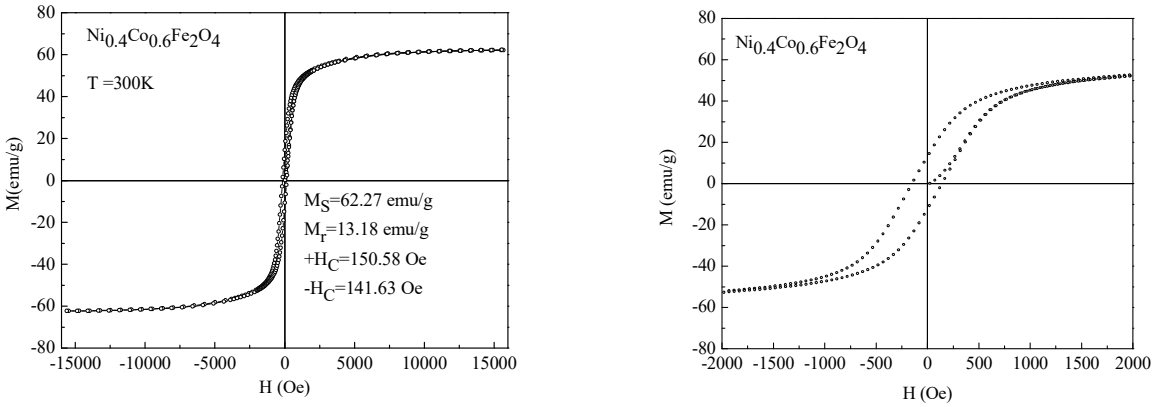

(d) The M-H loop for Ni(1-x)CoxFe2O4 , where x=0.6

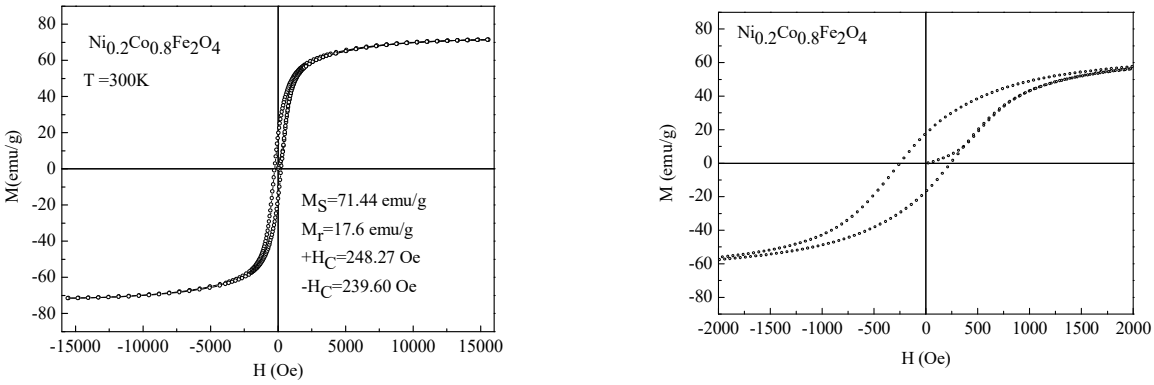

(e) The M-H loop for Ni(1-x)CoxFe2O4 , wherex=0.8

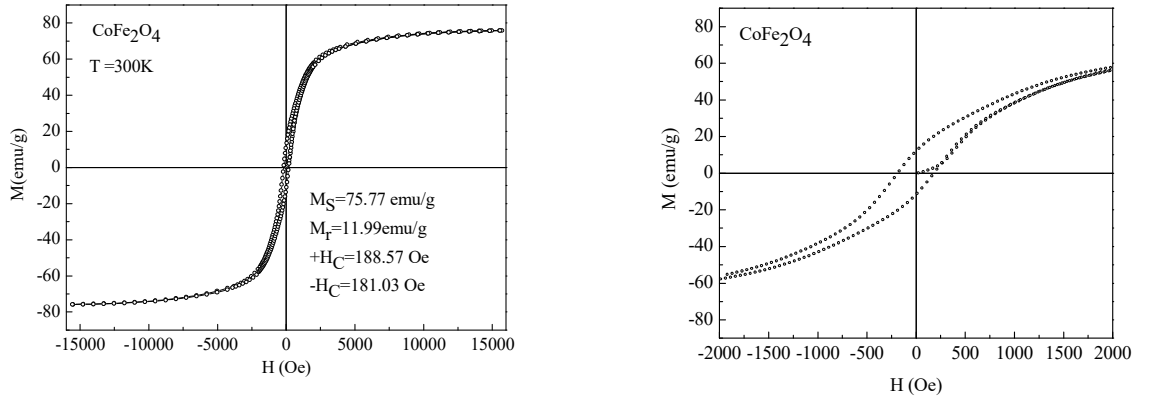

(f) The M-H loop for Ni(1-x)CoxFe2O4 , where x=1.0

Figure 5.16:(d-f) The M-H loop for $Ni_{(1-x)}Co_xFe_2O_4$ at 300K, sintered at 1200^0C

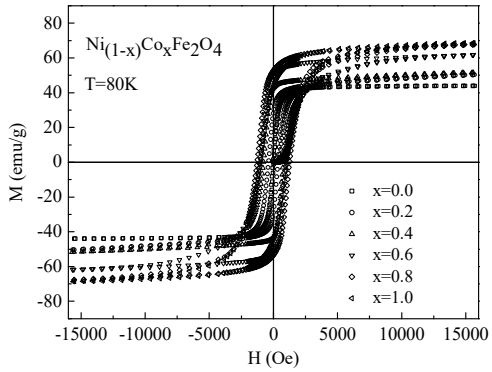

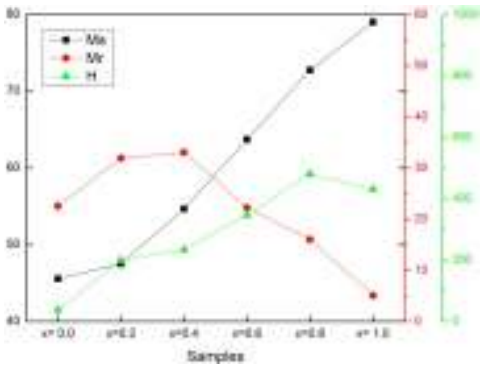

Figure 5.17. Saturation magnetization (M_s), Retentivity (M_r), Coercivity (H_c) for $Ni_{(1-x)}Co_xFe_2O_4$ at 80K , sintering condition 1200^0C

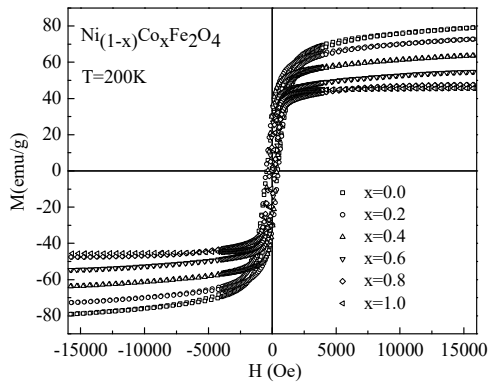

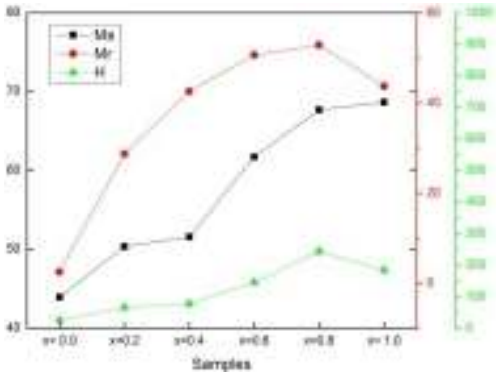

Figure 5.18. Saturation magnetization (M_s), Retentivity (M_r), Coercivity (H_c) for $Ni_{(1-x)}Co_xFe_2O_4$ at 200K , sintering condition 1200^0C

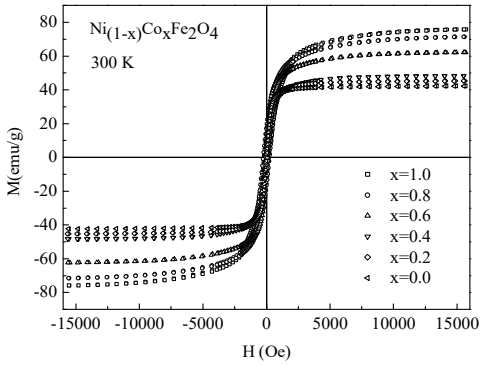

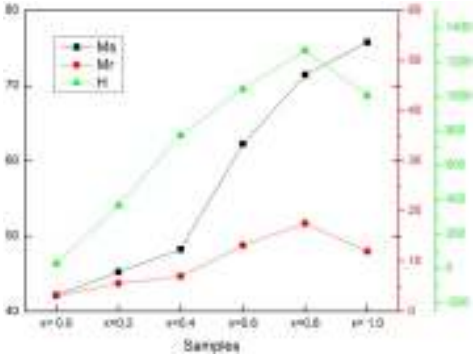

Figure 5.19. Saturation magnetization (M_s), Retentivity (M_r), Coercivity (H_c) for $Ni_{(1-x)}Co_xFe_2O_4$ at 300K , sintering condition 1200^0C

Table[5.3].Saturation magnetization (M_S), retentivity(M_r), coercivity(H_C), and hysteresis loss of Ni-Co ferrite samples at 80K.

Samples	M_s (emu/g)	M_r (emu/g)	H_C (Oe)
$NiFe_2O_4$	45.58	22.55	37.88
$Ni_{0.8}Co_{0.2}Fe_2O_4$	47.54	31.96	199.28
$Ni_{0.6}Co_{0.4}Fe_2O_4$	54.69	33.05	234.14
$Ni_{0.4}Co_{0.6}Fe_2O_4$	63.71	22.25	347.42
$Ni_{0.2}Co_{0.4}Fe_2O_4$	72.77	16.02	481.21
$CoFe_2O_4$	79.03	5.08	431.73

Table [5.4]. Saturation magnetization (M_S), retentivity(M_r), coercivity(H_C), and hysteresis loss of Ni-Co ferrite samples at 200K.

Samples	M_s (emu/g)	M_r (emu/g)	H_C (Oe)
$NiFe_2O_4$	43.95	2.51	29.16
$Ni_{0.8}Co_{0.2}Fe_2O_4$	50.36	28.71	367.65
$Ni_{0.6}Co_{0.4}Fe_2O_4$	51.59	42.59	773.24
$Ni_{0.4}Co_{0.6}Fe_2O_4$	61.74	50.67	1043.07
$Ni_{0.2}Co_{0.4}Fe_2O_4$	67.7	52.84	1266.72
$CoFe_2O_4$	68.67	43.73	1005.67

Table [5.5] Saturation magnetization (M_S), retentivity(M_r), coercivity(H_C), and hysteresis loss of Ni-Co ferrite samples at 300K.

Samples	M_s (emu/g)	M_r (emu/g)	H_C (Oe)
$NiFe_2O_4$	42.16	3.16	25.61
$Ni_{0.8}Co_{0.2}Fe_2O_4$	45.25	5.61	65.22
$Ni_{0.6}Co_{0.4}Fe_2O_4$	48.25	7.01	77.98
$Ni_{0.4}Co_{0.6}Fe_2O_4$	62.27	13.18	146.10
$Ni_{0.2}Co_{0.4}Fe_2O_4$	71.44	17.6	243.93
$CoFe_2O_4$	75.77	11.99	184.80

5.4 Thermal Properties

5.4.1 TG-DSC analysis

Differential Scanning Calorimetry(DSC) analysis determine important transition temperatures, determine heat of fusion of a crystal phase and the degree of crystallization, study crystal kinetic, determine heat capacity, determine heat of formation and sample purity. Whereas Thermogravimetry(TG) analysis study thermal degradation, chemical reaction resulting in changes of mass such as absorption, adsorption, desorption and sample purity. Figure 4.20(a-f) showed TG-DSC curves for the solid precursor of $Ni_{1-x}Co_xFe_2O_4$(where x=0,0.2,0.4,0.6,0.8 and 1.0) sintered at 1200^0C recorder under N_2 atmosphere with a heating rate 10^0 C min^{-1}.The Differential Scanning Calorimetry (DSC) curves showed tetragonal to Cubic phase change for the solid samples of $Ni_{1-x}Co_xFe_2O_4$(where x=0,0.2,0.4,0.6,0.8 and 1.0).At first desorption water molecules occurred around 100^0C.After removing water molecules Perovskite Tetragonal phase change occurred. For the Ni(1-x)CoxFe2O4 (where x=0, 0.2, 0.4, 0.6, 0.8 and 1.0) samples Tetragonal phase to Cubic phase transition temperature were 556^0C, 538^0C, 520^0C, 510^0C, 498^0C and 485^0C respectively [4.22, 4.23].TG curves showed that no weight loss during TG-DSC analysis. The TG experiment was conducted 25^0C to 600^{o}C.The TG curves showed slightly increased in weight within the sample due to N_2 gas consumption during the analysis [4.24, 4.25].

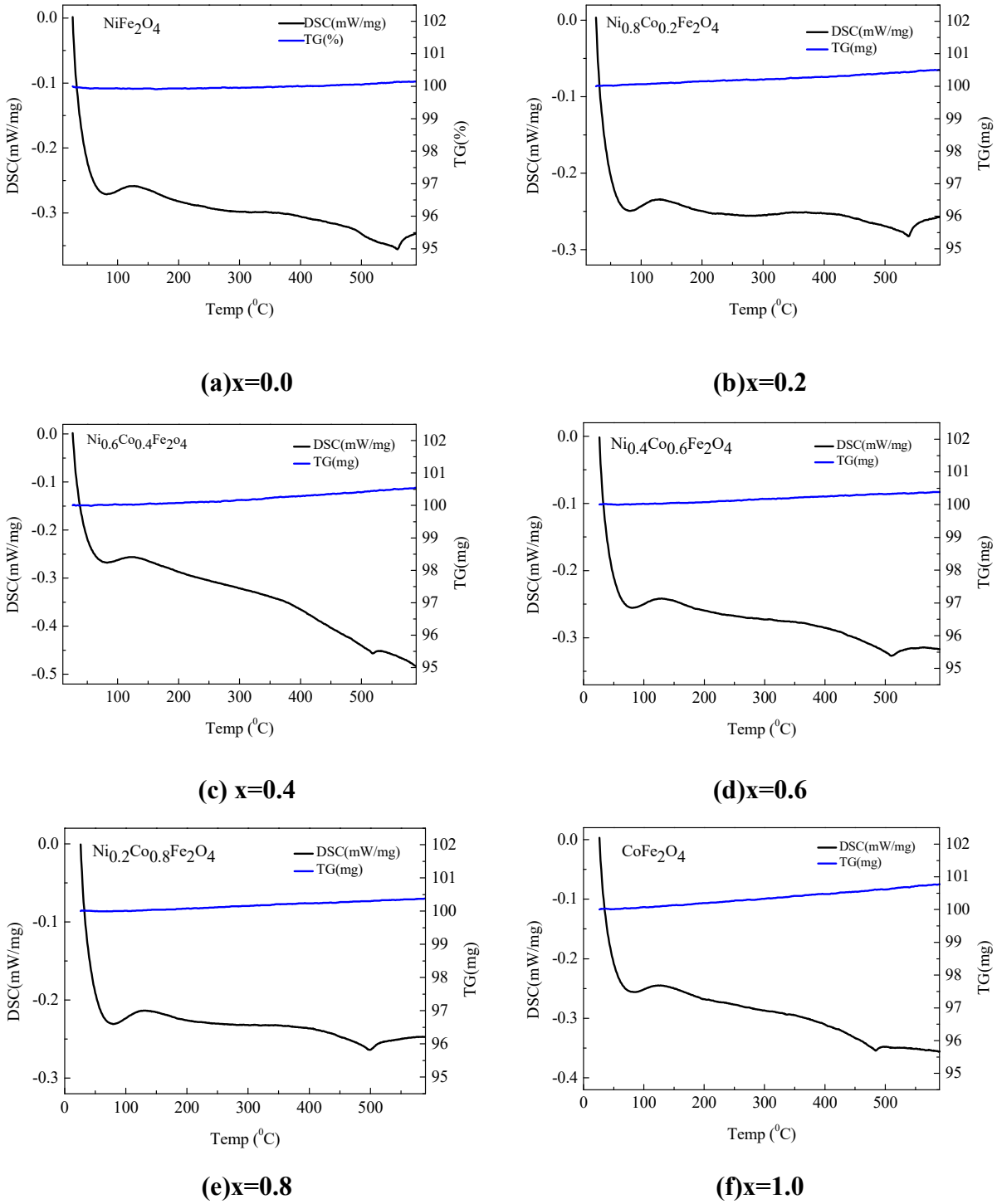

Figure 5.20:(a-f) TG-DSC curve of Ni-Co ferrites with the composition of $Ni_{1-x}Co_xFe_2O_4$(x=0.0,0.2,0.4,0.6,0.8 ,1.0),sintering temperature 1200^0C

5.4.2 Particle size analysis

As we discussed before Ni-Co ferrites with the composition $Ni_{(1-x)}Co_xFe_2O_4$ (where x=0, 0.2, 0.4,0.6, 0.8 & 1.0) were synthesized by solid state reaction method. The starting were synthesized by solid state reaction method. The starting materials for the preparation of the studied compositions were in the form of nano powder of ferrites ($NiFe_2O_4$ and $CoFe_2O_4$) of Inframat Advanced Materials, USA. The purity of our materials is up to 99.99%. From the figure 4.21(a-f), we observed that the particle size distribution of Ni –Co ferrites with the composition $Ni_{(1-x)}Co_xFe_2O_4$ (where x=0, 0.2, 0.4,0.6, 0.8 & 1.0).We found that boimodal distribution for $NiFe_2O_4$ and $CoFe_2O_4$.We also found that the avareage grain size range of $NiFe_2O_4$ and $CoFe_2O_4$.were 10 to 100 µm. Otherwise we found unimodal distribution for of Ni –Co ferrites with the composition $Ni_{(1-x)}Co_xFe_2O_4$ (where x= 0.2, 0.4,0.6 & 0.8). We also found that the avareage grain size range of of Ni –Co ferrites with the composition $Ni_{(1-x)}Co_xFe_2O_4$ (where x= 0.2, 0.4,0.6 & 0.8).were 1 to 10 µm.

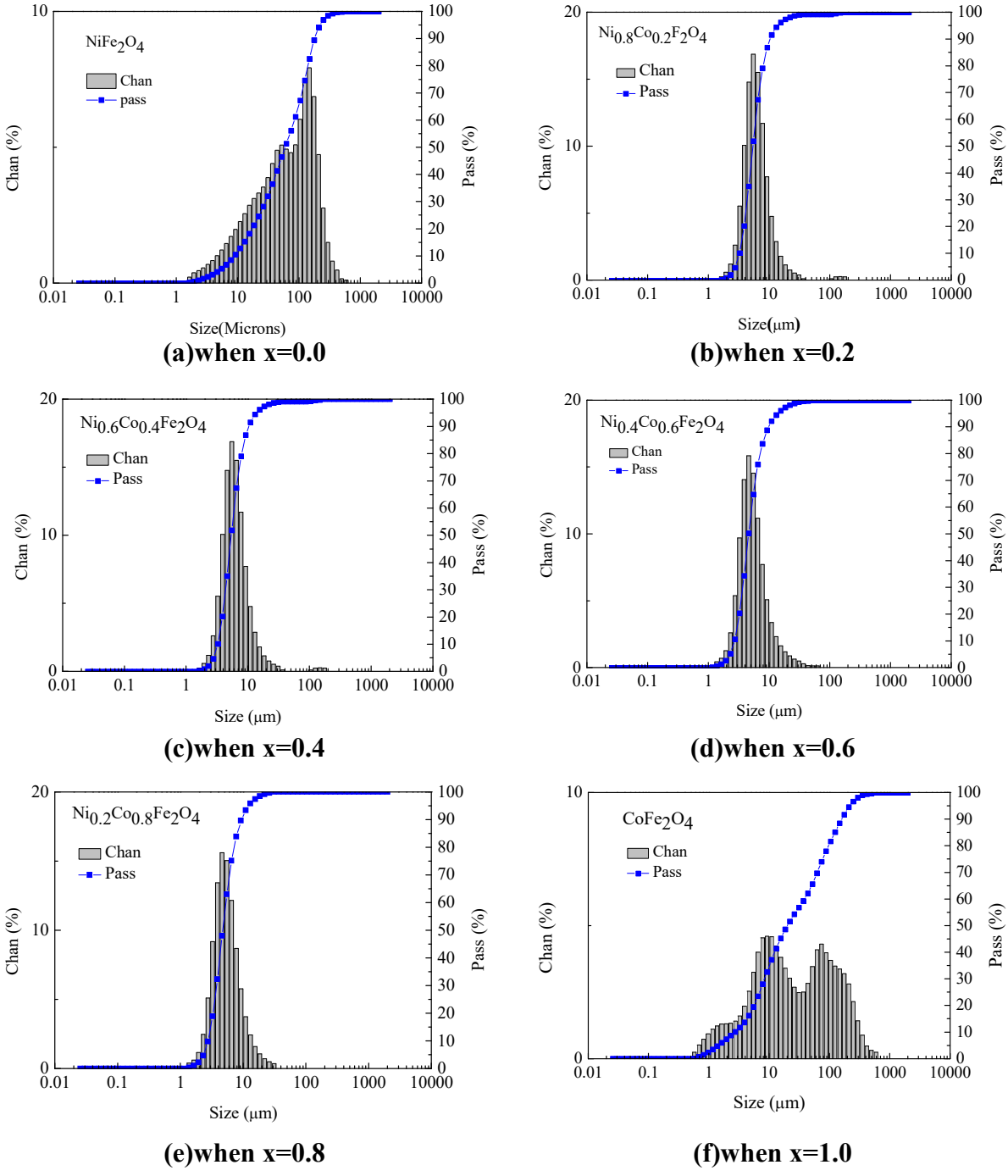

Figure 5.21:(a-f)Particle size distribution of Ni-Co ferrites with the composition $Ni_{1-x}Co_xFe_2O_4$ (x=0, 0.2, 0.4, 0.6, 0.8 &1.0),sintering temperature 1200^0C

5.5 Dielectric Properties

5.5.1Frequency dependence of dielectric constant

The dielectric behavior is one of the most important characteristics of ferrites which markedly depend on the preparation conditions, e.g. sintering time and temperature, type and quantity of additives. The dielectric constant (ε') results are due to the heterogeneous structure of the material. The frequency dependence of the dielectric constant for all the samples sintered at 1200^0C is shown in figure 4.22 and it can be seen that all the samples showed similar behavior, i.e. dielectric constant decreased initially with increase in frequency and reached a constant value at higher frequency. After a certain increase in frequency all the samples exhibit a frequency-independent behavior, which can be explained on the basis of Maxwell– Wagner interfacial type polarization, which is in agreement with Koop's phenomenological theory [4.26, 4.27]. The dielectric polarization in ferrites is similar with the conduction hopping mechanism. Hopping between Fe^{2+} and Fe^{3+} the local displacement of electrons in the direction of the applied field occurs and these electrons determine the polarization.

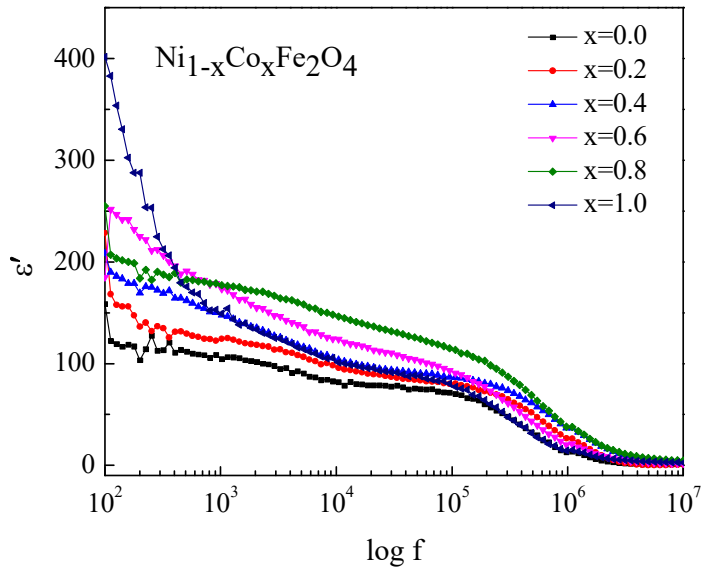

Figure 5.22: Frequency dependence of dielectric constant of $Ni_{1-x}Co_xFe_2O_4$ sintered at 1200^0C

The polarization decreased with increasing frequency and then reached a constant value due to the fact that beyond a certain external field frequency, and as a result electron exchange Fe^{2+} <=> Fe $^{3+}$ cannot follow the alternating field. The large value of the dielectric constant at lower frequency is due to the predominance of species like Fe^{2+} ions, interfacial dislocations piled up, oxygen vacancies, grain boundary defects, etc. [4.27, 4.28], while the decrease in ε with frequency is natural because of the fact that any species contributing to polarizability is found to show lagging behind the applied field at some higher frequencies.

Chapter Six

Conclusion

The research was undertaken to depict fabrication and characterization of $Ni_{(1-x)}Co_xFe_2O_4$ electromagnetic ceramic. The findings of the research are as follow:

- According to the X-ray diffraction pattern, at 1200^0C sintering condition confirmed the single phase cubic spinel structure of the $Ni_{(1-x)}Co_xFe_2O_4$ (where x = 0.0, 0.2, 0.4, 0.6, 0.8 & 1.00) ferrites.
- According to the Vegard's law, the lattice constant of $Ni_{(1-x)}Co_xFe_2O_4$ (where x = 0.0, 0.2, 0.4, 0.6, 0.8 & 1.00) sintered at 1200^0C we observed a correlation between the ionic radius & the lattice content i.e. the lattice constant increased linearly with increasing Co^{2+} content.
- We found that, The X-ray density and bulk density decrease significantly with the increasing Co content. for the composition of $Ni_{(1-x)}Co_xFe_2O_4$ (where x = 0.0, 0.2, 0.4, 0.6, 0.8 & 1.00) ferrites sintered at 1200^0C
- From the scanning electronic micrographs of $Ni_{(1-x)}Co_xFe_2O_4$ (where x = 0.0, 0.2, 0.4, 0.6, 0.8 & 1.00) samples sintered at 1100^0C, 1125^0C, 1150^0C, 1175^0C, 1200^0C and 1250^0C we observed that the average grain size of the sample increased with increasing sintering temperature. The possible reason for increase in grain size with increase in value x is relatively higher value of ionic radius of $Co^{2+}(0.745A^0)$ then $Ni^{2+}(0.69A^0)$.
- For the composition of $Ni_{(1-x)}Co_xFe_2O_4$ (where x = 0.0, 0.2, 0.4, 0.6, 0.8 & 1.00) ferrites sintered at 1200^0C confirmed that the Curie temperatures decreased linearly with the successive addition of Cobalt ions. We also measured the degree of compositional homogeneity by the temperature dependence of initial permeability at a constant frequency (100 KHz) for the toroid shaped samples of $Ni_{(1-x)}Co_xFe_2O_4$ (where x = 0.0, 0.2, 0.4, 0.6, 0.8 & 1.00) ferrites sintered at 1200^0C

- It is noticed that frequency dependence of the initial permeability (μ′) decreases with increasing C^{o2+} substitution in $N_{i1-x}C_{ox}F_{e2O4}$ (where x = 0.0, 0.2, 0.4, 0.6, 0.8 & 1.00) samples sintered at 110^{00}C, 112^{50}C, 115^{00}C, 117^{50}C, 120^{00}C and $1250\,^{0}$C.
- The detail hysteresis parameters such as Satuartion magnetization (M_s), Retentivity(M_r) and Coercivity(H_c) determined from M-H loop measured at 80K, 200K and 300K by the Vibrating sample Magnetometer (VSM) for $Ni_{(1-x)}Co_xFe_2O_4$ (where x = 0.0, 0.2, 0.4, 0.6, 0.8 & 1.00) ferrites sintered at 1200^0C. We found that, saturation magnetization, M_s measured at 80K was found much higher compared with data at 200K & 300K. M_s is found to increase with decreasing temperature and attained a maximum value corresponding to $CoFe_2O_4$ at any measurement temperature which may be attributed to higher magnetic moment of $CoFe_2O_4$ compared with $NiFe_2O_4$. We also established that a gradual increase in magnetic hardening was observed with increasing $CoFe_2O_4$ content with a maximum value of H_c at x=0.8.
- By The Differential Scanning Calorimetry (DSC) curves we measured tetragonal to Cubic phase change temperature for the solid samples of $Ni_{1-x}Co_xFe_2O_4$ (where x=0, 0.2, 0.4, 0.6, 0.8 and 1.0) sintered at 1200^0C.
- From the Thermogravimetry (TG) analysis we analyzed thermal degradation for the solid samples of $Ni_{1-x}Co_xFe_2O_4$ (where x=0, 0.2, 0.4, 0.6, 0.8 and 1.0) sintered at 1200^0C.We observed that no weight loss for these samples.
- By particle size distribution analysisi,we observed that the particle size distribution of Ni –Co ferrites with the composition $Ni_{(1-x)}Co_xFe_2O_4$ (where x=0, 0.2, 0.4,0.6, 0.8 & 1.0).We found that boimodal distribution for $NiFe_2O_4$ and $CoFe_2O_4$.We also found that the avareage grain size range of $NiFe_2O_4$ and $CoFe_2O_4$.were 10 to 100 μm. Otherwise we found unimodal distribution for of Ni –Co ferrites with the composition $Ni_{(1-x)}Co_xFe_2O_4$ (where x= 0.2, 0.4,0.6 & 0.8). We also found that the avareage grain size range of of Ni –Co ferrites with the composition $Ni_{(1-x)}Co_xFe_2O_4$ (where x= 0.2, 0.4,0.6 & 0.8).were 1 to 10 μm.

- The frequency dependence of the dielectric constant of $Ni_{1-x}Co_xFe_2O_4$(where x=0,0.2,0.4,0.6,0.8 and 1.0) sintered at 1200^0C was measured and we observed that all the samples showed similar behavior, i.e. dielectric constant decreased initially with increase in frequency and reached a constant value at higher frequency.

References

CHAPTER-1

1.1. A. Maqsood, K. Khan, M. A. Rehman and M. A. Malik, 2011, Journal of Alloys and Compound, Vol.509 (27), pp 7493–7499.

1.2. K. M. Batoo, F. A. Mir, M. S. A. El-sadek and N. A. Madhar, 2013, Journal of Nanoparticle Research, Vol. 15 (2067), pp 1-9.

1.3. A. K. M. A. Hossain, M. Seki, T. Kawai and H. Tabata, 2004, Journal of Appl. Phys., Vol. 96, pp- 1273**.**

1.4. A. Meenakshisundaram, N. Gunasekaran and V. Srinivasan, 1982, Phys. Status Solidi (a), Vol. 69, pp-15.

1.5. S. Hilpert, 1909, Ber. Deutseh. Chem. Ges. BD2, Vol. 42, pp- 2248.

1.6. J. L. Snoek, New developments in Ferrimagnetism, p-139.

1.7. T. Takai, 1937, J Electr. Chems., Vol. 5, pp-411.

1.8. L.Neel, 1948, Annales de Physique, Vol. 3, pp-137.

1.9. J. Smit and H. P. J. Wijn, 1959, Ferrites, Wiley New York, pp -369.

1.10. K. J. Standley, 1962, Oxide Magnetic Materials, pp -204.

1.11. J. S. Smart, 1955, Amer. J. Physics, Vol. 23 pp-356.

1.12. W. P. Wolf, 1961, Reports on Prog. In Phys., Vol. 24, pp-212.

1.13. E. W. Gorter, 1955, Proc I.R.E., Vol. 43, pp-1945.

1.14. E.C. Snelling, 1988, Soft Ferrites: Properties and Applications 2nd edition, Butterworths London, pp-1.

1.15. T. Suzuki, T. Tanaka & K. Ikemizu, 2001, J. Magn. Magn. Mater., Vol. 235, pp-159.

1.16. T. Giannakopoulou, L. Kompotiatis, A. Kontogeorgakos & G. Kordas, 2002, J. Magn. Magn. Mater., Vol. 246, pp-360.

1.17. E. Olsen & J. Thonstad, 1999, J. Appl. Electrochem., Vol. 29, pp-293.

1.18. C. O. Augustin, D. Prabhakaran. & L.K. Srinivasan 1993, J. Mater. Sci. Lett., Vol.12, pp-383.

CHAPTER-2

2.1. E.Ateia, M.A.Ahmed & A.K.El-Aziz, 2007, J. Magn. Magn. Mater., Vol. 311, pp.545-554.

2.2. A. Singh, J. Singh and H. S. Dosanjh, 2015, Journal of Chemical and Pharmaceutical Research, Vol. 7(2), pp-612-617.

2.3. N. B. Velhal, N. D. Patil, A. R. Shelke, N. G. Deshpande, and V. R. Puri, 2015, Journal of AIP Advances 5., Vol. 097166.

2.4. K. Kalpanadevi, C. R. Sinduja and R. Manimekalai, 2016, Journal of Bull. Chem. Soc. Ethiop., Vol. 30(1), pp-79-85.

2.5. K. B. Patil and M. S. Rathod, 2014, International Journal of Innovative Research in Science, Engineering and Technology, Vol. 3(6).

2.6. S. Joshi, M. Kumar and G. Srivastava, 2014, International Journal of Applied Engineering Research, Vol. 9(6), pp-713-718.

2.7. A. Maqsood, K. Khan, M. A. Rehman and M. A. Malik, 2011, J Supercond Nov Magn, Vol. 24, pp-617-622.

2.8. R. C. Kambale, P. A. Shaikh, C. H. Bhosale, K. Y. Rajpure and Y. D. Kolekar, 2009, Journal of Smart Mater. Struct., Vol. 18, pp-1-6.

CHAPTER-3

3.1. B.D. Cullity and C.D. Graham, 1972, Introduction to magnetic materials, Johan Wiley and Sons Inc., Hoboken New Jersey, p-2.

3.2. P. G. Hewitt, 1933, Conceptual Physics 7th Ed., Harper Collins College Publishers, New York.

3.3. Vowles & P. Hugh, 1932, Early Evolution of Power Engineering, Isis University of Chicago Press, Vol. 17 (2), pp-412.

3.4. J. Smith and H.P.J. Wijn, 1995, Ferrites- John Wiley and Sons. Publishers, New York, pp-1.

3.5. K. Thorne, 1999, Spacetime Warps and the Quantum: A Glimpse of the Future, ITP & CalTech.

3.6. N. Spaldin, 2003, Magnetic materials: Fundamentals and device applications, Cambridge University press. Cambridge.

3.7. J. Smith and H.P.J. Wijn, 1995, Ferrites, John Wiley and Sons. Publishers, New York, pp-46.

3.8. W. F. Smith and J. Hashemi, 2006, Foundations of Materials Science and Engineering -fourth Edit., Mc Graw-Hill., chapter 16, pp-888.

3.9. M. S. Vijaya & G. Rangarajan, 1999-2000, Materials Science, McGraw-Hill Publishing Company Limited, New Delhi, pp- 447.

3.10. K. J. Standley, 1972, Oxide Magnetic Materials 2nd ed., Oxford University Press.

3.11. W. H. Bragg, 1915, Nature, Vol. 95, pp- 561.

3.12. M. Grätzel 2001, Nature, Vol.414, pp- 338.

3.13. A. Goldman, 1990, Modern Ferrite Technology, Van nosttrand Reinhold New York.

3.14. D. Halliday, R. Resnick, and J. Walker, 2002, Fundamentals of Physics, 6th Ed., John Wiley & Sons, New York.

3.15. E. J. W. Verway and E. L Heilmann, 1947, J. Chem. Phys., Vol.15 (4), pp-174.

3.16. F. C. Romeign, 1953, Philips Res. Rep. 8, NR-5 pp-304.

3.17. J.Smith and H.P.J. Wijn, 1995, Ferrites: John Wiley and Sons. Publishers, New York, pp-17.

3.18. J. D. Jackson, 1998, Classical Electrodynamics: 3rd Ed., John Wisley & Sons, Inc. New York.

3.19. M. S. Vijaya and G. Rangarajan, 1999-2000, Materials Science, McGraw-Hill Publishing Company Limited, New Delhi, pp- 447.

3.20. B.D.Cullity, 1972, Introduction to magnetic materials, Addison-Wesley publishing Co.Inc., pp-110.

3.21. M. A. Omar, 1962, Elementary Solid State Physics (Principles & Applications) Wesley Publishing Company, Amsterdam.

3.22. D. S. Parasnis, Harper and Brothers 1961 Magnetism: From Lodestone to polar Wandering, New York.

3.23. J. R. Reitz, F. J. Milford and R. W. Chrisly, 1979, Foundations of Electromagnetic Theory, 3rd Ed. Addison, Wesley Publishing Company, London.

CHAPTER-4

4.1. G. F Dionne, 1987, J. Appl. Phys., Vol. 61 (8), pp-3868.

4.2. L. B. Kong, Z. W. Li, G. Q. Lin and Y. B. Gan, 2007, J. Am. Ceram. Soc., Vol. 90(7), pp-2104.

4.3. S. K. Sharma, Ravi Kumar, S. Kumar, M. Knobel, C. T. Meneses, V. V. Siva Kumar, V. R. Reddy , M. Singh and C. G. Lee, 2008, J. Phys.: Condens. Matter, Vol. 20, pp-235.

4.4. Soilah Zahi, Mansor Hashim and A. R. Daud, 2007, J. Magn. Magn. Mater.,Vol. 308, pp-177.

4.5. M. A. Hakim, D. K. Saha and A. K. M. Fazle Kibria, 2007, Bang. J. Phys., Vol. 3 pp-57.

4.6. A. Bhaskar, B. Rajini Kanth and S. R. Murthy, 2004, J. Magn. Magn. Mater.,Vol. 283, pp-109.

4.7. Z. Yue, J. Zhou, L. Li, and Z. Gui, 2001, J. Magn. Magn. Mater.,Vol. 233, pp-224.

4.8. P. Reijnen, 1965, 5th Int. Symp. React. In Solids : Elsevier Amsterdam, pp-562.

4.9.

CHAPTER-5

5.1. A. Verma, T.C. Goel, R.G. Mendiratta and R.G. Gupta, 1999, J. Magn. Magn. Mater.,Vol.192, pp 271-276.

5.2. L. Vegard, 1921, J. Phys., Vol.5, pp 17.

5.3. A. Maqsuod, K. Khan, M. A. Rehman and M. A. Malik, 2011, J Supercond Nov Magn., Vol.24, pp 617-622.

5.4. O. M. Hemida and M. M. Barakat, 2011, J. Magn. Magn. Mater.,Vol.223, pp 127.

5.5. A. Globus, H. Pascard and V. Cagan, 1977, J. Phys., Vol.38, pp 163.

5.6. K. H. Maria, S. Choudury and M. A. Hakim, 2013, International Nano Letters., Vol.3, pp 42.

5.7. Y. Koseoglu, 2013, J Supercond Nov Mahn., Vol.26, pp 1391-1396.

5.8. Y. Bai, J. Shou, Z. Gui, Z. Yue and L. Li, 2003, J. Magn. Magn. Mater., Vol.264, pp 44.

5.9. C. Kittel, 1976, Introduction to Solid State Physics 5th edn., John Wiley & Sons, New York, pp 32

5.10. J.H. Nam, W.G. Hur and J. H. Oh, 1997, J. Appl. Phys., Vol.81(8), pp 4794.

5.11. G.S. Shahane, A. Kumar, M. Arora and R.P. Pant, Krishanlal, 2010, J. Magn. Magn. Mater., Vol.322, p p1015-1019.

5.12. R. S. Devan, Y. D. Kolekar and B. K. Chougule, 2006, J. Phys. Condens. Mater., Vol. 18, pp 9809.

5.13. A. Goldman, 1999, Hand book of Modern Ferromagnetic Materials, Kulwer Academic Publishers Boston, USA.

5.14. G. C. Jain, B. K. Das, R. S. Khanduja and S. C. Gupta, 1976, J. Mater. Sci., Vol.II, pp 1335.

5.15. S. Chikazumi, 1966, Physics of Magnetism, John wiley and v sons, Inc, New York.

5.16. M. Srivastava, S. N. Shringi, R. G. Srivastava and N. G. Nandikar, 1976, Phys. Rev B, Vol.14, pp 2032.

5.17. Neel, L, 1948, Magnetic properties of ferrites. Ann. Phys. Paris, Vol. 3, pp 137–198.

5.18. A. Globus and P. Duplex, 1966, IEEE Trans. Magn., Vol.3, pp 441–445.

5.19. J.J Shorti, S.D. Kulkarn, C. E. Deshpande & S. K. Datte, 1999, Mater. Chem. Phys., Vol 59, pp 1-5.

5.20. ST Mahmud et al, 2006, J Magn. Magn. Mater, Vol 305, pp 269-274.

5.21. B.D.Cullity, 1972, Introduction to magnetic materials, Addison-Wesley publishing co. Inc., pp186.

5.22. M. A. Ati, H. Khudhair, S. Dabang, R. M. Rosnan and A.A. Ati, 2014, International Journal of science and Engineering Research, Vol. 5, pp 927-930.

5.23. P. P. Hankare, P. D. Kamble, M. R. Kadam, K. S. Rane and P. N. Vasambekar, 2007, Materials Letters, Vol. 61, pp 2769.

5.24. C. Fu, M. Syue, F. Wei, C. Cheng and C. Chou, 2010 J. Applied Physics, Vol.107, pp 519 .

5.25. E. V. Gopalan, K. A. Malini, D. S. Kumar, Y. Yoshida, I. A. Al-Omari, S. Sara-vanan and M. R. Anantharaman, 2009, J. Physics Condensed Matter, Vol.21, pp 1.

5.26. J.C. Maxwell, 1954, A Treatise on Elec. and Magn.,Oxford, New York, Vol.2.

5.27. C.G. Koops, 1951, Phys. Rev., Vol.83, pp 121.

5.28. K.W. Wagner, 1913, Ann. Phys., Vol.40, pp 817.

APPENDIX A

List of the Symbols

Angular frequency	ω
Wavelength	λ
Bulk density	ρ_B
X-ray density	ρ_x
Anisotropy constant	K_1
Bohr magneton	μ_B
Bragg's angle	θ
Cross-sectional area of toroid	S
Curie temperature	T_c
Dielectric constant	ε'
Exchange integral	J
Exchange-coupling constant	J_{ij}
Face centered cubic	f c c
Frequency	f
Grain diameter	D_m
Real part of initial permeability	μ'
Imaginary part of initial permeability	μ''
Impedance	Z
Inductance	L
Inter planner spacing	d
Lattice parameter	a
Loss factor	tan δ
Magnetization	M
Magnetic field	H
Neel temperature	T_N
Nelson-Riley function	F (θ)

Permeability in free space	μ_0
Porosity	P
Retentivity	M_r
Coercivity	H_c
Saturation magnetization	M_s
Sintering temperature	T_s
X-ray diffraction	XRD
Scanning electron micrographic	SEM
Vibrating sample magnetometer	VSM

APPENDIX B

List of Publication

a) Paper Presented in International and National Conferences /Seminars

1. **[106]:S. A. Ali**, M. A. Matin, M. A. Hakim, M. F. Islam **"Effects of $CoFe_2O_4$ Substitution on Magnetic Properties of $NiFe_2O_4$ Spinel Ferrite**" Presented on the 4th Intl. Conf. on Structure, Processing and Properties of Materials, SPPM2018, 1 – 3 March 2018, BUET, Dhaka